



**University of
Zurich^{UZH}**

Functional diversity from physiological forest traits across different spatial scales and optical sensors: attempts of mapping biodiversity from space

GEO 610 Master's Thesis

Author

Isabelle Helfenstein

13-762-372

Supervised by

Dr. Hendrik Wulf

Dr. Fabian D. Schneider (fabian.schneider@jpl.nasa.gov)

Faculty representative

Prof. Dr. Michael Schaepman

29.12.2018

Department of Geography, University of Zurich



**University of
Zurich^{UZH}**

GEO 610
Master Thesis
December 29, 2018

**Functional diversity from physiological forest traits across
different spatial scales and optical sensors**
Attempts of mapping biodiversity from space

Isabelle HELFENSTEIN
13-762-372

Supervised by:
Dr. Hendrik WULF
Dr. Fabian D. SCHNEIDER
Faculty representative:
Prof. Dr. Michael SCHAEPMAN

Remote Sensing Laboratories
Department of Geography
University of Zurich

Abstract

Global change affects biodiversity worldwide, which alters ecosystem productivity and stability. The increasing need for continuous global information on biodiversity of Earth's vegetation calls for new approaches to exploit existing satellite time-series. In this Master thesis, we adapt and test novel methods to map functional diversity by transferring these from airborne imaging spectroscopy platforms, APEX, to spaceborne multispectral satellites, Sentinel-2. We could identify changes in functional traits and functional biodiversity metrics between two dates of the year, namely July and September. We identified applicable spectral indices for physiological forest traits indicating forest health, stress, and potential productivity and compared their suitability for both sensors on varying spatial scales. We selected four functional traits forming the base data for functional diversity metrics, namely chlorophyll, anthocyanin, carotenoid and water content. Based on the highest scoring index for each trait, we successfully reproduced observations from previous studies at the spectral resolution of Sentinel-2. For all four traits, we selected corresponding indices that could be applied to Sentinel-2 and APEX data, namely $CI_{red-edge}$, RGR , $PSRI$, and $NDII$. Based on spatial scaling analysis from 20 m to 800 m, we observed significant change in two functional diversity metrics, namely functional richness and divergence. Both diversity metrics do not allow for quantitative comparisons across scales involving different numbers of pixels per unit. Qualitatively, the observed patterns of functional richness and divergence were comparable among the sensors for most parts, but not throughout the entire ecosystem. At coarser spatial resolution, mixed pixel effects could be noticed at the forest border and clearing areas, causing an increase in richness and decrease in divergence. Different approaches for masking vegetation, or specifically the forested areas, will improve presented results. Furthermore, including morphological information from laser scanning will provide the opportunity to characterize structural diversity and help to improve forest masking. Despite the challenges, there is a high potential in the presented approach. Mapping functional diversity from space will provide many opportunities to quantify biodiversity, ecosystem functioning and global environmental changes. Next steps include analysis of the approach at larger research areas, different ecosystems and throughout the phenological year.

Contents

Abstract	III
List of Figures	VII
List of Tables	XI
1 Introduction	1
2 Material and Methods	5
2.1 Study area	5
2.2 Remote Sensing data	5
2.2.1 Imaging spectroscopy data	6
2.2.2 Spaceborne Remote Sensing data	6
2.2.3 Dataset selection	6
2.2.4 Other data	8
2.3 Data preparation	9
2.3.1 Data pre-processing	9
2.3.2 Spectral resampling	9
2.3.3 Forest mask	9
2.4 Functional traits	12
2.4.1 Vegetation indices	12
2.4.2 Testing indices	17
2.5 Functional diversity	18
2.5.1 Multi-dimensional scale analysis	18
2.5.2 Functional diversity metrics	22
3 Results	25
3.1 Choice of vegetation indices	25
3.1.1 One-dimensional scale analysis	25
3.1.2 Comparing indices of rescaled APEX and Sentinel-2 datasets	27
3.1.3 Correlation of calculated indices	29
3.2 Functional traits	30
3.3 Multi-dimensional scale analysis	32
3.4 Functional diversity maps	34
3.4.1 Diversity calculated from 2 m APEX dataset	34
3.4.2 Differences in diversity maps due to rescaling	35

3.4.3	Differences in diversity maps due to sensor characteristics	40
4	Discussion	43
4.1	Functional traits	43
4.1.1	Identification of suitable functional traits and corresponding vegetation indices	43
4.1.2	Mapping functional traits	44
4.1.3	Outlook	46
4.2	Functional diversity	46
4.2.1	Four-dimensional scale analysis	46
4.2.2	Mapping functional diversity	47
4.2.3	The mixed-pixels problem	49
4.2.4	Adding Anthocyanin	50
4.2.5	Seasonal development of mapped physiological diversity	50
4.2.6	Behavior of diversity metrics with neighborhood area	51
4.2.7	Outlook	52
5	Conclusion	55
	Bibliography	57
A	Appendix - Additional Figures and Tables	69
B	Appendix - List of Abbreviations	83
B.1	Terms and Abbreviations	83
B.2	Abbreviations	84
B.3	Vegetation indices	85
B.4	Organizations	85
B.5	Missions	85
B.6	Software	86
	Acknowledgements	87
	Personal Declaration	89

List of Figures

2.1	Research site at the Laegern forest and location in Switzerland.	5
2.2	Histogram showing <i>NDVI</i> values at the research site in both summer and fall.	10
2.3	Final forest mask calculated at 2 m and 20 m resolution.	11
2.4	Example of one-dimensional scale analysis calculating within- and between-unit variance, for increasing unit side length.	17
2.5	Example of the calculation involved in a one-dimensional scale analysis.	19
2.6	Units considered for the scale analysis at a unitsize of 400 · 400 m.	20
2.7	Functional richness and divergence based on an example unit.	22
3.1	Scatterplots of the tested indices, calculated based on datasets for each sensor in both summer and fall.	28
3.2	Mapped functional traits (chlorophyll, anthocyanin, carotenoid, and water content) on the research site.	30
3.3	Mapped functional traits on research site in both summer and fall, at different sections of the research area.	31
3.4	Comparison of sensors in a four-dimensional scale analysis calculating richness from the functional traits chlorophyll, anthocyanin, carotenoid, and water content.	32
3.5	Comparison of sensors in a four-dimensional scale analysis calculating divergence from the functional traits chlorophyll, anthocyanin, carotenoid, and water content.	33
3.6	Functional richness based on 2 m APEX dataset in summer and fall.	34
3.7	Functional divergence based on 2 m APEX dataset in summer and fall.	34
3.8	Functional richness maps based on the A2, A20 and S20 dataset in summer and fall calculated in units with 60 m diameter.	36
3.9	Functional richness maps based on the A2, A20 and S20 dataset in summer and fall calculated in a 120 m diameter.	36
3.10	Functional divergence maps based on the A2, A20 and S20 dataset in summer and fall calculated in units with 60 m diameter.	38
3.11	Functional divergence maps based on the A2, A20 and S20 dataset in summer and fall calculated in a 120 m diameter.	38
3.12	Development of mean functional richness and divergence in summer and fall when calculated based on increasing neighborhood diameter for the whole ecosystem as well within the three subareas A, B and C.	39

3.13	Development of mean functional richness and divergence in summer and fall when calculated based on increasing neighborhood diameter. The panels show both the development of mean values when calculated based on the A20 dataset and the S20 dataset in large units.	39
3.14	Development of the correlation for richness and divergence with increasing neighborhood size in which they were calculated over the ecosystem.	41
3.15	Development of the correlation for the two functional diversity metrics with increasing unit size in which they were calculated, for each of the three subareas A, B and C. The resampled A20 dataset is compared with the A2 (left), the S20 dataset is compared with the A2 dataset (middle), as well as the A20 dataset and the 20 m S20 dataset (right).	42
4.1	Effect of niche partitioning on functional divergence.	48
4.2	Effect of mixed pixels on randomly generated data-points with clear differentiation/niche partitioning.	50
A.1	Comparison of APEX and Sentinel-2 pixels.	69
A.2	NDVI Mask, vegetation height mask based on the CHM and shadow mask.	70
A.3	Graphic representation of the three types of dataset, the spectrally resampled APEX dataset (A2), the spectrally and spatially resampled APEX dataset (A20) and the Sentinel-2 dataset (S20).	71
A.4	Graphic representation of the basic work-flow from remotely-sensed data to physiological diversity.	72
A.5	Example of circular pixel neighborhood and its weighing.	72
A.6	Performance of <i>CRI1</i> in the one-dimensional scale analysis.	74
A.7	Carotenoid describing <i>CRI1</i> calculated on the A2 dataset. <i>CRI1</i> seemed to not work properly on APEX data.	74
A.8	Difference of all functional traits calculated based on the A2 datasets.	76
A.9	Histograms showing the mapped functional traits chlorophyll, anthocyanin, carotenoid and water content on the research site.	77
A.10	One-dimensional scale analysis for each of the functional traits.	77
A.11	Scale analysis of A20 and S20 datasets, calculating functional richness.	78
A.12	Scale analysis of A20 and S20 datasets, calculating functional richness. Chlorophyll content is here described by <i>CI_{green}</i> instead of <i>CI_{red-edge}</i>	78
A.13	Scale analysis of randomly generated, normally distributed trait data calculated functional divergence five times.	78
A.14	Correlation of seasons for both functional richness and divergence maps, calculated from A2 data.	79
A.15	Seasonal difference of functional richness.	79
A.16	Seasonal difference of functional divergence.	80
A.17	Functional richness calculated based on the different datasets A2, A20, S20 in summer and fall based on 200 m unit size.	80

A.18 Functional divergence calculated based on the different datasets A2, A20, S20 in summer and fall based on 200 m unit size.	81
A.19 Development of within- and between-unit functional richness with increasing unit size in summer and fall in the four-dimensional scale analysis based on the A2 datasets.	81
A.20 Development of mean functional richness calculated based on the A20 dataset, with increasing unit area in summer and fall.	82
A.21 Effect of mixed pixels on randomly generated, normally distributed data-points without clear differentiation/niche partitioning.	82

List of Tables

2.1	Remotely-sensed data from the Laegern forest derived using APEX and Sentinel-2 in 2016.	6
2.2	Spectral bands and their spatial resolution of Sentinel-2 MSI sensors.	7
2.3	Phenological data from stations near the Laegern forest, indicating general leaf discoloration and general leaf fall.	7
2.4	Tested indices and type of traits.	16
2.5	Number of valuable pixels per unit (<i>ppu</i>) and number of units considered for every unit size within the scale analysis.	21
2.6	Unit size (diameter and area) of circular units, in meter and pixels, comparing data with 2 m pixels and 20 m pixels.	23
3.1	Tested indices and their corresponding trait in the one-dimensional scale analysis.	26
3.2	Correlation of the calculated indices on the A20 and S20 datasets.	26
3.3	Correlation of calculated indices with each other based on 20 m datasets, averaged over sensors and seasons.	29
3.4	Correlation of functional traits in both summer and fall.	30
A.1	Correlation of tested indices with each other, calculated based on A20 datasets averaged over seasons summer and fall.	73
A.2	Correlation of tested indices with each other, calculated based on S20 datasets averaged over seasons summer and fall.	73
A.3	Calculated variables of tested indices, calculated based on A20 and S20 datasets for each sensor at both summer and fall.	75

1 Introduction

Global environmental change is a continuing process. Anthropogenic changes, such as deforestation and forest degradation, shifts in climate (global warming) as well as atmospheric chemistry, eutrophication, fire suppression and drought can be noticed globally, lead to alterations in ecosystems and impact biodiversity (Brooks et al., 2002; Sodhi et al., 2004; Fearnside, 2005; Pandit et al., 2007; IPCC, 2013; Hautier et al., 2015). Changes in biodiversity related to environmental change affect productivity and stability of ecosystems (Hector and Bagchi, 2007; Cardinale et al., 2013; Bartomeus et al., 2013; Morin et al., 2014; Cusson et al., 2015; Jucker et al., 2014). The effects of changes in biodiversity on ecosystem services are visible, for example through food and wood provisioning, which is related to plant biomass and therefore productivity (Balvanera et al., 2006). An increase in diversity promotes ecosystem functioning and productivity, due to a more efficient usage of the given resources through niche partitioning (Loreau et al., 2001; Morin et al., 2011). Ecosystems characterized by higher diversity are more robust against disturbances, such as herbivory, pests and impacts of global environmental change (Jactel and Brockerhoff, 2007; Silva Pedro, Rammer, and Seidl, 2015). Diversity therefore provides insurance for ecosystem functioning due to a high number of different ecological strategies providing stability and resilience especially when facing disturbances and ecosystem changes (Loreau et al., 2003; Matias et al., 2013). Other positive effects of increased plant diversity on ecosystem services include erosion control, increases in decomposition, and ecosystem resistance to invasive species (Balvanera et al., 2006; Laureto, Cianciaruso, and Samia, 2015). Diversity loss, on the other hand, has an effect comparable to the effects of disturbances linked to environmental change, while also leading to greater exposition to disturbances caused by global anthropogenic changes (Tilman, Isbell, and Cowles, 2014).

Anthropogenic changes can alter interspecific interactions and produce unexpected changes in species distribution, community structure, and species diversity and have resulted in worldwide biodiversity loss (Harley, 2011). The preservation, conservation, and restoration of biodiversity should be a high global priority (Tilman, Isbell, and Cowles, 2014). Halting the rate of biodiversity loss and reducing its impact are international goals, which are manifested in the Aichi Targets for 2020 by the United Nations (UN) Convention on Biological Diversity, as well as the UN Sustainable Development Goals to be achieved by 2030 (Pereira et al., 2013; Tittensor et al., 2014; Brooks et al., 2015; FAO, 2018). Therefore, it is necessary to study the impacts, interactions and feedbacks of global environmental change on ecosystems and biodiversity.

Currently, there is a high demand in consistent time-series on a global scale to study the biodiversity of Earth's vegetation (Tittensor et al., 2014; Jetz et al., 2016). Observing functional diversity using satellite data will provide continuous, global coverage in space and time. Therefore, satel-

lite remote sensing is crucial to get long-term global coverage (Skidmore and Pettorelli, 2015). Advancing our scientific understanding on biodiversity states and changes on a global scale will help to assess the impact of environmental change on ecosystems and facilitates the prediction of future ecosystem functioning (Jetz et al., 2016). Furthermore, long-term observations provide a more detailed representation of the biosphere in Earth system models (Jetz et al., 2016). For a long time, access to satellite images was restricted for security or commercial reasons. Nowadays, data available from publicly funded space agencies build the basis for monitoring biodiversity and biodiversity change from space (Skidmore and Pettorelli, 2015). Making existing approaches to measure and map diversity suitable for satellite based data leads to new possibilities of large-scale analysis, possibilities of analysis throughout the phenological year (due to the fast revisiting time) or time-series of multiple years, also in remote areas and on large spatial scales.

Biodiversity is defined and detected in a variety of ways. Evenness of plant abundances and functional biodiversity from functional traits are linked to ecosystem functioning and stability as much as species richness, but only the latter is commonly used to define biodiversity (Polley et al., 2013). However, functional biodiversity allows measuring ecosystem functioning and stability, derived from remotely sensed data (Homolová, 2014; Jetz et al., 2016; Schneider et al., 2017).

The units within functional classification schemes are plant functional types (Cornelissen et al., 2003). They can be defined as groups of plant species with similarities in functioning at the organism level, roles within communities, responses to environmental factors or effects on ecosystems. These similarities are based on the fact that they tend to share a set of key functional traits (Homolová, 2014). A trait is any feature measurable at the individual level, from the cell to the whole-organism, without reference to the environment or any other level of organization (Violle et al., 2007). These functional traits can be morphological, including e.g. growth form and plant height, physiological, such as leaf nitrogen, phosphor or water content, or phenological, regarding e.g. leaf phenology to name a few. Several of the aforementioned traits are known and commonly used as plant functional traits (Pérez-Harguindeguy et al., 2013), and have been identified as essential biodiversity variables (EBV) (Pereira et al., 2013; Pettorelli et al., 2016). Not all of these can be derived using remotely sensed data, however, some of them can be measured well (Homolová, 2014; Schneider et al., 2017). Furthermore, functional traits respond to environmental conditions and are directly linked to growth, reproduction and survival (Violle et al., 2007; Liu et al., 2016). When focusing on the community scale (α -diversity) and ecosystems (β/γ -diversity), functional diversity offers more than functional traits (Cadotte, Carscadden, and Mirotnick, 2011), with γ -diversity of a landscape, or geographic area, being the product of the α -diversity of its communities and the degree of β -differentiation among them (Whittaker, 1972; Bello et al., 2009). Functional diversity was found to explain ecosystem functioning, similarly to species richness (Tilman et al., 1997; Polley et al., 2013). There is growing recognition of the fact that classifying terrestrial plant species on the basis of their function (into functional types) rather than their higher taxonomic identity, is a promising way forward for working on important ecological questions at the scale of ecosystems, landscapes or biomes (Cornelissen et al., 2003). Identifying the components of biodiversity that are closely related to ecosystem functioning is enormously important. These questions include those on vegetation responses to, as well as effects of the biosphere on, global

environmental changes. In this sense, functional diversity has proven to play an important role, since it is claimed to be an effective diversity measure for detecting a positive effect of biodiversity on ecosystem functioning and services (Laureto, Cianciaruso, and Samia, 2015; Balvanera et al., 2006). However, it remains unclear, whether remotely sensed functional diversity links similarly well to ecosystem functioning. Direct remotely-sensed measurements of plant traits by imaging spectroscopy are currently limited to only those traits with a clear spectral signature expressed in the dominant canopy layer. This leaves out a lot of traits, mainly regarding root and stem traits (Jetz et al., 2016). For a full understanding of the links between remote sensing and functional types a more complete integration of physical remote sensing concepts with a deep understanding of ecological theory is needed, requiring a high level of interdisciplinarity (Ustin and Gamon, 2010).

In 2017, Schneider et al. presented an approach on mapping functional diversity from remotely sensed data by combining morphological and physiological forest traits using airborne laser scanning and imaging spectroscopy data. This approach provides a baseline for measuring functional diversity using remotely-sensed data. Building on this approach, we explore possibilities of transferring it from airborne to spaceborne platforms to cover larger areas. This transformation generally comes at the expense of lower spatial and spectral resolution. The main objective of this Master thesis is to apply the given methodology suitable for satellite data and explore its potential as well as its limitations. Namely, we transfer mapping approaches of functional diversity from APEX to Sentinel-2. Due to a lack of suitable spaceborne laser scanning data, we focus on physiological traits only. Firstly, we analyze suitable physiological traits based on their robustness across different spatial scales and sensors. Spatial behavior and reaction to scaling of different trait describing vegetation indices are analyzed and compared in a scale analysis. Different vegetation indices and traits are calculated on both the APEX and the Sentinel-2 datasets, in order to find traits suitable for multiple types of data, with different spectral and spatial resolution. In a multidimensional scale-analysis, we compare the performance and scaling effects of the functional traits with functional diversity metrics, namely function richness and divergence. We compare the performance of functional metrics in a scale analysis to the one-dimensional functional traits. Secondly, we convolve the APEX imaging spectroscopy data to match the spectral and in a second step the spatial characteristics of Sentinel-2 data. Furthermore, the functional diversity metrics are calculated, mapped and compared using three datasets, (i) APEX in 2 m, (ii) APEX spatially re-sampled to 20 m and (iii) Sentinel-2 in 20 m. Rescaling APEX data reveals not only the potential of mapping functional diversity using current multispectral satellite data, but also future spaceborne imaging spectrometers with similar characteristics. However, when rescaling the underlying data from 2 m to 20 m pixel size, we expect some information loss. Furthermore, by using data collected at two mission dates in July and September, we identify changes in functional traits and functional biodiversity metrics between two dates of the year.

Our research questions are formulated accordingly:

1. How are different physiological traits and corresponding vegetation indices as well as functional diversity metrics affected by scaling effects? Which of them can be applied to multiple sensors?
2. To which extent are seasonal changes of the ecosystem between July and September visible through functional traits and biodiversity metrics?
3. To which extent do results from APEX data differ from resampled APEX data and from spaceborne data? How much of the initial diversity can be observed from spaceborne data, where are major differences?

Based on a previous study by Karadimou et al. (2016), we expect variations in diversity measurements due to scaling effects. Functional richness is expected to decrease with increasing pixel size. In comparison, we expect the effect of rescaling on functional divergence to be smaller, as no relationship with neighborhood area was observed (Karadimou et al., 2016). Furthermore, different datasets should yield in varying reflectance values due to changing observation geometries and atmospheric conditions. However, by spatially rescaling the APEX dataset, one can differentiate the impact of scaling and sensor changes on the diversity metrics.

2 Material and Methods

2.1 Study area

The study area covers the Laegern forest in Switzerland encompassing 12.8 km² ranging from 450 to 860 m a. s. l. (Figure 2.1). The semi-natural temperate mixed forest is predominantly characterized by shadow tolerant species such as European beech (*Fagus sylvatica*), Norway spruce (*Picea abies*) and Silver fir (*Abies alba*), while the more sunlit southwestern part comprises furthermore Ash (*Fraxinus excelsior*) and Sycamore (*Acer pseudoplatanus*) (Eugster et al., 2007). Compared to other temperate forests, the Laegern forest provides a high degree of biodiversity, considering species richness, as well as the distribution of individual age and stem diameter, due to the local management strategies (Eugster et al., 2007; Srinivasan et al., 2015; Schneider et al., 2017).

2.2 Remote Sensing data

In this study we analyzed two concurrent APEX and Sentinel-2 scenes from July and September, respectively. Furthermore, a canopy height model (CHM) was used in order to create a forest mask (see section 2.3.3).



FIGURE 2.1: Research site at the Laegern forest and location in Switzerland. Image and underlying data by swisstopo, Switzerland (2018).

TABLE 2.1: Remotely-sensed data from the Laegern forest derived using APEX and Sentinel-2 in 2016.

2016	APEX		Sentinel-2		δ
	[dd/mm]	[DOY]	[dd/mm]	[DOY]	[dd]
“Summer” June/July	07/07	189	24/06	176	13
“Fall” September	07/09	251	09/09	253	02

2.2.1 Imaging spectroscopy data

The Airborne Prism Experiment (APEX) is a push-broom imaging spectrometer covering the reflected wavelength range from 372 nm to 2540 nm (Schaepman et al., 2015). The imaging spectroscopy dataset includes 284 spectral bands in a 2 m spatial resolution. Both datasets were collected on cloudless days in 2016, namely July 7th and September 7th. In the following we will refer to the July acquisition as “summer” and the September acquisitions as “fall” (see Table 2.1).

2.2.2 Spaceborne Remote Sensing data

The European Space Agency (ESA) Sentinel-2 mission is a two satellite mission with a predicted lifespan of 15 years (Drusch et al., 2012). The Sentinel-2A satellite was launched in June 2015 and 2B in March 2017. The Sentinel-2 satellites Multi-Spectral Instrument (MSI) sensor has 13 spectral channels with a spatial resolution of 10 – 60 m (ESA, 2017; Korhonen et al., 2017). Sentinel-2 data enables improved monitoring possibilities offered by a higher temporal resolution, with a revisiting period of < 5 days (Drusch et al., 2012). In addition, a lot of Sentinel-2’s potential regarding vegetation remote sensing lies in the red edge spectral bands (bands 5 – 7, see Table 2.2), which improve the accuracy of various biophysical variables (Korhonen et al., 2017). To compare Sentinel-2 and APEX data, we focus on the spectral bands provided in 20 m resolution (see Figure A.1).

2.2.3 Dataset selection

Two images were studied per sensor, at two different states of the phenological year. The dates between APEX and Sentinel-2 acquisitions are closer in September (2 days), as compared to June/July (13 days, see Table 2.1). To assure that the acquisitions in September still took place during the photosynthetically active state of the forest, we analyzed the general leaf discoloration and leaf fall in 2016. General leaf discoloration is defined as the date, when 50% of the tree’s or stand’s summer leaf area turned yellow or brown (Verein GLOBE Schweiz, 2017b). General leaf fall, on the other hand, has been defined as the date, when 50% of the tree’s leaf area has fallen on the ground. Observations of the Swiss Phenology Network indicate general leaf discoloration around mid October and leaf fall by the end of October (MeteoSwiss, 2016). In more detail, specific dates on general leaf discoloration and general leaf fall have been observed for different tree

TABLE 2.2: Spectral bands and their spatial resolution of Sentinel-2 MSI sensors (Korhonen et al., 2017).

Band	Wavelength range [nm]	Resolution [m]
1 "Coastal aerosol" (CA)	433-453	60
2 "Blue" (B)	458-523	10
3 "Green" (G)	543-578	10
4 "Red" (R)	650-680	10
5 "Red edge 1" (RE1)	698-713	20
6 "Red edge 2" (RE2)	733-748	20
7 "Red edge 3" (RE3)	773-793	20
8 "Near infrared" (NIR)	785-900	10
8a "Near infrared narrow" (NIRn)	855-875	20
9 "Water vapor" (WV)	935-955	60
10 "Shortwave infrared"/"Cirrus" (C)	1360-1390	60
11 "Shortwave infrared 1" (SWIR1)	1565-1655	20
12 "Shortwave infrared 2" (SWIR2)	2100-2280	20

species at three stations close to the Laegern forest. Table 2.3 indicates the observed dates for European beech (*Fagus sylvatica*), a common species in the research site.

While yellowing can be referred to as the most obvious sign of leaf senescence, the process onset takes place long before the date of general leaf discoloration. By the time general leaf discoloration takes place, 50% of the leaf area already shows yellowing, which indicates yellowing onset taking place much closer to the mission days. Furthermore, chlorophyll degradation can even be detected before yellowing of the leaves becomes visible (Hanfrey, Fife, and Buchanan-Wollaston, 1996). By the time the leaf appears yellow to the human eye the chlorophyll content has fallen to around 50% of the amount in a mature green leaf (Hanfrey, Fife, and Buchanan-Wollaston, 1996; Buchanan-Wollaston, 1997) and therefore, signs of leaf senescence, such as chlorophyll decrease and anthocyanin increase can be detected before the time the leaf is senescing visibly. Therefore, the two points in time were compared especially considering differences in chlorophyll and anthocyanin content. The datasets collected in June and July are further referred to as "summer" images, while the ones collected in September are called "fall" images (see Table 2.1).

TABLE 2.3: Phenological data from stations near the Laegern forest, indicating general leaf discoloration and general leaf fall. Data from Swiss Phenology Network (Verein GLOBE Schweiz, 2017a).

Fagus sylvatica 2016	Oberehrendingen		Villnachern		Döttingen	
	[dd/mm]	[DOY]	[dd/mm]	[DOY]	[dd/mm]	[DOY]
General leaf discoloration	18/10	292	14/10	288	19/10	293
General leaf fall	30/10	304	30/10	304	01/11	306

2.2.4 Other data

2.2.4.1 Canopy Height Model

The Canopy Height Model (CHM), which was used to generate a forest mask (see Section 2.3.3), was created from airborne laser scanning data, which was acquired in August 2010, and registered to the Swiss national grid CH1903+ (Schneider et al., 2017).

2.3 Data preparation

2.3.1 Data pre-processing

The APEX data was pre-processed with the APEX Processing and Archiving Facility system (Hueni et al., 2009). Next, the data was atmospherically corrected in ATCOR4 and geo-rectified subsequently (Schläpfer and Richter, 2002; Schaepman et al., 2015; Hueni et al., 2017). The resulting surface reflectance data is characterized by a high spectral and spatial resolution with 284 spectral bands in the range of 400 nm – 2500 nm and a pixel size of 2 m. Sentinel-2 radiance data was corrected to surface reflectance in ATCOR3 according to Richter and Schläpfer (2017). Next, the datasets were converted to CH1903+/LV95, maintaining 20 m resolution using “gdalwarp” in QGIS.

2.3.2 Spectral resampling

To analyze indices, which can be calculated on datasets of both sensors, APEX and Sentinel-2, the APEX data was spectrally resampled to the resolution of the Sentinel-2 images based on the Sentinel-2 spectral response function (SRF) (“spectral resampling” in ENVI). The result was a new dataset with the same spectral resolution as the Sentinel-2 datasets and the spatial resolution of the APEX scenes (pixel size of 2 m). Those scenes will further be referred to as A2 scenes.

2.3.3 Forest mask

To only take fully illuminated forest pixels into consideration for further analysis, a combined forest and shadow mask was calculated. We developed a simple score based on three threshold requirements that result in the final forest mask, to define sunlit forest pixels (see Figure 2.3). A pixel which was assigned the value 1 in all three requirements (see 2.3.3.1 – 2.3.3.3), was included in the final forest mask and selected for further analysis. In order to compare results for both seasons, the forest mask was calculated separately and combined afterwards. The approach is outlined in detail in the following subsections, and illustrated using data of the A2 scenes.

2.3.3.1 Vegetation mask using NDVI

The *NDVI* (see 2.2 in section 2.4.1) is known to show a strong relationship to the Leaf Area Index (LAI) and therefore canopy density and biomass (Song, 2013). Although *NDVI* tends to saturate under moderate to high above-ground biomass, it can be useful for vegetation masking since it compensates for changing illumination conditions, surface slope, aspect, and other extraneous factors (Gitelson, 2004; Lillesand, Kiefer, and Chipman, 2015). A vegetation map was calculated using an *NDVI* (Eq. 2.2) threshold of 0.7, based on the histogram in Figure 2.2. Pixels with values ≥ 0.7 were assigned 1, and pixels < 0.7 were assigned 0 in both images, which were combined in the following step (see Figure 2.2 and A.2).

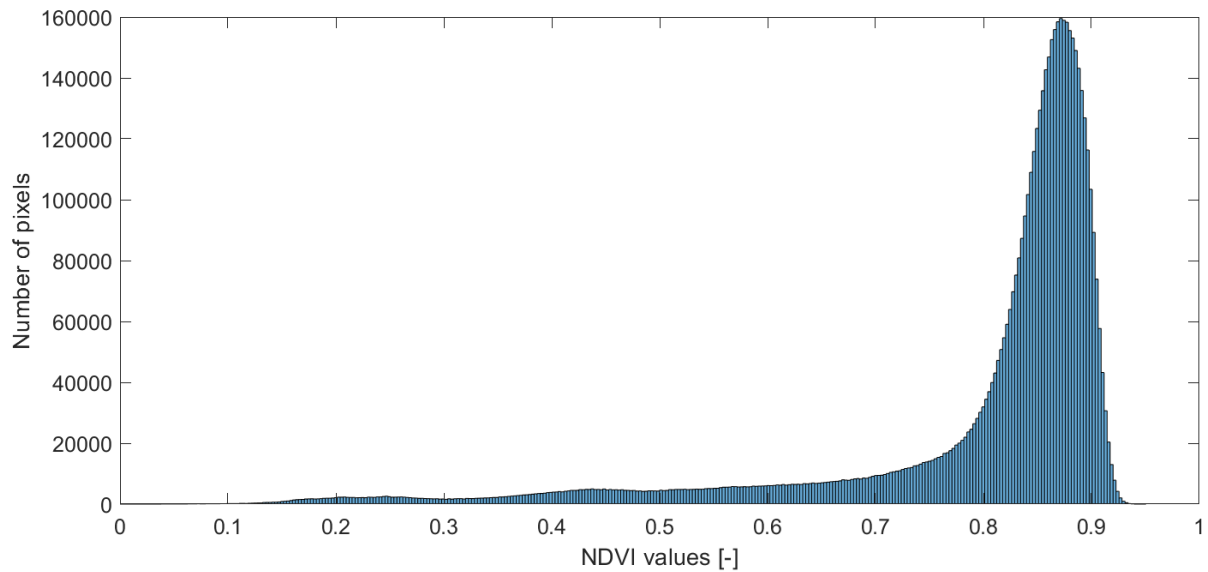


FIGURE 2.2: Histogram showing *NDVI* values at the research site in both summer and fall. The chosen threshold for the forest mask was set at 0.7.

2.3.3.2 Vegetation height mask

The mask based on vegetation height was calculated from the CHM. The critical canopy height, the threshold to exclude the forest edge and gaps, was chosen to be 4 m (Koukoulas and Blackburn, 2004). Pixels with values ≥ 4 m were assigned 1, and pixels < 4 m were assigned 0 (see Figure A.2).

2.3.3.3 Shadow mask

Pixels that are not fully illuminated can cause a variety of problems in spectral analysis. First of all, in datasets with high resolution, pixels of the same object, which is partly in shade, can cause higher heterogeneity within an object of the same spectral traits (Nagendra and Rocchini, 2008). Furthermore, information on surface properties could be lost due to the lower signal to noise ratio in shadows (Liu and Yamazaki, 2012). The presence of shadows can also lead to misleading results when comparing different images with changing sun-sensor geometry and thus BRDF effects, depending on season and time of the day (Liu and Yamazaki, 2012). In the topographically heterogeneous site of the Laegern forest, pixels which lie in the shade are certainly present. Using fully illuminated pixels is possible when excluding shadow. The effect of shadow is more dominant in infrared than in other parts of the spectrum. This is because the radiance ratio between shadow and sunlit areas decreases with increasing wavelength, as shadow regions are illuminated by diffuse light (Liu and Yamazaki, 2012; Rufenacht, Fredembach, and Susstrunk, 2014). In order not to unintentionally exclude dark pixels, which are dark green parts of conifers, bands in the infrared part of the spectrum were considered. The calculation therefore was based on channels 7 – 10 (780 – 1400 nm) in the red-edge and infrared part of the spectrum (see Table 2.2). To exclude potential shadow from the image, the total reflectance at selected channels was calculated, and

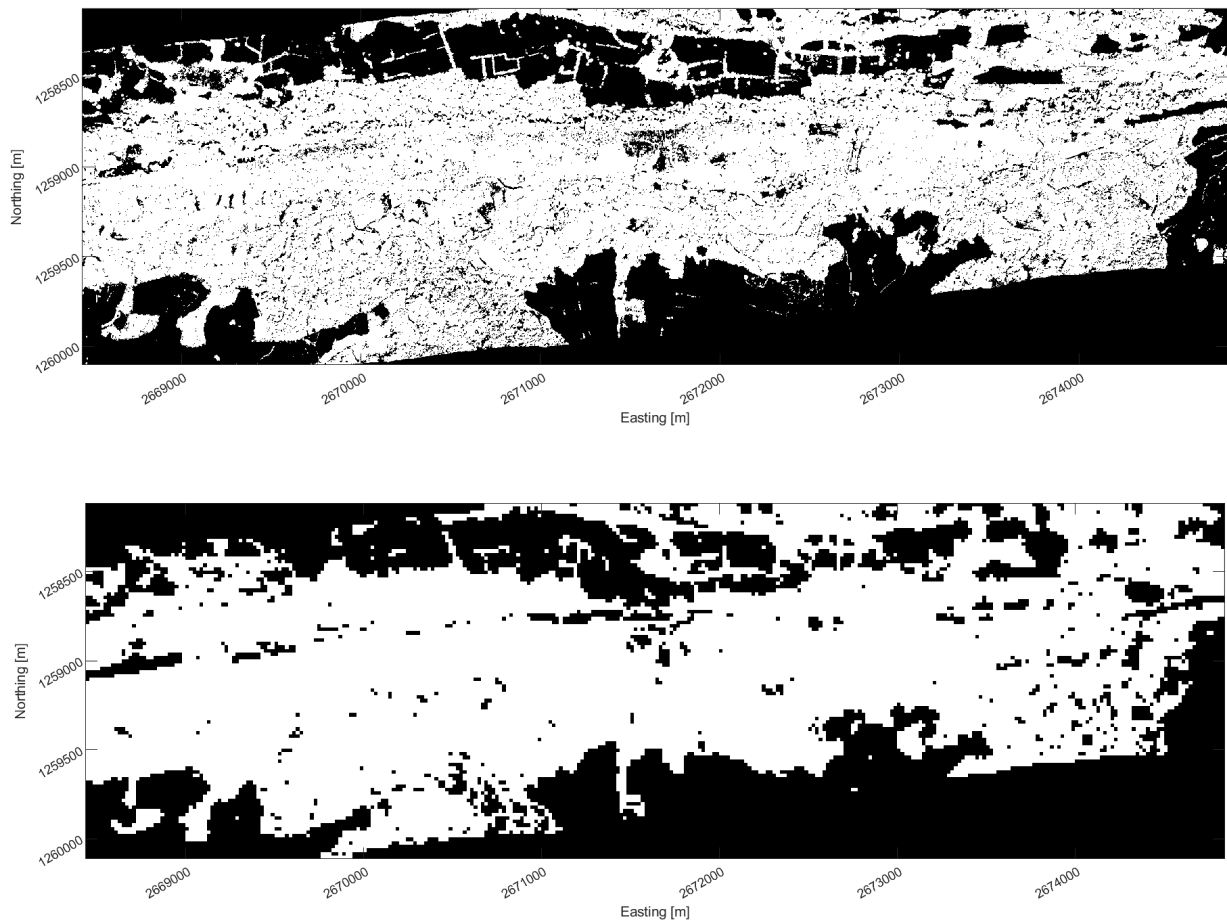


FIGURE 2.3: Final forest mask calculated at 2 m resolution (top) and final forest mask with 20 m resolution not rescaled but recalculated using the same parameters (bottom).

the darkest 2.5% of pixels were excluded. Pixels with values equal to the threshold or higher were assigned 1, and pixels lower than the threshold were assigned 0 (see Figure A.2).

2.3.3.4 20 m scene

To calculate the forest mask for the 20 m dataset, the CHM, as well as both APEX scenes were resampled to 20 m spatial resolution (“imresize” in MATLAB). The resulting scenes are APEX scenes with the same spectral and spatial resolution as the datasets acquired by Sentinel-2. The spectrally and spatially resampled APEX scenes will be further referred to as A20 scenes. The spaceborne data, acquired by Sentinel-2, will further be called S20 data. A graphic representation of the three types of datasets (A2, A20 and S20) can be found in Figure A.3. The 20 m shadow mask was calculated from the combination of the vegetation masks and shadow masks for either A20 and S20 data, in both seasons. The vegetation mask for the 20 m scenes was calculated according to the 2-m-resolution mask, using thresholds $NDVI \geq 0.7$, $CHM \geq 4$ m, and $\leq 5^{th}$ percentile of the summed channels 7 – 10 for the shadow mask (see Figure 2.3).

2.4 Functional traits

2.4.1 Vegetation indices

It is generally supported that correct estimates of functional diversity highly depend on the choice of meaningful traits (Tsianou and Kallimanis, 2016). Due to the used passive-optical spectroscopy data, only physiological traits were used. To describe functional traits, several vegetation indices (see Table 2.4) were collected and tested for usability, as further described.

The spectral relation between the reflection of light at different regions of the spectrum were found to be sensitive indicators for the presence and condition of vegetation, which shows typical reflection behavior in different spectral ranges. Mathematical combinations of channels are referred to as vegetation indices (VI) (Lillesand, Kiefer, and Chipman, 2015). Green vegetation mostly absorbs red light (R), whereas it reflects light at the near infrared (NIR) part of the spectrum due to heat protection. This spectral contrast is measured within pixels (Huete et al., 2002) and forms the basis for the calculation of many VIs (Henebry and De Beurs, 2013). Examples of VIs making use of the contrast of the reflection in red light and NIR are the Simple Ratio (*SR*) (Eq. 2.1) as a basic (Tucker and Sellers, 1986) and Normalized Difference Vegetation Index (*NDVI*) (Eq. 2.2) as a very common one (Huete et al., 2002). These indices are calculated using the surface reflectance ρ at the spectral bands R and NIR (band 4 and band 8 in the case of Sentinel-2, see Table 2.2) and can both be related to primary production and photosynthetic activity (Tucker and Sellers, 1986). While being functionally equivalent to the simple ratio, *NDVI* is representative of many variants sensitive to chlorophyll and photosynthetic vegetation (Huete et al., 2002). Another index used for estimating chlorophyll content and photosynthetic activity is the enhanced vegetation index (*EVI*) (Eq. 2.3), while showing less saturation in dense vegetation than *NDVI* (Huete, Liu, and Leeuwen, 1997). However, *EVI* is known as being more sensitive to topographic conditions than *NDVI*, because of the soil adjustment factor (Matsushita et al., 2007).

$$SR = \frac{\rho_{785-900}}{\rho_{650-680}} \quad (2.1)$$

$$NDVI = \frac{\rho_{785-900} - \rho_{650-680}}{\rho_{785-900} + \rho_{650-680}} \quad (2.2)$$

$$EVI = 2.5 \cdot \frac{\rho_{785-900} - \rho_{650-680}}{\rho_{785-900} + 6 \cdot \rho_{650-680} - 7.5 \cdot \rho_{458-523} + 1} \quad (2.3)$$

Like the *NDVI*, there are other indices used for monitoring, analyzing, and mapping temporal as well as spatial distributions of physiological characteristics of vegetation (Gitelson, 2004). Pigment contents can be estimated, such as chlorophyll, carotenoids and anthocyanin, as well as water content. To find VIs that describe functional traits, suitable for further calculations, various indices have been collected. The first requirement to the VIs was that they are supported by the spectral resolution of the Sentinel-2 MSI sensor. This limited the selection of indices and corre-

sponding functional traits. Furthermore, they should show reasonable and similar results in both Sentinel-2 and APEX scenes as well as at different spatial scales, to be universally applicable.

2.4.1.1 Chlorophyll content

Chlorophyll is a green pigment, responsible for capturing light during photosynthesis (Grimm, 2001; Jetz et al., 2016). The following indices known for the estimation of chlorophyll content were observed. Clevers and Gitelson (2013) presented the red-edge chlorophyll index ($CI_{red-edge}$) (Eq. 2.4) and the green chlorophyll index (CI_{green}) (Eq. 2.5) along with testing the results for canopy chlorophyll and nitrogen content. Major advantages are their linearity with chlorophyll content and the absence of a saturation effect.

$$CI_{red-edge} = \frac{\rho_{773-793}}{\rho_{698-713}} - 1 \quad (2.4)$$

$$CI_{green} = \frac{\rho_{773-793}}{\rho_{543-578}} - 1 \quad (2.5)$$

In 2007, Dash and Curran presented a vegetation index, designed for the Medium Resolution Imaging Spectrometer (MERIS), on the Envisat satellite. MERIS terrestrial chlorophyll index ($MTCI$) (Eq. 2.6) is strongly related to chlorophyll content at different spatial scales. As heritage of MERIS, this $MTCI$ is the basis of one of the products of Ocean and Land Color Instrument (OLCI) Sentinel-3, called the OLCI Terrestrial Chlorophyll Index ($OTCI$) (Knaeps et al., 2012; Vuolo et al., 2012; Clevers and Gitelson, 2013).

$$MTCI = \frac{\rho_{733-748} - \rho_{698-713}}{\rho_{698-713} + \rho_{650-680}} \quad (2.6)$$

Clevers and Gitelson (2013) observed best results in estimating canopy chlorophyll and nitrogen content using $CI_{red-edge}$, CI_{green} and $MTCI$. $NDVI$ -type of indices, namely normalized difference red-edge ($NDRE1$, Eq. 2.7 and $NDRE2$, Eq. 2.8) were tested as well.

$$NDRE1 = \frac{\rho_{733-748} - \rho_{698-713}}{\rho_{733-748} + \rho_{698-713}} \quad (2.7)$$

$$NDRE2 = \frac{\rho_{773-793} - \rho_{698-713}}{\rho_{773-793} + \rho_{698-713}} \quad (2.8)$$

The red-edge position (REP) (Eq. 2.9) has often been used as an estimate for chlorophyll content. With the limited number of Sentinel-2 red-edge bands, the REP can be derived easily (Clevers and Gitelson, 2013).

$$REP = 705 + 35 \cdot \frac{\frac{\rho_{650-680} + \rho_{773-793}}{2} - \rho_{698-713}}{\rho_{733-748} - \rho_{698-713}} \quad (2.9)$$

Depth of the chlorophyll absorption 670nm relative to 550nm and 700nm is expressed in the modified chlorophyll absorption ratio index (*MCARI*) (Eq. 2.10) (Daughtry et al., 2000). *MCARI* is known to be sensitive to background reflectance properties and is difficult to interpret at low LAI. It is further sensitive to LAI, chlorophyll, LAI-chlorophyll interaction and background reflectance.

$$MCARI = [(\rho_{698-713} - \rho_{650-680}) - 0.2 \cdot (\rho_{698-713} - \rho_{543-578})] \cdot \frac{\rho_{698-713}}{\rho_{650-680}} \quad (2.10)$$

To compensate for the variations of reflectance characteristics of background materials (soil and non-photosynthetic components), which is mostly the case at low chlorophyll concentrations, and therefore to increase this sensitivity at low chlorophyll values, the transformed chlorophyll absorption ratio index (*TCARI*) (Eq. 2.11) was presented (Haboudane et al., 2002; Wu et al., 2008).

$$TCARI = 3 \cdot ((\rho_{698-713} - \rho_{650-680}) - 0.2 \cdot (\rho_{698-713} - \rho_{543-578})) \cdot \frac{\rho_{698-713}}{\rho_{650-680}} \quad (2.11)$$

In order to solve the problem of sensitivity to underlying soil in canopy reflectance properties, Daughtry et al. (2000) combined *MCARI* with a soil line vegetation index like the optimized soil-adjusted vegetation index (*OSAVI*) (Eq.2.12, Eq.2.13). This can also be done with the *TCARI* (Eq. 2.14) (Haboudane et al., 2002; Wu et al., 2008), and proved to achieve accurate estimations of chlorophyll content (Kooistra and Clevers, 2016; Jay et al., 2017). In order to achieve a positive correlation with chlorophyll content, the *TCARI/OSAVI* ratio was inverted.

$$OSAVI = (1 + 0.16) \cdot \frac{\rho_{785-900} - \rho_{650-680}}{\rho_{785-900} + \rho_{650-680} + 0.16} \quad (2.12)$$

$$\frac{MCARI}{OSAVI} = \frac{[(\rho_{698-713} - \rho_{650-680}) - 0.2 \cdot (\rho_{698-713} - \rho_{543-578})] \cdot \frac{\rho_{698-713}}{\rho_{650-680}}}{(1 + 0.16) \cdot \frac{\rho_{785-900} - \rho_{650-680}}{\rho_{785-900} + \rho_{650-680} + 0.16}} \quad (2.13)$$

$$\frac{TCARI}{OSAVI} = \frac{3 \cdot ((\rho_{698-713} - \rho_{650-680}) - 0.2 \cdot (\rho_{698-713} - \rho_{543-578})) \cdot \frac{\rho_{698-713}}{\rho_{650-680}}}{(1 + 0.16) \cdot \frac{\rho_{785-900} - \rho_{650-680}}{\rho_{785-900} + \rho_{650-680} + 0.16}} \cdot (-1) \quad (2.14)$$

2.4.1.2 Anthocyanin content

Leaf senescence results in several observable effects. Chlorophyll decrease and anthocyanin increase take place long before visible yellowing (Dhindsa, Plumb-Dhindsa, and Thorpe, 1981). Anthocyanin content can be derived using Anthocyanin Reflectance Index 1 and 2 (*ARI1* and

$ARI2$) (Eq. 2.15 and 2.16), while Gitelson, Chivkunova and Merzlyak (2009) also referred to $ARI2$ as modified Anthocyanin Reflectance Index ($mARI$).

$$ARI1 = \frac{1}{\rho_{543-578}} - \frac{1}{\rho_{698-713}} \quad (2.15)$$

$$ARI2 = \frac{\rho_{785-900}}{\rho_{458-523}} - \frac{\rho_{785-900}}{\rho_{543-578}} = mARI \quad (2.16)$$

The Red Green Ratio (RGR) (Eq. 2.17) (Sims and Gamon, 2002) is a broad band index also sensitive to red pigments but readily calculable from all multispectral sensors. Hence, it may be regarded as a (less sensitive) substitute where wavelengths for ARI are not available (Hill, 2013).

$$RGR = \frac{\rho_{650-680}}{\rho_{543-578}} \quad (2.17)$$

2.4.1.3 Carotenoid content

Another pigment to be detected in the canopy is carotenoid. Carotenoids are orange and yellow pigments involved as antioxidants in the xanthophyll cycle for avoiding damage under stress conditions (Havaux, 2014; Jetz et al., 2016). The Carotenoid Reflectance Index 1 ($CRI1$) (Eq. 2.18) is sensitive to yellow pigments (Hill, 2013).

$$CRI1 = \frac{1}{\rho_{458-523}} - \frac{1}{\rho_{543-578}} \quad (2.18)$$

The structure-insensitive pigment index ($SIPI$) on the other hand, is linked to the carotenoid-chlorophyll ratio (Penuelas, Baret, and Filella, 1995; Sims and Gamon, 2002; Merzlyak, Solovchenko, and Gitelson, 2003). $SIPI$ includes channel 1, which means, it can only be calculated from Sentinel-2 data in 60 m spatial resolution. The Plant Senescence Reflectance Index ($PSRI$) (Eq. 2.19) utilizes narrow bands within the visible (VIS) and NIR spectral region (Hill, 2013). It can be related to the $SIPI$, while maintaining 20 m resolution.

$$PSRI = \frac{\rho_{650-680} - \rho_{543-578}}{\rho_{733-748}} \cdot (-1) \quad (2.19)$$

2.4.1.4 Water content

This trait describes the total amount of water in a leaf or canopy relative to its dry mass (Jetz et al., 2016). Changes in water content can be related to drought stress. The Normalized Difference Infrared Index ($NDII$) (Eq. 2.20) utilizes the 1610 nm SWIR1 band (band 11, see Table 2.2) available from Sentinel-2 and is comparable to the Normalized Difference Water Index ($NDWI$), which is not available using Sentinel-2 bands, while it is a little more robust in dryland environments

than the NDWI (Hill, 2013). Moisture Stress Index (*MSI*) (Eq. 2.21) can be used to detect water stress at the canopy level, involving the NIR and SWIR region of the spectrum (Dotzler et al., 2015). However, when inverted, index values increase with larger moisture contents, as shown by Dotzler et al. (2015).

$$NDII = \frac{\rho_{785-900} - \rho_{1565-1655}}{\rho_{785-900} + \rho_{1565-1655}} \quad (2.20)$$

$$MSI = \frac{\rho_{1360-1390}}{\rho_{785-900}} \cdot (-1) \quad (2.21)$$

TABLE 2.4: Tested vegetation indices and their corresponding type of trait, namely chlorophyll (green), anthocyanin (red), carotenoid (orange) and water content (blue).

Trait	Indices		
Chlorophyll	<i>CIred - edge</i> (2.4)	<i>CIgreen</i> (2.5)	<i>MTCI</i> (2.6)
	<i>NDRE1</i> (2.7)	<i>NDRE2</i> (2.8)	<i>REP</i> (2.9)
	<i>MCARI/OSAVI</i> (2.13)	<i>TCARI/OSAVI</i> (2.14)	
Anthocyanin	<i>ARI1</i> (2.15)	<i>ARI2</i> (2.16)	<i>RGR</i> (2.17)
Carotenoid	<i>CRI1</i> (2.18)	<i>PSRI</i> (2.19)	
Water content	<i>NDII</i> (2.20)	<i>MSI</i> (2.21)	

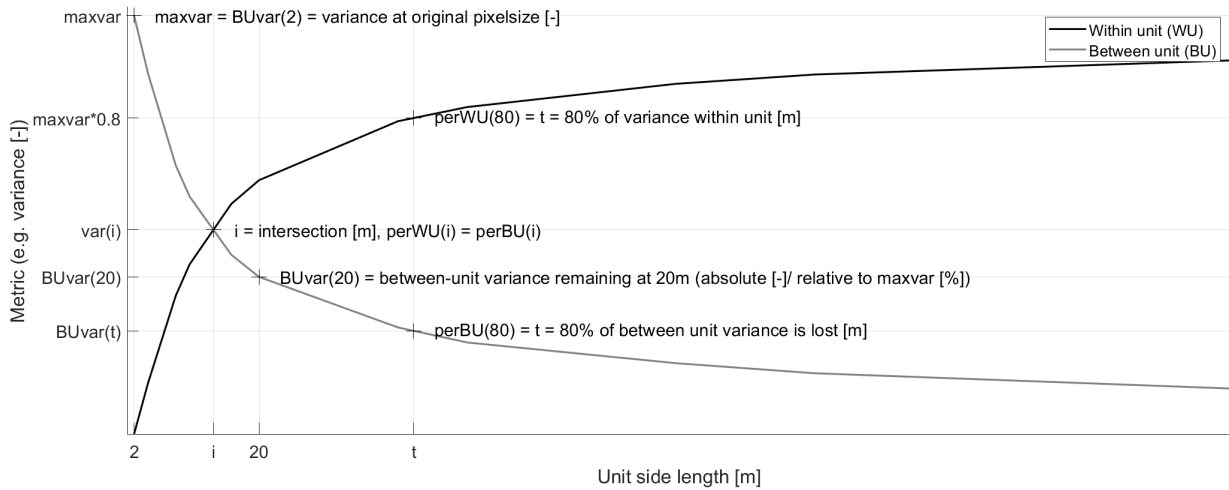


FIGURE 2.4: Example of one-dimensional scale analysis calculating within- and between-unit variance, for increasing unit side length. Calculated variables were the intersection of within- and between-unit variance (i), between-unit variance at unit size 20 m ($BUvar(20)$) and the unit side length at which 80% of the variance is explained within the units (t).

2.4.2 Testing indices

We tested fifteen VIs (see Table 2.4) to find those suitable for both APEX and Sentinel-2 scenes, whereas eight describe chlorophyll content and three are related to anthocyanin content. Furthermore, carotenoid and water content are described by two indices each. The aim of this analysis is to select indices that reveal similar characteristics in scale analysis for both scenes and sensors. The highest scoring index per trait was used for further calculation of functional diversity metrics.

2.4.2.1 One-dimensional scale analysis

The indices that can be used for the calculation of functional diversity metrics were compared in a scale analysis. This was analyzed in one dimension, calculating within- and between-unit variance (Violle et al., 2012). With increasing unit size, within-unit (WU) variance increases, and between-unit (BU) variance decreases (see Figure 2.4). For each calculated index, the intersection of within- and between-unit variance (i) was detected. At this unit size, the same extent of trait dissimilarity emerges from intra-unit trait variability than between-unit differences (Bello et al., 2011). The higher this value, the more information can still be derived at lower spatial resolution. Furthermore, the pixel size where 20% of the initial between-unit variance ($maxvar$, variance at 2 m resolution) is still measurable (t), was detected. Lastly, the between-unit variance at a unit size of 20 m ($BUvar(20)$) was measured. The vegetation indices should deliver comparably high values of i , $BUvar(20)$, and t , as well reasonable values when comparing the two seasons and when comparing with other indices describing the same functional trait (see Section 3.1.1).

2.4.2.2 Comparing sensors

The same calculated index for the resampled APEX dataset and the Sentinel-2 dataset should perform similarly. To test this hypothesis, different statistics were calculated from index values and compared between the sensors for both summer and fall scenes.

These statistics comprise (i) the difference of the mean values, (ii) coefficient of variation (cv), and (iii) the mean proportion of outliers. First, the difference of the mean values between two seasonal scenes indicates their similarity on an absolute scale. Second, the cv is defined as the ratio of standard deviation and mean. It permits comparison free from scale effects (Brown, 1998). The difference in cv throughout the sensors shows the difference in variability of the calculated index through sensors.

The higher this difference value, the larger the difference between the sensors in their variance behavior. Furthermore, average cv indicates the total variability of the results. Lastly, the mean proportion of outliers was calculated. Outliers were defined as values more than three scaled median absolute deviations away from the median (Leys et al., 2013). The number of outliers was divided by the number of pixels. The smaller the proportion of outliers per scene, the more meaningful is the calculated index.

2.4.2.3 Correlation of calculated indices

To test the correlation between the calculated indices, the correlation was calculated between all the datasets. The mean correlation of the two seasons and sensors was analyzed afterwards. High correlation was expected within traits, while low correlation was expected between traits. VIs that show relatively high correlation with other indices describing the same functional trait seem to show a more meaningful and consistent result.

2.5 Functional diversity

2.5.1 Multi-dimensional scale analysis

A scale analysis was computed to derive intra- and inter-unit properties. According to de Bello et al. (2011) intra-unit variability can be defined as within-unit diversity or the extent of trait dissimilarity because of intra-unit trait variability. Correspondingly, inter-unit variability can be defined as between-unit functional diversity or the extent of trait dissimilarity in a community because of the discrepancy between-units. The scale analysis was performed using a function $y = f(x)$. In this case, it was performed one-dimensionally (calculating intra and inter-unit variance), as well as four-dimensionally (calculating intra and inter-unit richness and divergence). In the multi-dimensional case, the function was adapted to $y = f(x_1, x_2, \dots, x_{dim})$, with dim being the number of dimensions. Accordingly, four instead of one trait maps were used for the calculation. Each pixel therefore was assigned four values. The trait map was aggregated to spatial

$y = f(x)$

$U1_1$	$U1_2$	$U2_1$	$U2_2$
$U1_{..}$	$U1_{ppu}$	$U2_{..}$	$U2_{ppu}$
$U3_1$	$U3_2$	Un_1	Un_2
$U3_{..}$	$U3_{ppu}$	$Un_{..}$	Un_{ppu}

Example variance $y = \text{var}(x)$

1	1	2	3
2	1	2	3
2	2	2	4
2	3	3	4

1. Between-unit (BU)

$\bar{U1} = \frac{1}{ppu} \sum_{i=1}^{ppu} U1_i$	$\bar{U2} = \frac{1}{ppu} \sum_{i=1}^{ppu} U2_i$
$\bar{U3} = \frac{1}{ppu} \sum_{i=1}^{ppu} U3_i$	$\bar{Un} = \frac{1}{ppu} \sum_{i=1}^{ppu} Un_i$

$BU = f(\bar{U1}, \dots, \bar{Un})$

1.25	2.5
2.25	3.25

BUvar = var(1.25, ..., 3.25) = 0.6823

2. Within-unit (WU)

$U1 = f(U1_1, \dots, U1_{ppu})$	$U2 = f(U2_1, \dots, U2_{ppu})$
$U3 = f(U3_1, \dots, U3_{ppu})$	$Un = f(Un_1, \dots, Un_{ppu})$

$WU = \frac{1}{n} \sum_{i=1}^n U_i$

0.25	0.33
0.25	0.917

WUvar = mean(0.25, ..., 0.917) = 0.4367

FIGURE 2.5: Example of the calculation involved in a one-dimensional scale analysis.

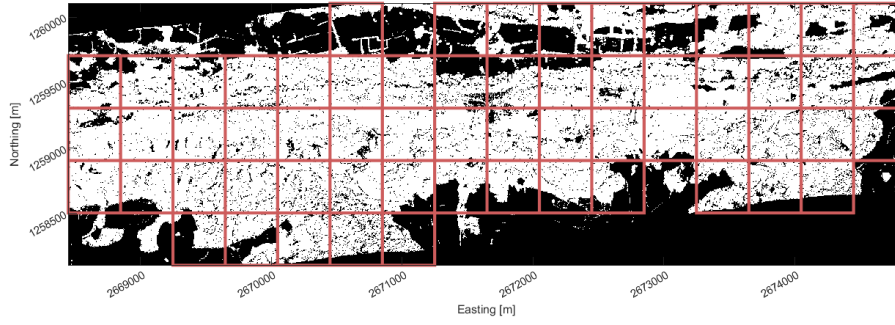


FIGURE 2.6: Units considered for the scale analysis at a unit size of $400 \cdot 400$ m at the research site. At this unit size, the condition to be taken into consideration is that 20% of the pixels within the unit are classified as forest (ppu).

units within the study area of $2 \cdot 6.4$ km. Unit size was increased stepwise while maintaining the quadratic shape of units (see Figure 2.6). The smallest unit size was $4 \cdot 4$ m, leading to 449'539 units within the extent n = number of units and the largest unit size was $800 \cdot 800$ m, leading to 66 units within the extent. For every step, calculated traits were aggregated by taking the average of the pixels within the units. Between-unit and within-unit variance, richness, and divergence were calculated at each unit size (Wiens, 1989; Scholtz et al., 2018). To determine the extent of trait dissimilarity because of the difference between-units of a specific size (BU), pixel values U_{ppu} within each unit were combined to a new value (\bar{U}) using the mean calculation (Eq. 2.22), with ppu being the number of pixels per unit. The resulting n values were calculated using the given function (Eq. 2.23).

$$\bar{U} = \frac{1}{ppu} \sum_{i=1}^{ppu} U_i \quad (2.22)$$

$$BU = f(\bar{U}_1, \dots, \bar{U}_n) \quad (2.23)$$

To determine the extent of trait dissimilarity because of within-unit trait variability at a specific unit size (WU), the trait variability was firstly calculated within every unit of interest (Eq. 2.24). The resulting n values were then averaged. (Eq. 2.25).

$$U = f(U_1, \dots, U_{ppu}) \quad (2.24)$$

$$WU = \frac{1}{n} \sum_{i=1}^n U_i \quad (2.25)$$

An example of the calculation in the one-dimensional case using variance (Eq. 2.26) is illustrated in Figure 2.5.

$$var(x) = \frac{\sum_{i=1}^n (x_i - \bar{x})^2}{n - 1} \quad (2.26)$$

TABLE 2.5: Number of valuable pixels per unit (*ppu*) and number of units considered for every unit size within the scale analysis. For divergence, where euclidean distance is calculated which required too much computation effort. Therefore, point clouds larger than 45'000 pixels were limited to not exceed this number.

Area	Unit side length	Percentage of valid pixels	2 m pixel			20 m pixel		
			Unit side length	Units considered	Pixel number per Unit	Unit side length	Units considered	Pixel number per Unit
16ha	400 m	20%	200p	66	8'000	20p	65	80
4ha	200 m	25%	100p	242	2'500	10p	237	25
1ha	100 m	33%	50p	879	825	5p	862	9
64a	80 m	33%	40p	1'371	528	4p	1'326	6
25a	50 m	50%	25p	3'258	313			
16a	40 m	50%	20p	5'043	200	2p	5'072	2
4a	20 m	75%	10p	17'852	75	1p	19'118	1
256 m ²	16 m	75%	8p	27'942	48			
100 m ²	10 m	75%	5p	71'786	19			
64 m ²	8 m	75%	4p	113'502	12			
16 m ²	4 m	75%	2p	466'986	3			
4 m ²	2 m	100%	1p	1'902'937	1			

Due to masking, units contain different numbers of valid pixels. Therefore, only units with a valuable amount (depending on unit size) of valid pixels were used in the calculation, while making sure that the same number of pixels per unit (*ppu*) was considered. The threshold of valid pixels per unit was set low (20%) at a large unit size, because of the need for a reasonable number of units and a large number of pixels per unit. At a smaller unit size the minimum percentage of valid pixels per unit increased, due to an increased number of units and a decreasing number of pixels per unit (see Figure 2.6, Table 2.5).

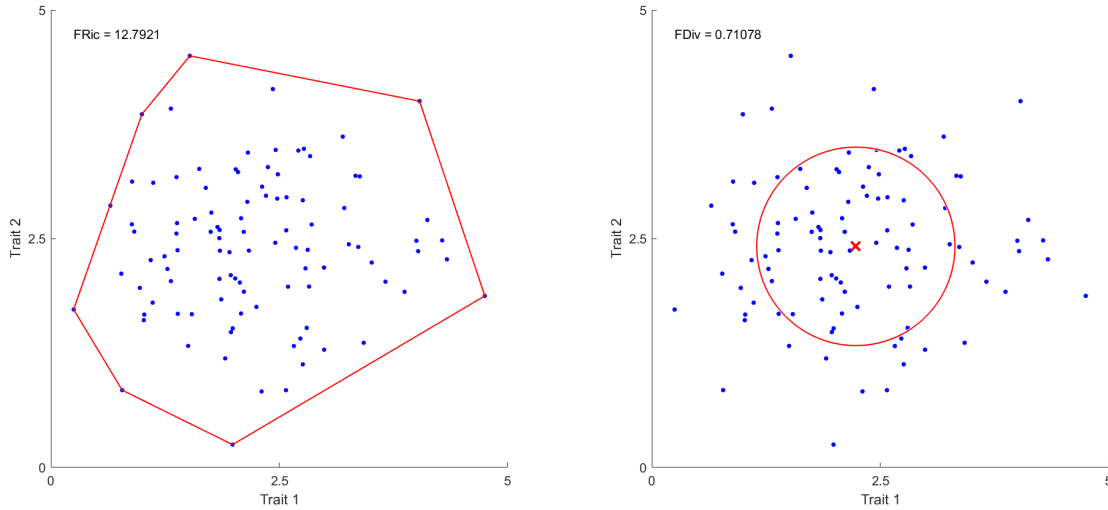


FIGURE 2.7: Functional richness (left) and divergence (right) based on an example unit with 100 pixels and an example data range of 0-5.

2.5.2 Functional diversity metrics

As functional diversity metrics, functional richness and divergence were calculated to compare the scaling effects on functional diversity metrics, according to Schneider et al. (2017). A graphic representation of the work-flow from VI data to physiological diversity metrics is shown in Figure A.4. Functional evenness was not considered here, as both functional divergence and evenness sufficiently describe how sample points are distributed within the community niche. Both, functional divergence and evenness, behave similarly according to Schneider et al. (2017), which is why the more complex functional evenness was not taken into consideration due to long computation times of the minimum spanning tree (Villéger, Mason, and Mouillot, 2008; Schneider et al., 2017). This leaves two functional diversity metrics, of which one is a measure of niche extent and the other one of distribution. Both vary independently from each other (Mason et al., 2005).

Functional richness describes the extent of the functional space occupied by a species, individuals or pixels (see Figure 2.7). It was calculated by mapping pixels of a certain neighborhood in a functional space, whose axes are defined by the functional traits (Villéger, Mason, and Mouillot, 2008; Schneider et al., 2017). Richness is the volume of the convex hull of the mapped pixels in a multi-dimensional trait space (“convhull” in MATLAB). Functional divergence is a measure of the distribution of values in space. It shows high values if all values are equally far away from the common center (Villéger, Mason, and Mouillot, 2008; Schneider et al., 2017). It was calculated using the number of pixels mapped in the functional space (S), the euclidean distance between every pixel i and the center of gravity (dG_i) and the mean distance of all pixels to the center of gravity (dG) (Eq. 2.27 – 2.28).

$$\Delta|d| = \sum_{i=1}^S \frac{1}{S} \cdot |dG_i - \overline{dG}| \quad (2.27)$$

TABLE 2.6: Unit size (diameter and area) of circular units, in meter and pixels, comparing data with 2 m pixels and 20 m pixels. The unit area includes one hundred times more pixels compared to 20 m if the pixels are 2 m in size. Furthermore, equivalent square side length, the side length of a square unit with the identical area, is given for each of the circular units.

unit diameter [m]	20	40	60	120	200
unit area [m ²]	314.2	1256.6	2827.4	11310	31416
unit area in 2 m pixel [ppu]	78.54	314.2	706.9	2827.4	7854.0
unit area in 20 m pixel [ppu]	0.785	3.142	7.068	28.27	78.54
equivalent square side length [m]	17.72	35.45	53.17	106.4	177.3

$$FDiv = \frac{\overline{dG}}{\Delta|d| + \overline{dG}} \quad (2.28)$$

Functional richness and functional divergence were used in the scale analysis and their behavior through scale was analyzed. Furthermore, diversity maps were calculated using different sizes (20 m, 40 m, 60 m, ...) of neighborhoods to compare the results of different underlying datasets, namely the spectrally resampled 2 m APEX dataset, the spectrally and spatially resampled 20 m APEX datasets and the 20 m Sentinel-2 dataset. A neighborhood of 10 m on a 2 m dataset creates a circular shape with a radius of 5 m, which are 2.5 pixels. This neighborhood therefore has a size of 5 · 5 pixels. By maintaining the same area as the units from the scale analysis, diameters were transformed to the side length l of a square with the same area as the circle with diameter d (see Table 2.6). Their relationship is expressed as $l = \frac{\sqrt{\pi \cdot d}}{2}$. At 20 m the neighborhood has a radius of 5 pixels and has the same area as a unit with a unit side length of 17.7 m (see Figure A.5) and 60 m, which has the same area as a unit with a side length of 53.2 m, leads to 15 pixel radius for the neighborhood. At the 20 m dataset, the calculation takes place based on unitsizes larger than 60 m.

3 Results

3.1 Choice of vegetation indices

We tested fifteen indices to find those suitable for both sensors (see Table 2.4). These indices correspond to four functional traits, namely chlorophyll, anthocyanin, carotenoid, and water content. For each trait, the highest scoring index was chosen to derive functional diversity metrics.

3.1.1 One-dimensional scale analysis

The indices and their corresponding trait were tested in a one-dimensional scale analysis, which was performed on the spectrally resampled 2 m APEX (A2) dataset. Resulting values are shown in Table 3.1 and explained in Figure 2.4. The first analyzed value is the intersection (i), at which unit size variance is equally explained within-unit and between-units. The highest values of i were found for chlorophyll content (12 m – 18 m), followed by carotenoid content, anthocyanin and water content (7 m – 13 m). This finding leads to the conclusion that water content shows variation at a smaller scale than chlorophyll content. In comparison, a random model was set-up, where underlying normally distributed fictive trait data was generated randomly. The resulting intersection i was calculated to be 3.5 m. All of the traits showed stronger results and reaction to auto-correlation, except CRI1 (see A.6). Furthermore, the between-unit variance remaining at a unit size of 20 m, the size of Sentinel-2 pixels, ($BUvar(20)$) was calculated relative to 2 m unit size and in absolute values. Those values vary between 12% – 30% and 0.01 – 0.05 respectively (see Table 3.1). Lastly, the unit size where 80% of the variance is explained within-unit and no more between-unit (t) ranges between 15 m – 75 m. On the random model, 80% of the variance was explained at 6.1 m.

Within the chlorophyll describing indices, highest values of i were achieved by $CI_{red-edge}$, CI_{green} , $NDRE2$ and $TCARI/OSAVI$, while CI_{green} shows the lowest difference between seasons. $MTCI$ showed lowest results, especially in fall, which was the only result of a chlorophyll describing index smaller than 10 m. At 20 m unit size, most relative variance was explained by $TCARI/OSAVI$ in fall. Lowest values were achieved by $MTCI$ and $NDRE1$, which on the other hand achieved highest absolute values. Absolute variance at 20 m was found to be higher in fall, except for $MCARI/OSAVI$. Highest values for t were achieved by $TCARI/OSAVI$, $CI_{red-edge}$ and $NDRE2$, of which the latter two happen to consist of similar bands, followed by CI_{green} . All of them achieved $t > 60$ m, while the rest achieved results of $t < 50$ m. Weakest results for t were achieved by $MTCI$ and $MCARI/OSAVI$. Regarding anthocyanin, best results of i were achieved

TABLE 3.1: Tested indices and their corresponding trait in the one-dimensional scale analysis. The corresponding traits are chlorophyll (green), anthocyanin (red), carotenoid (orange) and water content (blue). The first analyzed values are the intersection (i), at which unit size variance is equally explained within-unit and between-units. Secondly, the between-unit variance remaining at a unit size of 20 m ($BUvar(20)$) is calculated relative to 2 m unit size and absolute values. Lastly, the unit size where 80% of the variance is explained within-unit and no more between-unit (t) was calculated for each index.

Index	i [m]		BUvar(20) [%]		BUvar(20) [-]		t [m]	
	July	September	July	September	July	September	July	September
<i>CIred – edge</i>	18.4	16.7	20.65	23.44	0.0315	0.0377	71.5	65.9
<i>CIgreen</i>	17.5	18.3	19.53	26.44	0.0334	0.0388	60.1	65.7
<i>MTCI</i>	15.5	9.6	29.05	13.42	0.0226	0.0359	43.7	33.9
<i>NDRE1</i>	14.2	11.9	16.45	14.60	0.0320	0.0420	48.3	37.8
<i>NDRE2</i>	17.8	16.2	20.30	23.50	0.0295	0.0377	72.3	64.8
<i>REP</i>	15.7	14.1	32.65	24.70	0.0275	0.0317	46.6	42.8
<i>MCARI/OSAVI</i>	13.7	11.9	20.08	16.24	0.0423	0.0327	36.3	33.6
<i>TCARI/OSAVI</i>	15.1	21.5	21.84	35.42	0.0250	0.0260	63.7	90.9
<i>ARI1</i>	10.4	15.1	24.36	35.18	0.0141	0.0321	25.6	37.1
<i>ARI2</i>	13.4	17.2	27.09	38.89	0.0240	0.0324	39.0	40.6
<i>RGR</i>	13.6	12.0	17.20	16.67	0.0331	0.0348	42.9	34.6
<i>CRI1</i>	NaN	NaN	81.39	88.08	0.0104	0.0227	234.0	243.7
<i>PSRI1</i>	16.1	17.5	24.85	31.47	0.0276	0.0326	69.7	76.2
<i>NDII</i>	13.0	12.3	20.92	21.82	0.0182	0.0382	43.5	34.9
<i>MSI</i>	7.6	7.4	13.07	12.04	0.0144	0.0334	20.9	17.3

TABLE 3.2: Correlation of the calculated indices on the A20 and S20 datasets (different sensors). The corresponding traits are chlorophyll (green), anthocyanin (red), carotenoid (orange) and water content (blue).

Index	<i>CIred – edge</i>	<i>CIgreen</i>	<i>MTCI</i>	<i>NDRE1</i>	<i>NDRE2</i>	<i>REP</i>	<i>MCARI/OSAVI</i>	<i>TCARI/OSAVI</i>
Summer	0.36	0.26	0.22	0.27	0.35	0.27	0.22	0.14
Fall	0.39	0.18	0.23	0.28	0.41	0.29	0.21	0.19
Index	<i>ARI1</i>	<i>ARI2</i>	<i>RGR</i>	<i>CRI1</i>	<i>PSRI</i>	<i>NDII</i>	<i>MSI</i>	
Summer	0.003	0.01	0.15	0.047	0.14	0.21	0.053	
Fall	0.034	0.036	0.16	0.07	0.11	0.32	0.14	

by *ARI2*, followed by *RGR* and *ARI1*. Most between variance at 20 m was explained by *RGR* in absolute values, even if this index achieved weakest results for relative values. Considering t , highest results were achieved by *ARI2*, while *RGR* shows a high value in summer, but a low value in fall.

CRI1 performed weakly (for more information see Figure A.6), from which it can be concluded that this index does not work for the APEX properties (for more information see Figure A.7). This is also visible in the correlation of A20 and S20 datasets (see section 3.1.2). *PSRI* achieved acceptable results, when comparing to the other functional traits. There was a slightly higher variance, i , and t in fall for this carotenoid describing index. Water content seems to show variation at a smaller scale, compared to other described traits. Both indices seemed to achieve stable results in the scale analysis. They show higher absolute variance at 20 m in fall and higher i and t in summer. However, *NDII* shows higher values for i , relative $BUvar(20)$ and t than *MSI*.

3.1.2 Comparing indices of rescaled APEX and Sentinel-2 datasets

Tested indices and their corresponding trait on 20 m datasets (rescaled APEX A20 and Sentinel-2 S20) were compared graphically in boxplots (see Figure 3.1) and using calculated values (see Table A.3). *CIred – edge*, *NDRE1* and *NDRE2* show a larger difference regarding seasons in the S20 datasets, where the S20 fall scene showed lower values, than the other three. The inverted case can be found for *CRI1* and *ARI2*, where the fall scene for Sentinel-2 show much higher values than the others. *MTCI* and *CRI1* show large differences of mean values, as well as averaged *cv*. *MTCI* overall shows much lower values in Sentinel-2 than the resampled APEX scenes. Furthermore, chlorophyll content shows lower values at fall scenes for every chlorophyll describing index, except *TCARI/OSAVI*, which is the only one that has produced higher values in fall. *CIgreen* shows slightly higher values for Sentinel-2, however seems to show a balanced result. Results for *REP* show one scene (S20 summer) being much higher than the others. *MCARI/OSAVI* produced comparably low values, however showing a quite balanced result. Difference in *cv* turned out to be high for *CIred – edge*, *MTCI*, *REP* and *CRI1*. The proportion of outliers is rather high for *TCARI/OSAVI*, *NDRE1*, *NDRE2*, *CRI1*, *ARI1* and *NDII*. Regarding correlation of A20 and S20 datasets, as shown in Table 3.2, *MCARI/OSAVI* and *TCARI/OSAVI* achieved weakest results, followed by *MTCI* and *CIgreen*. Relatively good results were achieved by *REP*, *NDRE1* and *NDRE2*. The index describing chlorophyll with the most correlation between APEX and Sentinel-2 was *CIred – edge*.

Considering anthocyanin indices, *ARI2* seems to show weak results, as the values in fall seem lower for A20, but higher for S20 scenes. On the other hand, *ARI1* and *RGR* seem to show reasonable results, with anthocyanin values being higher in fall. The correlation values for the datasets were highest for *RGR* and lowest for *ARI1* and *ARI2*. Regarding *ARI1* and *ARI2*, correlation showed large difference between seasons. *PSRI* values seem reasonable and higher in summer than in fall on both sensors. Correlation of dataset for *PSRI* is rather low, as shown in Table 3.2. Indices describing water content show similar results with higher values in summer, compared to fall. *NDII* shows slightly higher values on the S20 scenes. Differences between seasons are much higher on A20 scenes, compared to S20 for *MSI*. In addition to the better performance of *NDII* in one-dimensional scale analysis, correlation between datasets was higher for *NDII* than *MSI*. Regarding water content, correlation of sensors is higher in fall. This could be explained by the smaller difference in time between the mission dates.

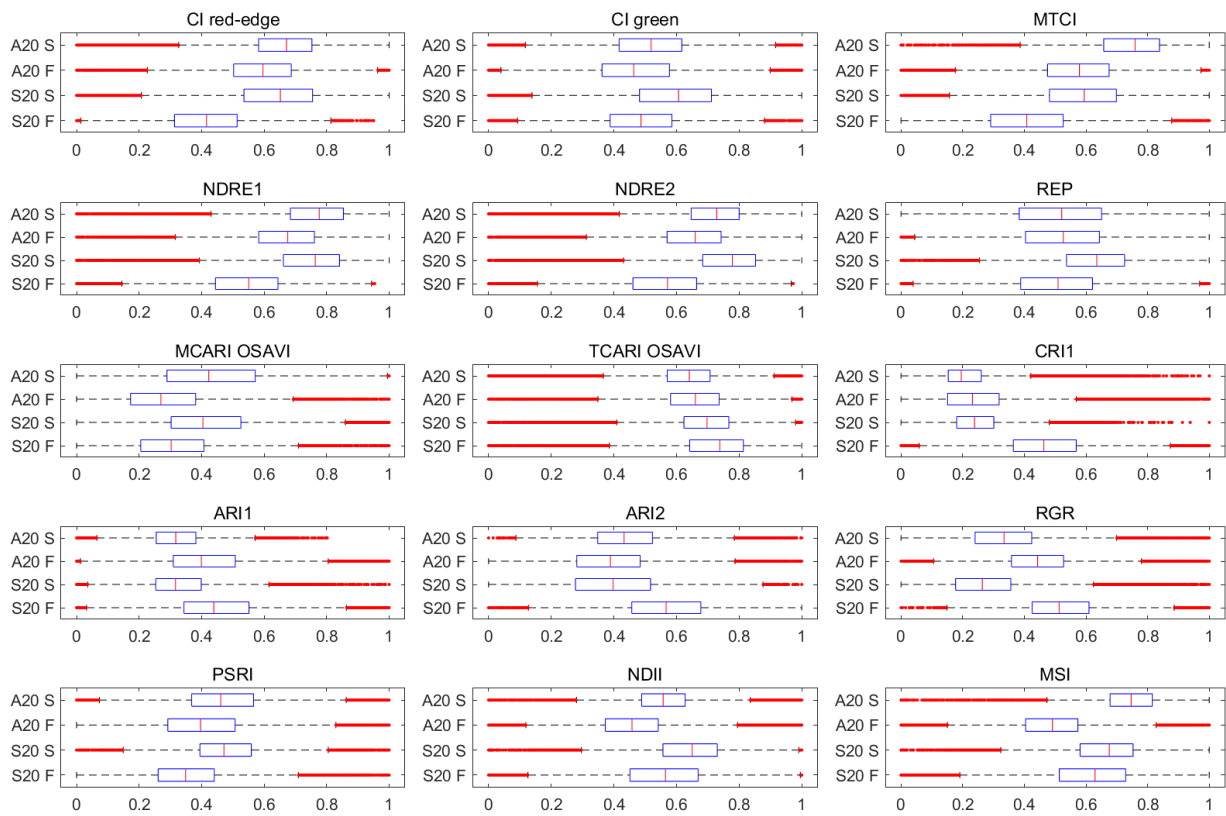


FIGURE 3.1: Scatterplots of the tested indices, calculated based on A20 and S20 datasets for each sensor in both summer (S) and fall (F). In each plot, all four datasets are shown for the corresponding index, in order A20 summer, A20 fall and S20 summer and S20 fall (from top to bottom).

3.1.3 Correlation of calculated indices

Table 3.3 shows correlation averaged over both seasons and sensors. The data averaged over the seasons summer and fall per sensor can be found in the Appendix (see Table A.1 and A.2). Considering the chlorophyll describing indices, *REP*, *MCARI/OSAVI* and *TCARI/OSAVI* correlate rather weak compared to the others. While *REP* shows similar results for both sensors, *MCARI/OSAVI* and especially *TCARI/OSAVI* correlate much stronger with other indices describing chlorophyll in the S20 scenes. This leads to the conclusion that *MCARI/OSAVI* and *TCARI/OSAVI* ratios show weak results on the selected data. Especially *TCARI/OSAVI* does not seem to work properly for the characteristics of the APEX datasets. Indices describing anthocyanin show high variation, which can be explained with the relatively low anthocyanin values in the ecosystem. The same can be observed at correlation values of *CRI1* and *PSRI*, which can be explained by *CRI1* not showing reasonable values. The indices describing water content, on the other hand, show high positive correlation, and seem to both show reasonable results.

TABLE 3.3: Correlation of calculated indices with each other based on 20 m datasets, averaged over sensors (A20, S20) and seasons (summer, fall). The corresponding traits are chlorophyll (green), anthocyanin (red), carotenoid (orange) and water content (blue). $r^2 = 0$ means no correlation, while $r^2 = 1$ means perfect correlation.

Index	<i>CIred-edge</i>	<i>CIgreen</i>	<i>MTCI</i>	<i>NDRE1</i>	<i>NDRE2</i>	<i>REP</i>	<i>MCARI/OSAVI</i>	<i>TCARI/OSAVI</i>	<i>ARI1</i>	<i>ARI2</i>	<i>RGR</i>	<i>CRI1</i>	<i>PSRI</i>	<i>NDII</i>	<i>MSI</i>
<i>CIred-edge</i>	1	0.83	0.84	0.93	0.99	0.67	0.19	0.70	0.33	0.52	-0.51	0.28	-0.20	0.59	0.53
<i>CIgreen</i>	0.83	1	0.62	0.79	0.83	0.46	0.41	0.75	0.55	0.51	-0.32	0.29	-0.53	0.29	0.24
<i>MTCI</i>	0.84	0.62	1	0.86	0.83	0.46	0.11	0.48	0.02	0.28	-0.37	-0.04	-0.18	0.52	0.55
<i>NDRE1</i>	0.93	0.79	0.86	1	0.94	0.38	0.33	0.64	0.22	0.53	-0.63	0.21	-0.10	0.54	0.53
<i>NDRE2</i>	0.99	0.83	0.83	0.94	1	0.66	0.19	0.71	0.34	0.52	-0.53	0.29	-0.19	0.59	0.54
<i>REP</i>	0.67	0.46	0.46	0.38	0.66	1	-0.31	0.50	0.35	0.19	0.02	0.23	-0.28	0.42	0.30
<i>MCARI/OSAVI</i>	0.19	0.41	0.11	0.33	0.19	-0.31	1	-0.04	-0.18	0.40	-0.57	-0.11	0.10	0.01	0.10
<i>TCARI/OSAVI</i>	0.70	0.75	0.48	0.64	0.71	0.50	-0.04	1	0.78	0.36	-0.24	0.54	-0.39	0.36	0.28
<i>ARI1</i>	0.33	0.55	0.02	0.22	0.34	0.35	-0.18	0.78	1	0.17	0.10	0.63	-0.51	0.07	-0.08
<i>ARI2</i>	0.52	0.51	0.28	0.53	0.52	0.19	0.40	0.36	0.17	1	-0.56	0.68	0.06	0.36	0.32
<i>RGR2</i>	-0.51	-0.32	-0.37	-0.63	-0.53	0.02	-0.57	-0.24	0.10	-0.56	1	-0.23	-0.59	-0.50	-0.52
<i>CRI1</i>	0.28	0.29	-0.04	0.21	0.29	0.23	-0.11	0.54	0.63	0.68	-0.23	1	-0.02	0.18	0.05
<i>PSRI</i>	-0.20	-0.53	-0.18	-0.10	-0.19	-0.28	0.10	-0.39	-0.51	0.06	-0.59	-0.02	1	0.24	0.29
<i>NDII</i>	0.59	0.29	0.52	0.54	0.59	0.42	0.01	0.36	0.07	0.36	-0.50	0.18	0.24	1	0.94
<i>MSI</i>	0.53	0.24	0.55	0.53	0.54	0.30	0.10	0.28	-0.08	0.32	-0.52	0.048	0.29	0.94	1

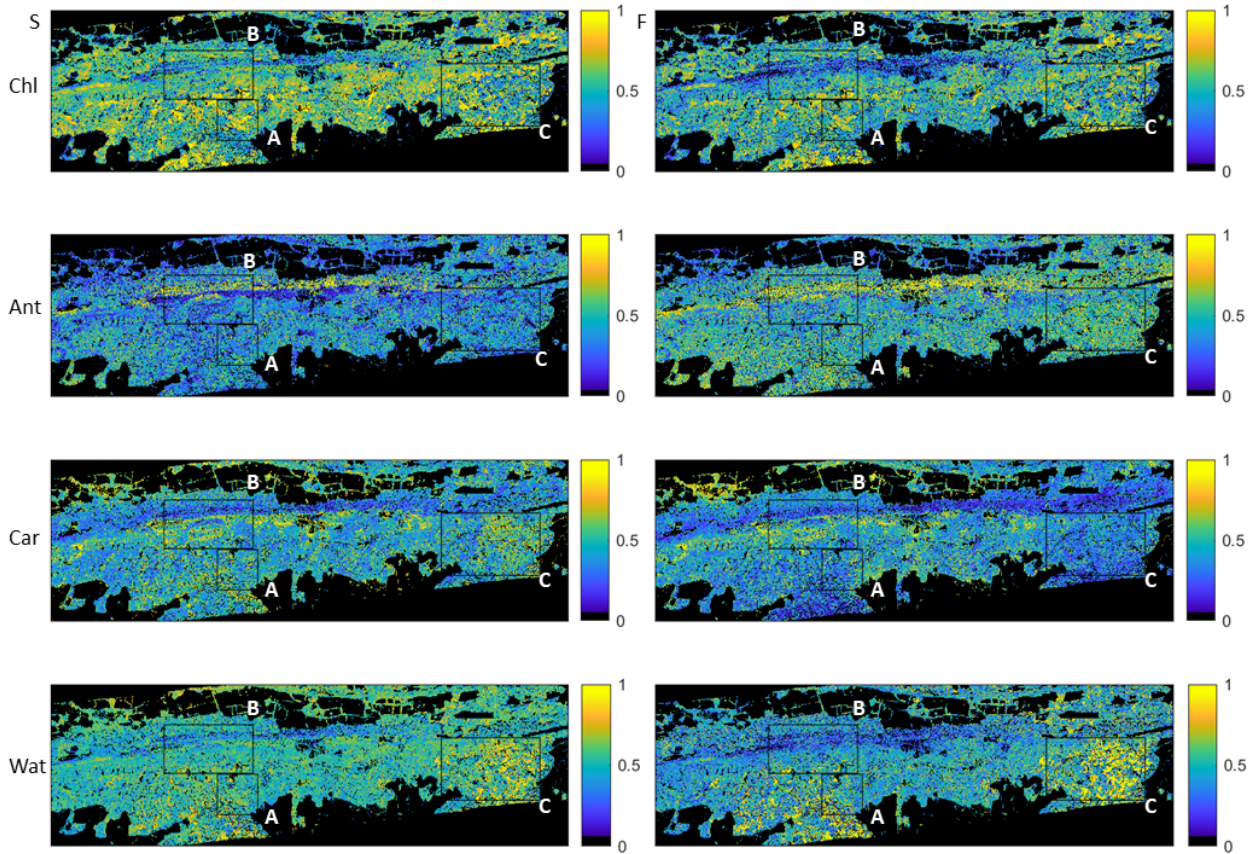


FIGURE 3.2: Mapped functional traits in both summer (left) and fall (right). The mapped functional traits are chlorophyll, anthocyanin, carotenoid, and water content (from top to bottom). Values are normalized from 0 to 1.

3.2 Functional traits

Based on the results in the tests (see section 3.1), an index was chosen to represent each functional trait. To describe the chlorophyll content, $CI_{red-edge}$ was selected. It achieved best results in the test, followed by CI_{green} and $NDRE2$, which also seemed to be suitable for further analysis. For the anthocyanin content, RGR was chosen, as $ARI1$ and $ARI2$ achieved weaker results in our tests. The carotenoid content is described by $PSRI$, and the water content is described by $NDII$, due to better results in the scale analysis and higher correlation of A20 and S20 based results.

Figure 3.2 and 3.3 show the mapped functional traits for both summer and fall. In summer, chlorophyll content correlates most with anthocyanin, followed by water content and least with

TABLE 3.4: Correlation of functional traits in both summer (left) and fall (right).

Index	Chlorophyll	Anthocyanin	Carotenoid	Water
Chlorophyll	1	0.2038	0.1082	0.1946
Anthocyanin	0.2038	1	0.3322	0.2273
Carotenoid	0.1082	0.3322	1	0.0455
Water	0.1946	0.2273	0.0455	1

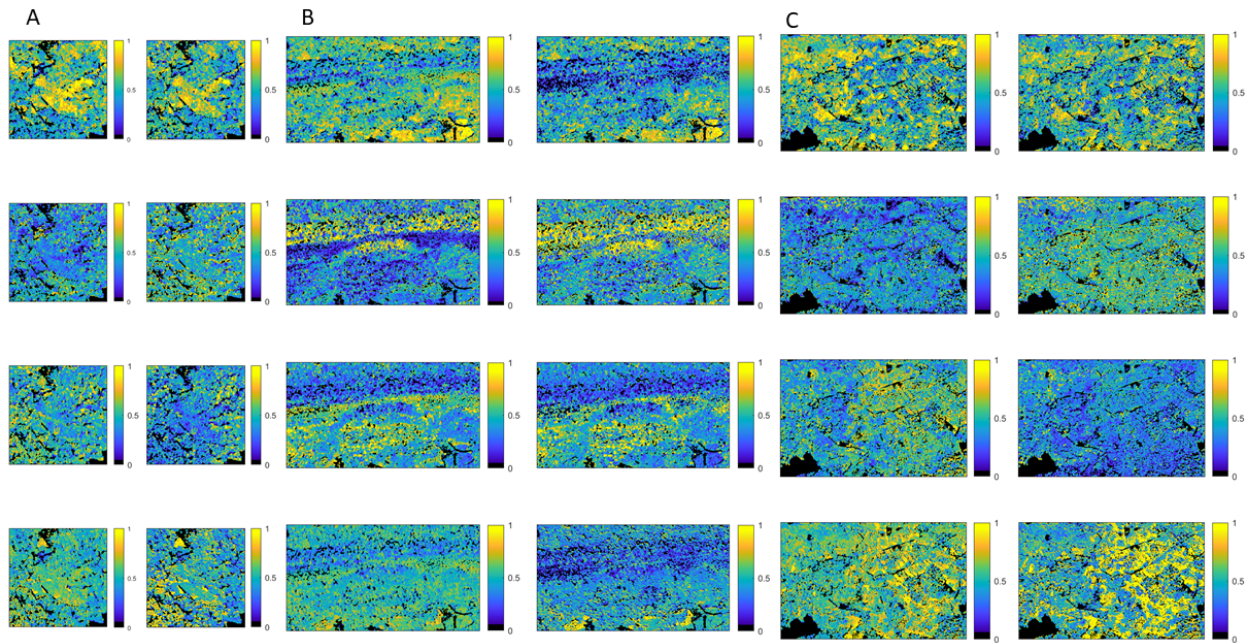


FIGURE 3.3: Mapped functional traits on research site in both summer (left) and fall (right) in different sub-areas (A to C, left to right) of the research area. The mapped functional traits are chlorophyll, anthocyanin, carotenoid, and water content (from top to bottom).

carotenoid content. Anthocyanin and carotenoid content show the highest correlation values, followed by water content. In fall, the chlorophyll and the anthocyanin content, as well as water content correlated more than in summer. Chlorophyll and carotenoid contents correlate less than in summer. The anthocyanin and carotenoid contents show even higher correlation, while anthocyanin and water content become more independent. The same applies for the carotenoid and water contents, which still show the lowest correlation (see Table 3.4).

Furthermore, the spatial detail of increase and decrease of the traits is shown in Figure A.8. As shown in the histogram of traits (see Figure A.9), the chlorophyll, carotenoid and water content each decrease towards fall, while anthocyanin increases. Variance increased towards fall regarding all the four traits with varying degrees of severity. The values of the chlorophyll content decrease towards fall, particularly in patches with high values. The values near the ridge also decrease towards September. Variance of the chlorophyll content increases towards fall from 0.0315 to 0.0377. Anthocyanin levels are relatively low, so the differences are exaggerated by rescaling. In fall, anthocyanin levels rise. The differences at the ridge decrease. Along the north and south slopes the values rise. The variance increases hardly, compared to the other traits from 0.0331 to 0.0348. Overall, variance of carotenoid content values increases from 0.0276 to 0.0326. Water content seems to be more evenly distributed in summer than in fall. The variance of water content increases the most strongly towards fall from 0.0182 to 0.0382, which is also visible in the images. These differences are also visible in the one-dimensional scale analysis of traits (see Figure A.10).

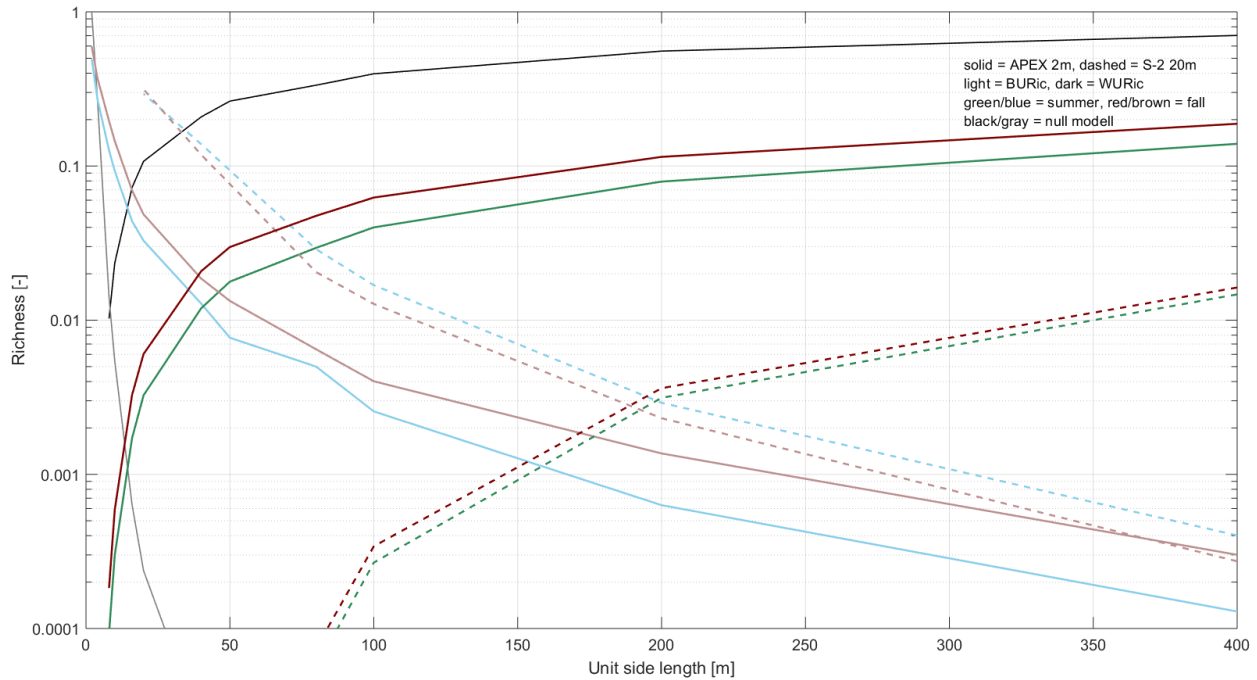


FIGURE 3.4: Comparison of sensors in a four-dimensional scale analysis calculated from the functional traits chlorophyll, anthocyanin, carotenoid, and water content. For the analysis, functional richness was calculated based on the A2 datasets (solid line) and the S20 datasets (dashed line) for both summer (blue/green) and fall (red/brown). Additionally, a 2 m dataset, with randomly generated, normally distributed trait data was tested as well (black/grey).

3.3 Multi-dimensional scale analysis

In order to test the performance of functional richness and divergence, we analyzed their scaling behavior and compared it to the results of the scale analysis of functional traits.

Just as the variance in the one-dimensional scale analysis, functional richness calculated in four-dimensions increases with area and saturates at a certain value. The intersection of within and between functional richness is higher than within- and between-unit variance in the one-dimensional scale analysis. The A2 dataset showed intersections at 40.81 m in summer and 39.04 m in fall (see Figure 3.4). This leads to the conclusion that functional richness is more stable when scaled than the individual traits. Regarding the 20 m datasets, rescaled A20 summer dataset achieved 242.74 m and the fall dataset achieved 249.72 m. The S20 dataset showed an intersection of 203.35 m in summer, and 192.34 m in fall. However, richness is 10 times lower at the intersection i , compared to the values calculated from the A2 dataset. Like variance in scale analysis, richness seems to saturate, however, at a larger unit side length (> 400 m). At 400 m, the value of within-unit richness explains 30% (28.23% in summer, 31.6% in fall) of the maximum between-unit functional richness. Values calculated based on the S2 dataset are 10 times lower. Similar values of within-unit richness are achieved at unit sizes, where a similar number of pixels is given per unit (e.g. 40 m for 2 m pixels, 400 m for 20 m pixels). Values of between-unit functional richness approach each other as the unit size increases. With regard to the fall scenes, the values for between-unit richness are equally small for A2 and S20 with a unit side length of 400 m.

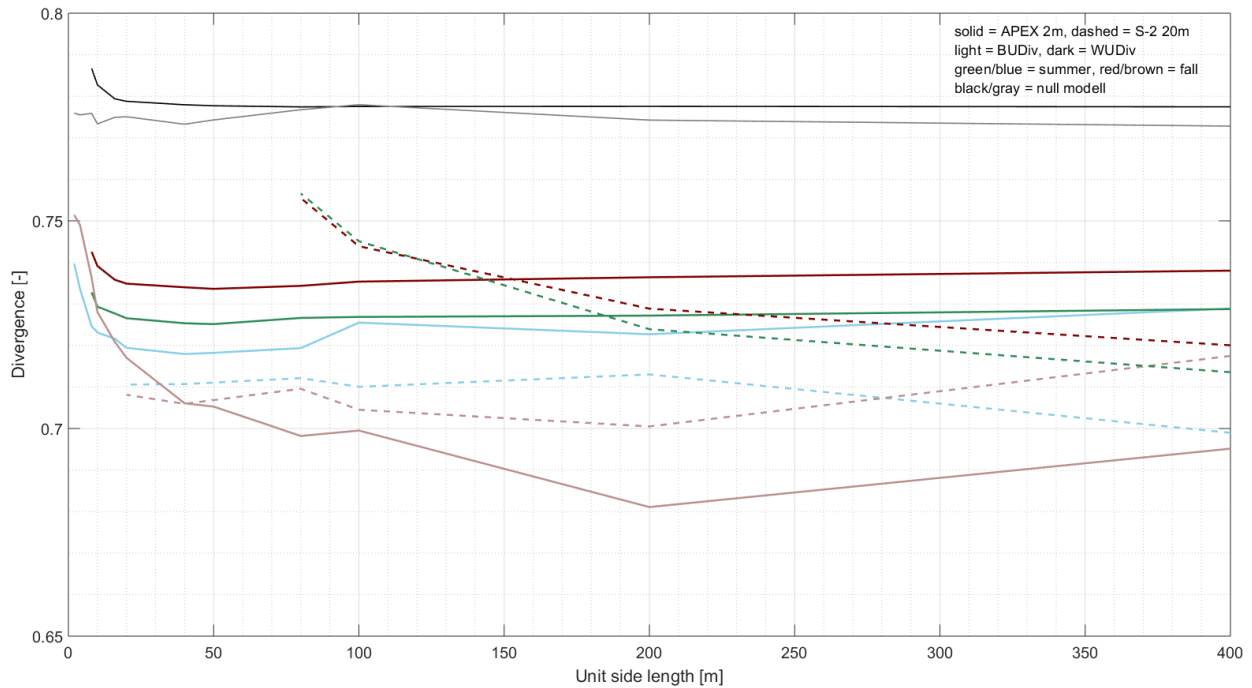


FIGURE 3.5: Comparison of sensors in a four-dimensional scale analysis calculated from the functional traits chlorophyll, anthocyanin, carotenoid, and water content. For the analysis, functional divergence was calculated based on the A2 datasets (solid line) and the S20 datasets (dashed line) for both summer (blue/green) and fall (red/brown). Additionally, a 2 m dataset, with randomly generated, normally distributed trait data was tested as well (black/grey).

Functional richness is higher in fall regarding within- and between-unit richness. This, on the other hand, is not the case for between-unit richness calculated for the Sentinel-2 datasets, while it is the case for the resampled 20 m APEX dataset (for more information see Figure A.11). This could be explained by the chlorophyll and carotenoid contents showing lower values in fall for the Sentinel-2 dataset (see Figure 3.1). However, this difference is also present when calculated with *CIgreen*, which does not show this seasonal difference (for more information see Figure A.12). Functional divergence is scale invariant here, however highly dependent on the number of pixels (see Figure 3.5) and was shown to have no correlation with area. Regarding the A2 dataset-based scale analysis, within-unit divergence saturates at around 20 m unit side length, and the 20 m datasets divergence saturates at 200 m unit side length. This corresponds to 100 pixels per unit, no matter how large these pixels are. Regarding between-unit divergence, saturation took place at 20 m in summer and 100 m in fall on the 2 m dataset. However, between-unit divergence shows a high amount of variability (see random model in the Appendix, Figure A.13). When there are < 5000 units considered (side length of ≥ 40 m, see Table 2.5), calculated mean APEX divergence shows a comparably high variability. A larger research area could therefore improve the results here. Based on the 20 m datasets, no such effect was visible with increasing area. Compared to the randomly generated dataset with a divergence of 0.77, the 2 m summer scene showed divergence values around 0.72. The fall dataset showed values of 0.73 for within-unit and 0.69 for between-unit divergence. While within-unit divergence saturates at a lower level for the 20 m datasets than the A2 datasets, between-unit divergence is lower in the summer scene, and higher in fall.

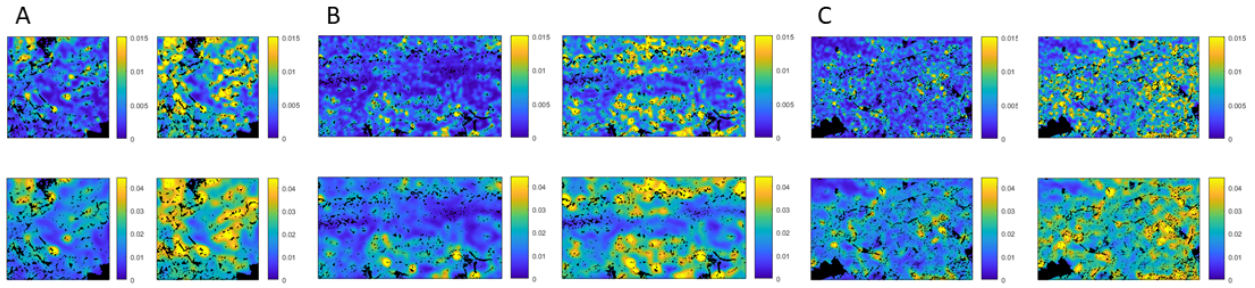


FIGURE 3.6: Functional richness based on the A2 dataset in summer (left) and fall (right). Top images are calculated in 20 m diameter and bottom images are calculated in 40 m diameter. Richness maps calculated in 60 m diameter are shown below (Figure 3.8).

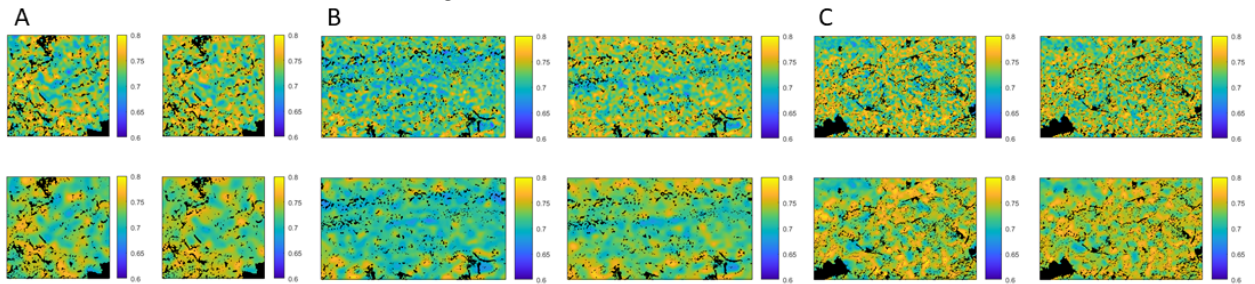


FIGURE 3.7: Functional divergence based on the A2 dataset in summer (left) and fall (right). Top images are calculated in 20 m diameter and bottom images are calculated in 40 m diameter. Divergence maps calculated in 60 m diameter are shown below (Figure 3.10).

3.4 Functional diversity maps

Functional diversity maps were calculated using different sizes of circular neighborhood to compare the results of different underlying datasets, namely the spectrally resampled 2 m APEX (A2) dataset, the spectrally and spatially resampled 20 m APEX (A20) datasets and the 20 m Sentinel-2 (S2) dataset. Diversity maps based on the A2 datasets were calculated for different unit sizes with diameters ranging from 20 m to 120 m, while the ones based on A20 and S20 were calculated for units with diameters ranging from 40 m to 700 m. Maps of functional diversity metrics are shown in Figures 3.6 – A.18.

3.4.1 Diversity calculated from 2 m APEX dataset

Regarding the diversity maps from the A2 datasets, functional richness is higher in fall compared to summer at all different unit sizes. The same applies to the variance of the calculated richness values. The relationship to the slope, which was observed by Schneider et al. in 2017, is visible on the summer as well as on the fall map. The highest values of richness were found on the northern and the southern slope, while the lowest values were observed around the ridge. The correlation of richness maps between summer and fall is $r^2 = 0.4745$ for 20 m unit size, increases strongly towards $r^2 = 0.6197$ for 60 m, and increases more slowly towards $r^2 = 0.6801$ for 120 m and $r^2 = 0.7127$ for 200 m. Correlation furthermore seems to saturate at around $r^2 = 0.7$ and does not further increase (see Figure A.14). The spatial differences of the richness values (see Fig-

ure A.15) show the highest increase in functional richness in the southern-most part of the forest (south of subarea B), similar to the increasing values of chlorophyll and water content in this area. The same applies to the north-facing slope, where a slight decrease in chlorophyll, carotenoid and water contents was observed towards fall, while anthocyanin increases. Around the ridge, functional richness shows a slight decrease towards fall.

In subarea A, where comparably high values of chlorophyll content were observed, low values of functional richness were found. The increase of richness around the patch does not affect the patch of juvenile forest. While the patch of high, multi-layered and dense canopy in subarea B is still visible on the map based on 20 m and 40 m units (see Figure 3.6), it vanishes at larger units (see Figure 3.9 – A.17). The east-west course of the ridge and the transition of communities is visible at 120 m. The functional richness in subarea C is high at the edges of the section.

Functional divergence values are higher in fall than in summer at all unit sizes. At unit sizes > 40 m, the variance of functional divergence is higher in summer, than in fall. The highest values of divergence appear in the southern areas and at the northern slope, which is visible especially on the fall maps. This area is characterized by deeper, acidic Cambisol and Podsol soils (Schneider et al., 2017; Grotzinger et al., 2008). The lowest values can be found around the ridge, characterized by a steep slope and a shallow Regosol on loose ground (Lukito, Kouno, and Ando, 1998; Grotzinger et al., 2008; Schneider et al., 2017). The correlation of divergence maps between the seasons is increasing with unit size, as it is $r^2 = 0.2125$ for a 20 m diameter, increases strongly towards $r^2 = 0.4973$ for 60 m and less strongly to $r^2 = 0.6430$ for 120 m and $r^2 = 0.7265$ for 200 m. For 200 m, the correlation between seasons is most similar for richness and divergence. The correlation is higher for divergence than richness for 120 m unit size, which is not the case with smaller units. The spatial differences of divergence values (see Figure A.16) show an increase at the north-facing slope, while decreasing on the south facing slope.

The patch of juvenile forest in subarea A, that shows low values in functional richness, also shows low values of functional divergence (see Figure 3.7). Those patterns are still visible at larger units with 60 m and 120 m (see Figure 3.11). In subarea B, the east-west course of the mountain ridge is visible in the divergence maps, more clearly in fall, compared to summer. The juvenile forest at the ridge, is visible due to low values of divergence, even at units with diameters of 200 m. This area is also characterized by a steep slope. Subarea C is characterized by high values of functional divergence.

3.4.2 Differences in diversity maps due to rescaling

The results for the calculated functional richness are shown in Figures 3.13, 3.8, 3.9 and A.17. The first thing that stands out is that the functional richness is much higher for the A2 datasets, as well as higher for the A20, compared to the S20 dataset. This can be seen from the color scales in Figures 3.8, 3.9 and A.17 and in the left panels of Figure 3.12. Richness depends on the unit size, which also means the number of pixels. This number of pixels is a hundred times larger for A2 datasets than for A20 datasets. As visible in Figure 3.12, if the area is 10 times larger (same number

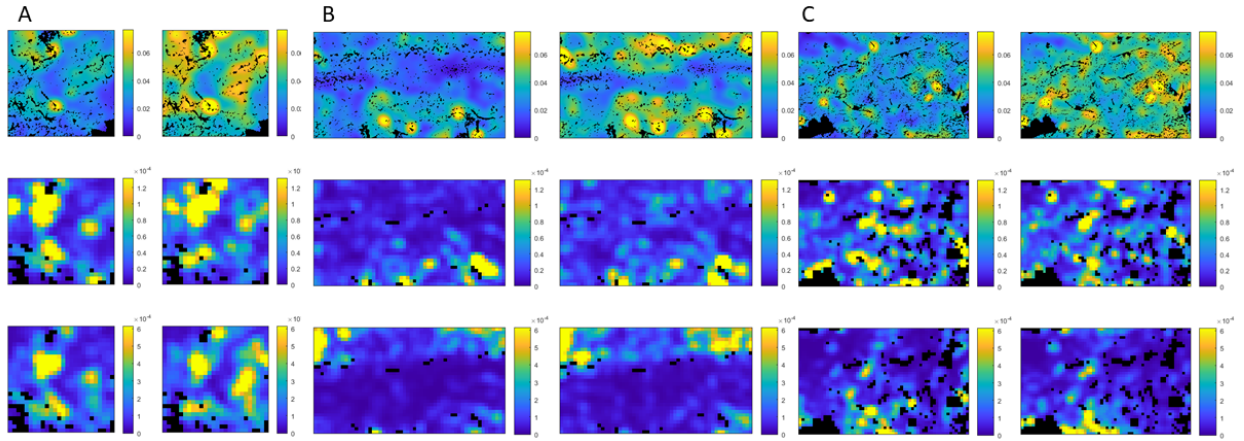


FIGURE 3.8: Functional richness maps based on the A2 (top), A20 (middle) and S20 (bottom) dataset in summer (left) and fall (right) calculated in units with 60 m diameter in the three subareas (A – C).

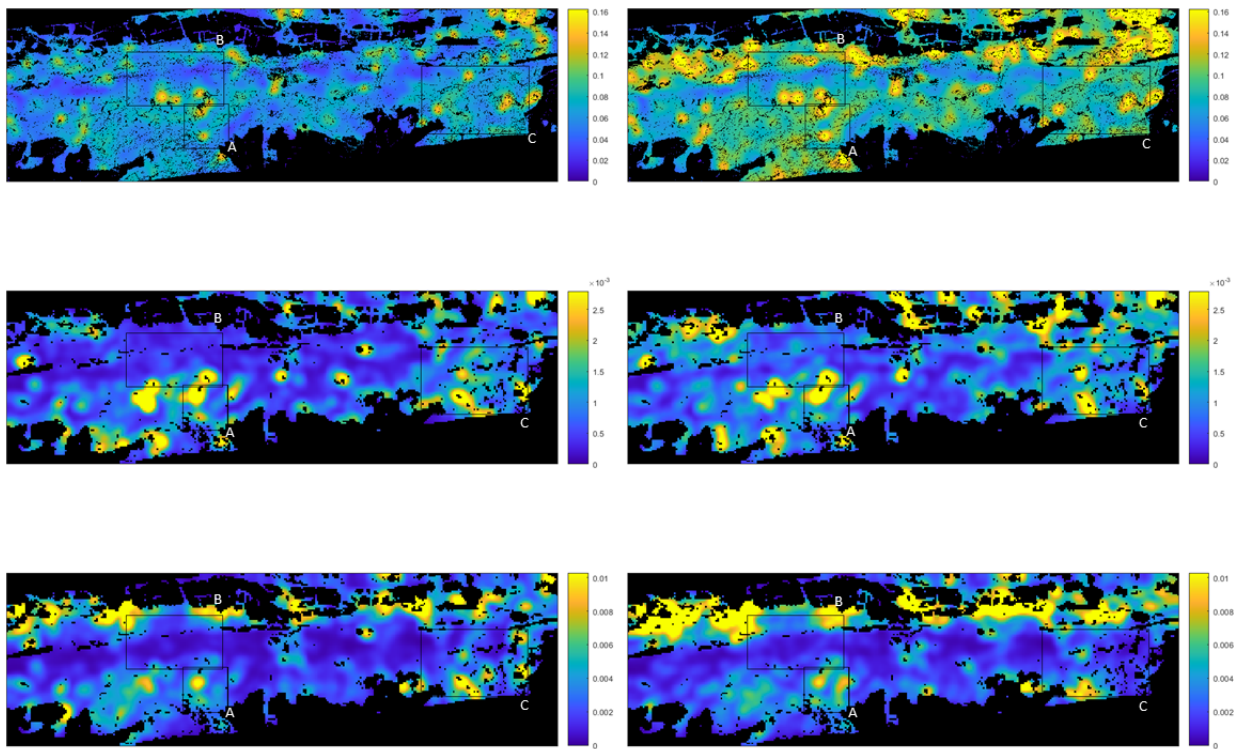


FIGURE 3.9: Functional richness maps based on the A2 (top), A20 (middle) and S20 (bottom) dataset in summer (left) and fall (right). The calculation is based on 120 m diameter which corresponds to a square unit with a side length of 106.35 m.

of pixels), the values will be of similar size. At 40 m diameter for the A2 dataset and 400 m for the A20 dataset, which both are units with a diameter of 20 pixels, values of mean functional richness are of similar size, however, a little lower still on the A20-based map. This is due to mixed pixels, which consist of averaged values. This lowers the functional richness even more for the rescaled dataset. At the same unit size, the values share a relationship of approximately a factor of 50. However, patterns throughout the whole ecosystem are visible in both datasets, so that richness is highest in subarea A and lowest in subarea B in maps based on both datasets.

The results for the calculated functional divergence are shown in Figures 3.10, 3.11, A.18 and 3.13. Divergence is higher in fall than in summer, which is visible in both the A2 and the A20-based map. Functional divergence values are also higher for the A2-based dataset, however showing a smaller increase than functional richness. This is because of divergence not reacting to any change of unit area (Karadimou et al., 2016). For all areas, except C (which increases), functional divergence decreases and saturates at a certain unit size. This value is characteristic for different spatial resolutions, being much higher for the A20 and the S20 datasets. Divergence is highest in subarea C and lowest in subarea B. In summer, the mean functional divergence in subarea B of the A2-based map decreases towards 60 m unit diameter and increases again. This pattern is also visible in the A20-based maps, where the increase takes place at much larger unit diameters. The increasing behavior of mean divergence in subarea C, which is observed in A2-based maps, is not visible in the A20-based maps. However, it is visibly higher in all maps, than the mean functional divergence in other subareas.

The similarities of the A2 and A20 dataset in behavior and relationship of subareas show that these patterns remain after resampling the dataset spatially. Based on this observation, the conclusion can be made that other differences between the A20 and the S20 dataset are not due to consequences of lower spatial or spectral resolutions. Differences, especially of functional divergence, are lower in fall, which once again could be due to higher values of anthocyanin and the lower difference in time between the mission dates.

The correlation of the calculated richness is low when calculated at diameters of 40 m ($r^2 = 0.07$ in summer and $r^2 = 0.08$ in fall), however, higher as for divergence ($r^2 = 0.058$ in summer and $r^2 = 0.052$ in fall). The correlation of functional richness between A2 and resampled A20 dataset calculated at 60 m diameter is $r^2 = 0.1$ in summer and $r^2 = 0.11$ in fall, while $r^2 = 0.12$ in summer and $r^2 = 0.21$ in fall for a diameter of 200 m. The increase of correlation is similar from 40 m to 60 m for both seasons, however much stronger in fall at larger units, while the correlation only slightly increases in summer. Furthermore, the correlation of functional richness shows saturation at larger units. The correlation of functional divergence between A2 and A20 datasets calculated at 60 m diameter is $r^2 = 0.1$ in summer and $r^2 = 0.09$ in fall. The correlation is increasing strongly towards 120 m ($r^2 = 0.2$), while similar for seasons with the correlation in summer being a little higher. The correlation increases strongly and similar for both seasons. While the correlation between the datasets is higher for richness at 60 m unit size, on for divergence increases strongly with unit size and is clearly higher for 200 m (see Figure 3.14). Furthermore, correlation is more similar between seasons for divergence, compared to richness, especially at unit sizes ≤ 120 m.

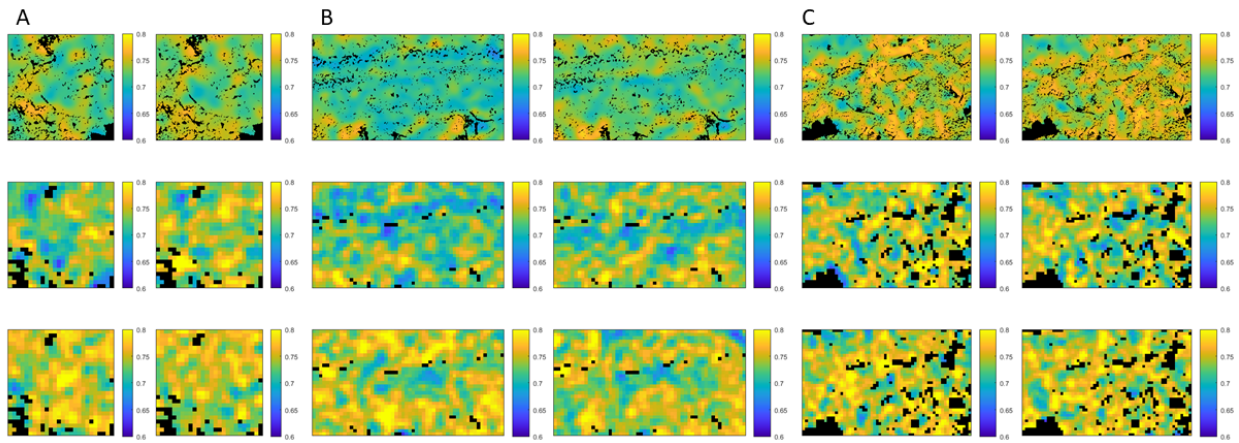


FIGURE 3.10: Functional divergence maps based on the A2 (top), A20 (middle) and S20 (bottom) dataset in summer (left) and fall (right) calculated in units with 60 m diameter in the three subareas (A – C).

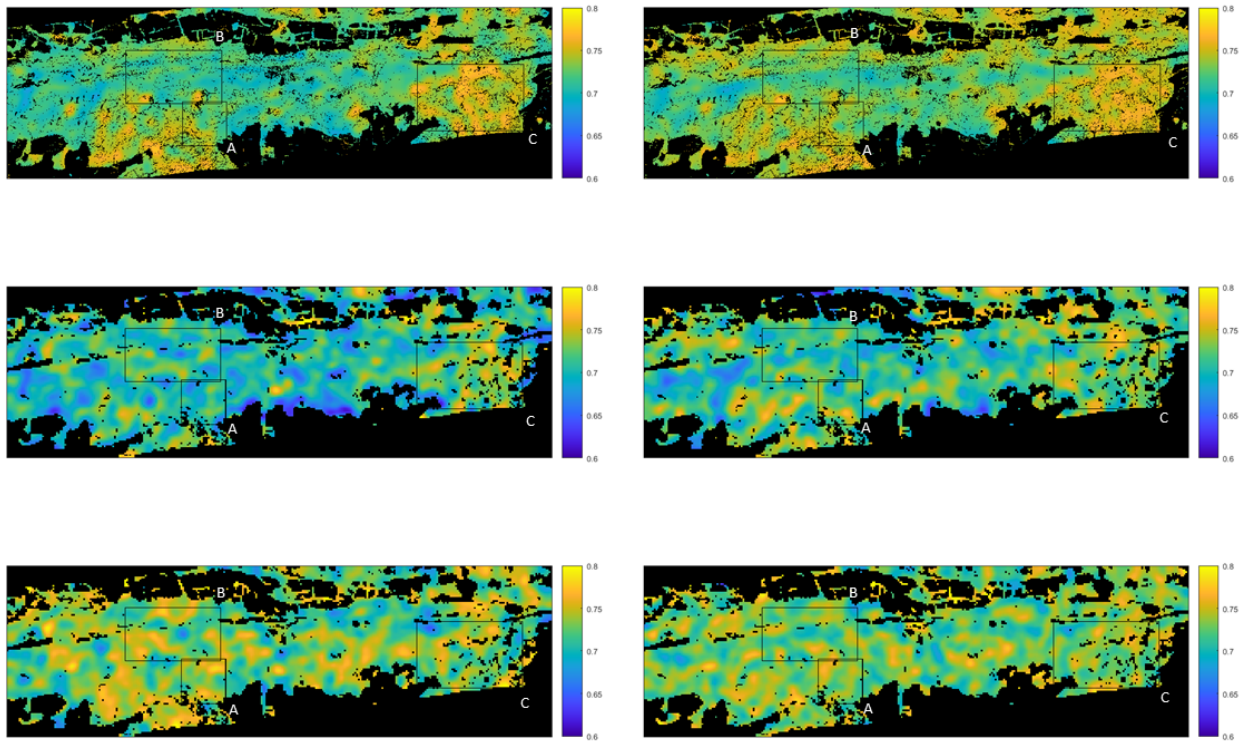


FIGURE 3.11: Functional divergence maps based on the A2 (top), A20 (middle) and S20 (bottom) dataset in summer (left) and fall (right). The calculation is based on 120 m diameter which corresponds to a square unit with a side length of 106.35 m.

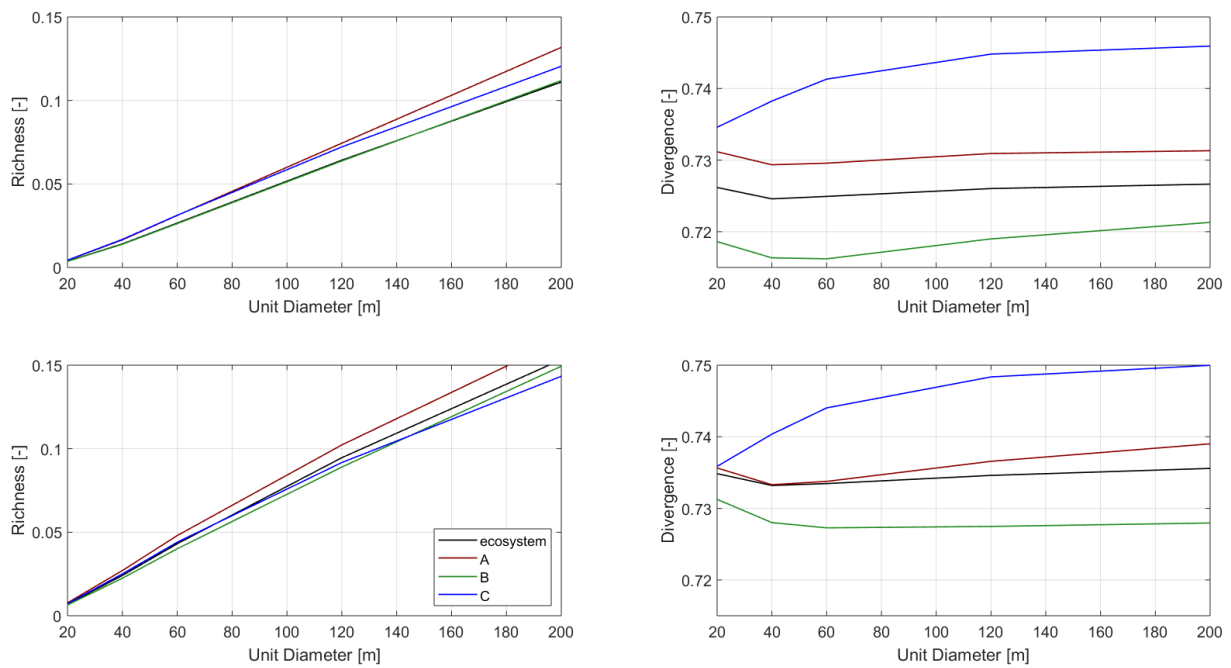


FIGURE 3.12: Development of mean functional richness (left panels) and divergence (right panels) in summer (upper panels) and fall (lower panels) when calculated based on increasing unit diameter for the whole ecosystem (black) as well within the three subareas A (red), B (green) and C (blue). The panels show the development of mean values when calculated based on the A2 dataset in calculated smaller units (20 m – 200 m diameter).

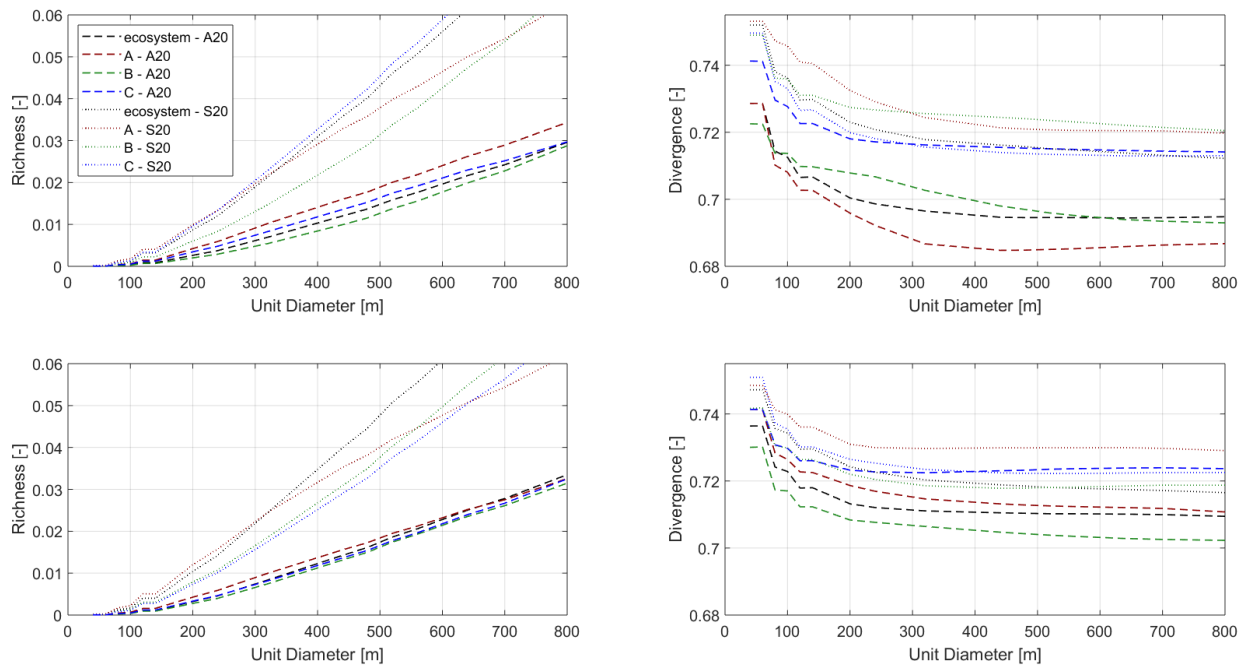


FIGURE 3.13: Development of mean functional richness (left panels) and divergence (right panels) in summer (upper panels) and fall (lower panels) when calculated based on increasing unit diameter for the whole ecosystem (black) as well within the three subareas A (red), B (green) and C (blue). The panels show both the development of mean values when calculated based on the A20 dataset (dashed) and the S20 dataset (dotted) in large units (40 m – 800 m).

For 200 m, correlation of functional divergence for the fall datasets ($r^2 = 0.31$) is higher than in summer ($r^2 = 0.25$).

The correlation of the A2 and S20 datasets is much lower than the correlation of A2 and A20 datasets. Correlation of functional richness between A2 and A20 scenes is higher in fall and even higher between A2 and S20, which can be explained by the smaller difference in time between the two images, compared to the summer images (see Table 2.1). The correlation for richness is low in summer ($r^2 < 0.04$) and increases hardly with unit size ($r^2 = 0.06$ for 200 m). The correlation for richness in fall is similarly low at 40 m, however increasing with unit size ($r^2 = 0.21$ for 200 m). Regarding the correlation of functional divergence maps, the correlation is low for units with diameters < 60 m ($r^2 < 0.015$). In fall, the correlation shows a high increase ($r^2 = 0.13$ for 200 m), compared to summer ($r^2 = 0.09$ for 200 m). The correlation of divergence seems more independent of seasons compared to richness, when comparing A2 with both A20 and S20 datasets. In fall, the correlation is higher and also increasing more strongly with unit size. This could be explained by higher values of anthocyanin, the higher variance of traits, and the smaller difference in time between the images.

3.4.3 Differences in diversity maps due to sensor characteristics

Regarding the maps calculated from the S20 and A20 dataset, the correlation is low for 60 m and 40 m diameter ($r^2 = 0.01$ for divergence and $r^2 = 0.07$ for richness). The correlation for both diversity metrics starts increasing rapidly at larger units. In summer, the correlation is highest at a diameter of 320 m ($r^2 = 0.17$ for richness and $r^2 = 0.27$ divergence). For this unit size, values for the fall datasets are $r^2 = 0.3557$ for richness and $r^2 = 0.1992$ for divergence. In fall, correlation does not show a maximum (tested < 700 m), however correlation tends to be less strongly increasing at unit sizes > 320 m. The highest correlation values for the fall datasets are at a diameter of 700 m, which are $r^2 = 0.5002$ for richness and $r^2 = 0.4446$ for divergence. In fall, the correlation of richness is higher than the one of divergence. On the other hand, the opposite behavior was observed in summer for units > 100 m. A correlation decrease of divergence at 320 m and higher could emerge from information loss, due to the limited size of the research area.

In the functional richness maps based on 60 m units, the patch in subarea A is visible, due to low values of richness within and high values on the edges of the patch. This was detected in the maps based on all three types of data (see Figure 3.6). At higher unit sizes (120 m and 200 m diameter), where the patch is no longer visible, high values of richness in the north-western part of subarea A are visible in all richness maps (see Figure 3.9 and A.17). Higher values of functional richness in the 2 m maps, compared to 20 m maps, are due to the much higher number of pixels per unit (100 times more). In subarea B, low values around the ridge are visible. A major problem at the A20 and S20 based maps are mixed pixels, which lead to high values around clearings and at the forest edges, especially on the north facing slope. At subarea B, sparse canopy around the ridge does not have the same effect, as clearings and forest edge. In the S20 based maps, especially high values of richness are observed on the north facing slope. This can be explained by either the

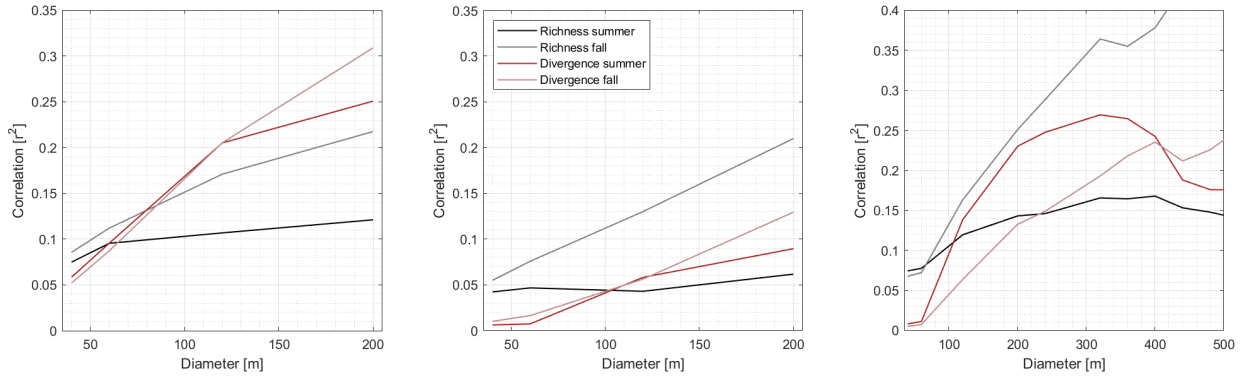


FIGURE 3.14: Development of the correlation for richness (black/grey) and divergence (red/light red) with increasing neighborhood size in which they were calculated over the ecosystem. The resampled A20 dataset is compared with the A2 dataset (left), the S20 dataset is compared with the A2 dataset (middle), as well as the A20 and the S20 dataset (right).

presence of mixed pixels, or the much steeper angle of view of Sentinel-2, compared to APEX. The values on the north slope lead to an override of the values on the south slope.

Correlation in the subareas between the three diversity map types (A2, A20 and S20) is shown in Figure 3.15. In subarea A, the correlation of A2- and A20-based maps is much higher for richness, compared to divergence. As visible in Figure 3.8 and 3.9, the patch in subarea A is visible in maps calculated from all datasets. This is also true for the correlation between A2 and S20 based maps. This leads to the conclusion that in subarea A less information is lost when calculating functional richness at lower spatial resolution. When comparing the correlation for both sensors, at 20 m spatial resolution, the correlation is much higher for functional divergence. In subarea B, the east-west course of the ridge is visible at 120 m and 200 m unit sizes, in all divergence maps. However, the ridge is especially visible in the fall scenes. This is also visible in the correlation of A2 and S20 datasets and A2 and A20 correlation of divergence, which is higher in fall scenes. When comparing datasets, the highest correlation is visible within divergence maps. Regarding subarea C, correlation is higher for functional richness at all unit sizes, with a maximum at 120 m diameter, when comparing A2 and A20 datasets. At larger unit sizes, correlation of divergence maps rises, and becomes more important, compared to smaller units. When comparing A2 and S20 datasets, the scenes are more similar, when comparing divergence maps, with a peak at 120 m. Regarding functional richness, no correlation could be found between A2 and S20-based maps. However, when comparing A20 and S20 maps, functional divergence shows similar patterns of correlation compared to subarea A and B, as well as the whole ecosystem, being relatively high ($r^2 = 0.2 - 0.4$). On the other hand, functional richness shows high correlation between the two sensors, and an even higher correlation in fall. The correlation between rescaled images and sensors, both diversity metrics show values depending on the subarea.

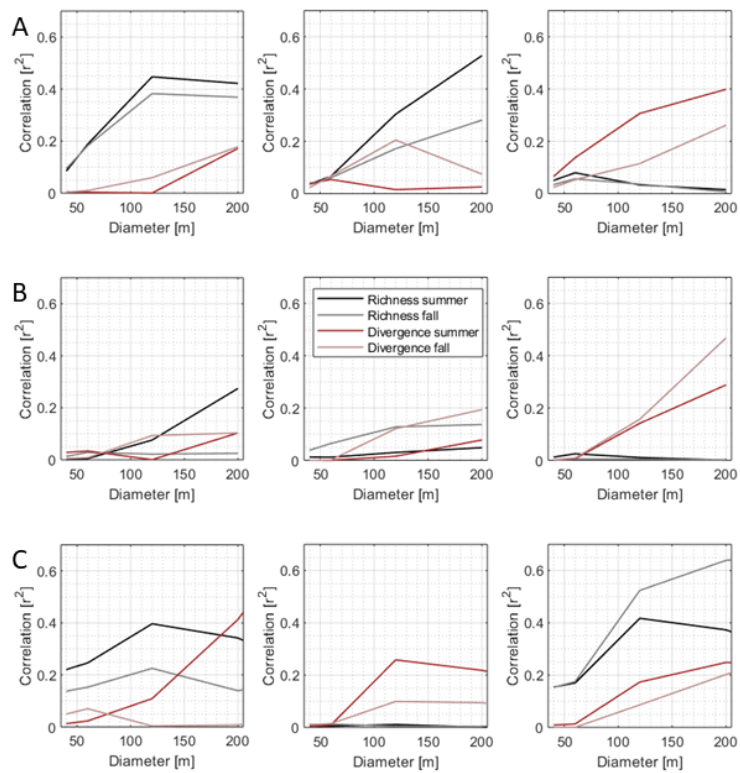


FIGURE 3.15: Development of the correlation for richness (black/grey) and divergence (red/light red) with increasing unit size in which they were calculated, for each of the three subareas A, B and C (from top to bottom). The resampled A20 dataset is compared with the A2 dataset (left), the S20 dataset is compared with the A2 dataset (middle), as well as the A20 and the S20 dataset (right).

4 Discussion

Discrepancies between different research fields hamper the transfer of findings from ecosystem services to ecosystem functioning and vice versa. Ecosystem service studies are often conducted at larger spatial scales and usually do not investigate the underlying ecosystem functions related to specific services. In contrast, ecosystem functioning is biased to small scale ecosystems and/or based on experimental designs (Laureto, Cianciaruso, and Samia, 2015). The first step towards bridging these gaps between ecosystem functioning and ecosystem services, is measuring functional diversity at large scales. Furthermore, identifying various links between traits and ecosystem services will provide a better understanding of how biodiversity affects ecosystems, representing an important tool for conserving ecosystem services and functions (Bello et al., 2011; Laureto, Cianciaruso, and Samia, 2015). Quantifying functional diversity on large scales creates the link between ecosystem functioning and ecosystem services. This link paves the way for future studies, directly predicting impacts of global environmental changes, which affect ecosystem functioning and ecosystem services on a global scale.

In 2017, Schneider et al. presented an innovative method of mapping functional diversity continuously through space. The next step of transferring this method to satellite systems is presented in this study. The performance of functional traits and diversity metrics was tested at different spatial scales over different seasons using two different optical sensors. We analyzed functional traits and functional diversity metrics based on three datasets, namely a spectrally resampled APEX dataset (A2), the spatially and spectrally resampled APEX dataset (A20) and a Sentinel-2 satellite dataset (S20). The latter two datasets have the same spatial resolution of 20 m.

4.1 Functional traits

4.1.1 Identification of suitable functional traits and corresponding vegetation indices

Different indices were tested on their scalability and suitability for multiple sensors based on the A2 data. All of the indices, except *CRI1*, showed stronger results and reactions to autocorrelation in the scale analysis, compared to the random model. 80% of the initial variance is no more between-units but within-units (t) at 40 m for water and anthocyanin content, which tend to show variation at smaller scales, compared to carotenoid and chlorophyll content for which 80% of the original variance at 2 m spatial resolution was found within-units at a side length of 60 m. The same is visible for the variance remaining at 20 m, the resolution of Sentinel-2, being 16% for carotenoid and chlorophyll content, and 13% anthocyanin and water content.

To enable the most accurate comparison of sensors, it is crucial to check the suitability of the sensors for each index before calculating diversity metrics. This was done using a qualitative comparison of boxplots of two sensors and quantitatively using correlation between datasets. Thus we could answer our research question on how different physiological traits and diversity metrics are affected by scaling effects, and which of the traits can be applied to multiple sensors. Many of the chlorophyll indices worked good on both datasets. *CIred – edge* has been proven to correlate well with chlorophyll content in various studies and has also proven to be suitable and stable in the tests carried out here (Peng and Gitelson, 2011; Clevers and Gitelson, 2013; Clevers et al., 2017). Based on our results, we expect best results from *CIred – edge*, *CIgreen* and *NDRE2* in this order. All of which performed good in our tests and are known to deliver reasonable results. Based on findings in the literature and our experience with its performance, we recommend *CIred – edge* and *CIgreen* as an alternative, if there is no red-edge band available (Peng and Gitelson, 2011; Clevers and Gitelson, 2013; Clevers et al., 2017). Water content also achieved reasonable results. We recommend *NDII*, but *MSI* worked as well. Both *NDII* and if necessary *MSI* can be recommended. Hardest to determine were the anthocyanin and carotenoid content, due to spectral properties. These indices showed potential for failure on one of the sensors, such as *CRI1* and *ARI1*. Most potential for improvement can be found here. Nevertheless, *RGR* and *PSRI* achieved the strongest and most stable results.

4.1.2 Mapping functional traits

Mapped functional traits are shown in Figure 3.2 and 3.3 for both summer and fall. All four mapped functional traits delivered reasonable results and differences between the seasons. The spatial patterns of increase and decrease of traits when comparing July and September are shown in Figure A.8. As shown in the histogram of traits (see Figure A.9), chlorophyll, carotenoid and water content decrease towards fall, while anthocyanin increases.

Low values of chlorophyll are observed in areas where conifers make up most of the forest mixture, and are also measured directly on the north side of the ridge. The highest chlorophyll values are measured on the southern slope, in patches especially where less than 50% beech (*Fagus sylvatica*) is observed. Especially young forests show high chlorophyll values. Young forests and trees usually show high productivity and therefore high values of chlorophyll, as they invest a lot of energy in biomass accumulation and growth (Finegan, 1984; Day, Greenwood, and White, 2001; Acker et al., 2002). A patch described by Schneider et al. (2017), where small juvenile forest, likely affected by disturbance caused by a winter storm was also visible here (subarea A), characterized by high values of chlorophyll content (see Figure 3.3, subarea A). These values decrease towards fall, particularly in patches with high chlorophyll content and near the ridge. A slight decrease in chlorophyll content between DOY 189 and 251 seems plausible (Demarez et al., 1999; Zhang, Chen, and Thomas, 2007). The highest decrease was observed in higher areas near the ridge on the south facing part, where the juvenile forest seems to react early to seasonal changes and the corresponding stress. A slight increase in chlorophyll content was observed in lower areas on the south-facing slope, where areas are characterized by evergreen needle forest.

Anthocyanin levels are known to be comparably low during summer, so the differences are exaggerated by rescaling (Ustin et al., 2009; Schneider et al., 2017). Rescaled values are relatively low as well, with one exception near the ridge, where the values are especially low on the south side and particularly high on the north side. Anthocyanin rise can be caused by stress, which seems plausible on the shallow soils and the lower light income on the steep north-facing slope below the ridge (Schneider et al., 2017). Young forests tend to be less robust to stress, as most of the energy is allocated to growth rather than defense, health and reproduction (Loehle, 1988; Herms and Mattson, 1992; Obeso, 2002). In the western third, high values of anthocyanin are observed in a patch on the south side of the ridge (see Figure 3.3, subarea B). This area has been described with morphological characteristics by Schneider et al. (2017). The area characterized by low values of anthocyanin on the south side of the ridge in subarea B is described as multi-layered, low and sparse canopy, while the bright patch is described as high, multi-layered and dense canopy. The same patch is visible when calculating carotenoids, where it is described by lower values than its surroundings. Values of anthocyanin content increase towards fall (Dhindsa, Plumb-Dhindsa, and Thorpe, 1981). A higher increase in anthocyanin content was observed in higher areas on the south-facing areas near the ridge, similarly to the patterns of chlorophyll decrease. This is reasonable, considering the seasonal cycle of plants in temperate and boreal biomes is primarily controlled by temperature and day length (Menzel, 2002). Consequently, plant phenology is mainly regulated by temperature: low temperature initiates winter dormancy. Laegern forest has a gradient in altitude of 450-860 m a.s.l (Eugster et al., 2007), the higher altitudes at the ridge lead to lower temperatures and therefore ease earlier changes that can be attributed to leaf senescence.

Carotenoid values are higher on the southern than on the northern slope, which can be explained by the protective function of carotenoids from high radiation income in summer by release of excess energy through fluorescence (Ustin et al., 2009; Schneider et al., 2017). In fall, the values of carotenoid content decrease in patterns similar to the increase in chlorophyll, especially in the lowest areas of the southern slope, where more than 50% conifers are present in the mixture, such as subarea C (Schneider et al., 2017; GIS-ZH, 2018). These observations of carotenoid decrease could be explained by the less steep solar angle in September and the resulting lower radiation, enabling higher productivity. Areas remaining highly exposed to radiation income at higher altitudes show less decrease in carotenoids. Carotenoids function as antioxidants and appear as protectors during stress (Lewandowska and Jarvis, 1977; Gamon et al., 2016). In deciduous trees, carotenoid content decreases during senescence (Goodwin, 1958), while in coniferous trees, values of carotenoid content were observed to decrease towards fall and increase again in winter (Lewandowska and Jarvis, 1977; Ensminger et al., 2004; Gamon et al., 2016). High values of carotenoid protect the needles during the cold of winter. Based on this, it is expected that the values of measured carotenoid content rise again during fall senescence in communities with a high proportion of coniferous trees in the mixture, while staying low in deciduous trees, until the onset of leaf fall in mid October (Verein GLOBE Schweiz, 2017b).

Water content tends to be more evenly distributed in summer than in fall. The lowest values were observed on the northern slope just below the ridge. All in all, the highest values of water content are located similarly to where Schneider et al. (2017) observed them, namely on the

southern slope in the east and in the west in flatter areas with deeper, acidic soils. These areas are dominated by evergreen coniferous needle trees. These values increase even more towards fall, i.e. in the dense coniferous forests, while they drop sharply around the ridge, where the communities are characterized by a young forest. The juvenile forest near the mountain ridge further shows the strongest decrease in water content, while the lower areas on the south facing areas only show a slight increase in water content. This is similar to patterns in chlorophyll decrease and could be explained by soil depth being higher in lower areas of the south facing slope. In these areas of deeper, less rocky, further developed soils, the roots are deeper and the water capacity of the soil is higher, which leads to a more balanced water regime.

4.1.3 Outlook

In summary, all of the four traits worked to describe the ecosystem under the coarser spectral resolution. Regarding seasonal changes of functional traits, a lot of information on the development of traits could be gained by comparing multiple seasons, throughout the phenological year or through multiple years. Furthermore, observing the development of physiological traits throughout the daily cycle, could deliver a lot of new information about communities.

Using future spaceborne imaging spectrometers, more functional traits and dimensions could be added to the analysis, depending on the spectral properties of the sensor in regard. This could for example be cellulose content, (Nagler et al., 2003), leaf area or leaf mass per unit area (Wijk and Williams, 2005; Jiang et al., 2008), other minerals, such as phosphorus content (Mutanga and Kumar, 2007), nitrogen content (Martin et al., 2008), nonstructural carbohydrates (NSC) (Asner and Martin, 2015), phenolics (Asner, Martin, and Suhaili, 2012; Kokaly and Skidmore, 2015), sugar or starch. Global trait databases support this task (Kattge et al., 2011). By adding morphological information from laser scanning data to derive functional traits, results could further be improved (Schneider et al., 2017; Dalponte et al., 2018).

4.2 Functional diversity

Furthermore, we answered the question to which extent the results from data acquired at high spectral and spatial resolution (A2) differ from spatially resampled A20 data, as well as multi-spectral spaceborne S20 data and how much of the initial diversity, derived from A2 data can be observed from data collected from space.

4.2.1 Four-dimensional scale analysis

It has been shown by the four-dimensional scale analysis that functional diversity varies on a larger spatial scale than functional traits alone. Similar to variance in the one-dimensional scale analysis, functional richness calculated in four dimensions increases with neighborhood area and saturates at a certain value (Karadimou et al., 2016). For a unit size of 40 m, the same amount of

physiological richness is found between and within-units in the scale analysis of the A2 data. This is an increase by a factor of two compared to the traits on their own. The scale analysis showed similar behavior, when calculated based on A20 and S20 datasets, however, functional richness is lower at the same unit size due to a lower number of pixels per unit (*ppu*) and because of small scale diversity being averaged out at lower spatial resolution. This can be explained with the area-diversity relationship (Karadimou et al., 2016). The value of functional richness is 20 times lower in the 20 m datasets compared to the 2 m dataset. Functional divergence shows similar patterns in the form of strong differences due to the resampling of the data. Divergence is scale invariant, and showed negative, positive or no correlation with area, depending on plot and community (Karadimou et al., 2016). However, it seems highly dependent on the number of pixels (see Figure 3.5). The value drops and saturates at a unit size much higher in the A20/S20 data, compared to the A2 data.

4.2.2 Mapping functional diversity

We found that mapping functional diversity based on 20 m spatial resolution is possible, however, not without information loss. The properties of functional diversity metrics lead to spatial effects when resampling to lower spatial resolutions. Figures 3.12 and 3.13 show the development of functional diversity metrics with unit size at the whole ecosystem, as well as the three subareas A, B and C. Subarea B shows the ridge, which is the dominant feature of the ecosystem. The shallow and rocky soil, steep slopes and high radiation, especially on its southern slope, act as environmental filter (Schneider et al., 2017). Tree types that withstand shallow and rocky soil as well as the high light income, profit from the absence of competitive species, such as beech (*Fagus sylvatica*) and spruce (*Picea abies*) under these conditions. On the south side of the ridge, the mixture of trees contains light demanding species, such as oak (*Quercus sp.*), hornbeam (*Carpinus*) and lime tree (*Tilia sp.*). On the north side of the ridge, the ground is steep, unstable, and characterized by less light input (data by the state government, GIS-ZH, 2018). The species mixture contains more beech (*Fagus sylvatica*), ash (*Fraxinus excelsior*), and maple species (*Acer sp.*). On both sides of the ridge the conditions are harsh and resource availability is low. This requires one-sided adaptation by the species. The reduced trait variability towards the ridge was visible in all richness maps. As visible in Figures 3.12 and 3.13, subarea B shows the lowest values of richness at all unit sizes, and in all sensors. In fall, physiological richness rises especially on the north-facing slope. Senescence onset is driven by temperature and day-length which is locally dependent on topography (Menzel, 2002). Therefore small scale location differences could drive the onset of senescence and therefore ease earlier changes that can be attributed to leaf senescence, such as light stress in the north-facing slope, leading to higher functional richness in fall. Regarding functional divergence, subarea B also shows the lowest values. In the 20 m based maps, this is also visible. However, it is much less pronounced, especially in S20 maps (see Figure 3.10, 3.11 and A.18). This could be explained by the one-sided distribution of traits used in this harsh location. At the ecosystem level, the mountain is again dominated by the ridge as the most prominent landscape feature. Therefore, regarding γ -diversity, the behavior of physiological richness and divergence is very similar

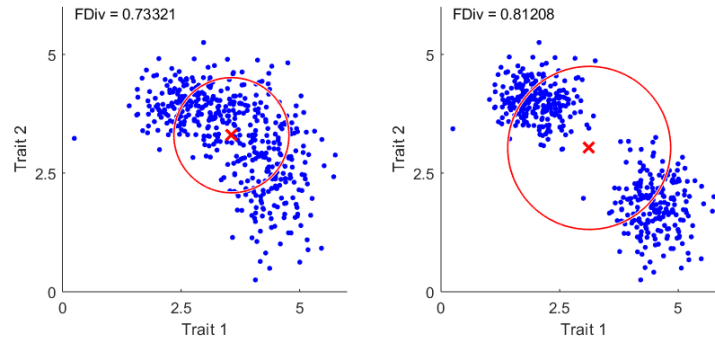


FIGURE 4.1: Effect of niche partitioning on functional divergence shown on randomly generated data-points.

between subarea B and the whole ecosystem (see Figures 3.12 and 3.13). The main difference was an overall lower richness and divergence at subarea B. Contrarily, subarea C shows highest values of divergence, which can be explained by the mixture of coniferous and deciduous trees, leading to an even distribution of traits (Mason et al., 2005; Schneider et al., 2017). The vigorous, advantageous stands, are dominated by beech (*Fagus sylvatica*) and spruce (*Picea abies*). It is rather dark and dominated by high concurrence, rather than resource shortage. The physiological traits are evenly distributed throughout the mixture. Functional divergence is highest in subarea C in both the A2 and the resampled A20 dataset. Divergence shows higher values, in parted niches (see Figure 4.1, Mason et al., 2005). On the other hand, functional richness is comparably low in subarea C, which can be explained by the low level of diversity in the mixture. Lastly, subarea A shows the highest values of richness at smaller scales, and does not increase that much at larger units. This can be explained by the size of the units out-ranging the size of the patch of juvenile forest within subarea A. Functional divergence is rather high at smaller scales, compared to other areas, and decreasing towards larger units as well, which could also be explained by the patch of juvenile forest being averaged out, and the pattern disappearing at larger scales. This can be observed at unit sizes of 120 m and higher. Overall, patterns like the low richness at the ridge or the high divergence at subarea C are visible in all types of diversity maps. However, at unit sizes of 120 m and higher, some attributes get lost, namely the patch in area A. It is visible at all sensors that the divergence is higher in fall, which can be explained by higher levels of anthocyanin. However, at the ridge, where the highest increase of anthocyanin values was observed, values of divergence decrease. The correlation of different datasets also varies strongly between patches, depending on the values of the diversity metrics and community. Using a combination of both divergence and richness is recommended. Except for subarea A, the same relative patterns of richness and divergence could be observed. This means that this information is not lost during resampling. However, direct comparison is not recommended here, as the values of richness and divergence are directly linked to the number of pixels per unit and for this reason the differences in scales of values are immensely high. Differences between A20 and S20 therefore can be further explained by differences in illumination, angle of view, sensor specification, altitude, and time, instead of the difference in spatial resolution of the underlying data.

When comparing original and rescaled APEX datasets (A2 and A20), fall scenes show stronger

correlation with each other and a high increase of correlation with unit size, as well as correlations of divergence maps showing higher increase with unit size, compared to richness. The low correlation at unit sizes < 60 m matches the observation in Figure 3.13, in which values of richness and divergence neither rise nor fall at units smaller than 60 m. We assume that edge effects, which disturb the visible patterns when fewer than 3×3 pixels per unit are considered, are the reason for the poor quality of the analysis. We recommend minimum sizes of three times the pixel size as unit diameter in circular and side length in square units, in order to avoid these effects when working on large areas, especially for divergence. In small areas, features can be qualitatively visible when using functional richness (e. g. subarea A). The highest correlation between sensors was visible at either 120 m and 320 m diameter in circular units, which corresponds to 100 m and 280 m square unit side length. The higher correlation in fall could be due to higher variance, higher values of anthocyanin or a smaller difference in time between the missions. Adding anthocyanin content adds value to the calculation, especially in fall. Furthermore, the variance of results increase in the fall scene, most likely due to higher values of anthocyanin in fall. Lastly, higher correlation was observed in fall, which can be explained by higher values on anthocyanin in fall, higher variance or due to the smaller difference in time between the mission dates. Regarding the subareas, A20 and S20 correlate mostly through functional divergence, while A2 and resampled A20 correlate mostly through richness. However, this is depending on the subarea, and therefore the forest type (see Figure 3.15). Over the whole ecosystem, A20 and S20 correlate mostly through both metrics and especially in fall. This could be due to higher values of variance, or closer mission dates in fall. When rescaling (A2 to A20), more information is left when calculating richness from the resampled dataset. When rescaling and comparing, the use of both metrics is recommended.

4.2.3 The mixed-pixels problem

A common problem at coarse spatial resolutions, especially in relation to the objects, are pixels where a large proportion are mixed as they include both object and background (Hsieh, Lee, and Chen, 2001; Jones and Sirault, 2014; Chen et al., 2018). This is the case at the edges of objects or in low resolution images. This problem increases as the spatial resolution of the image becomes coarser to a point where the pixel size approaches or becomes greater than the object size. At Laegern forest, the average crown diameter is around 6 m. Therefore, mixed pixels are likely to cause problems at the given 20 m pixel size (Schneider et al., 2017). The effect of mixed pixels on the functional richness maps is visible by higher values of richness near forest edges and clearings. This is observed around clearings on the south facing slope, and on the north facing slope. This could be explained with a different angle of view of the sensors and different illumination. On functional divergence maps, the effect of mixed pixels can also be observed, however, with a different phenomenon. Mixed pixels near the forest edge and clearing tend to show higher values of richness and lower values of divergence. This seems plausible regarding the concept of richness and divergence. Pixel values lying off the niches would increase the value of richness and decrease the values of divergence (see Figure 4.2 and A.21). The local effects of mixed pixels were so high that other patterns and properties are no longer observable. This could explain why

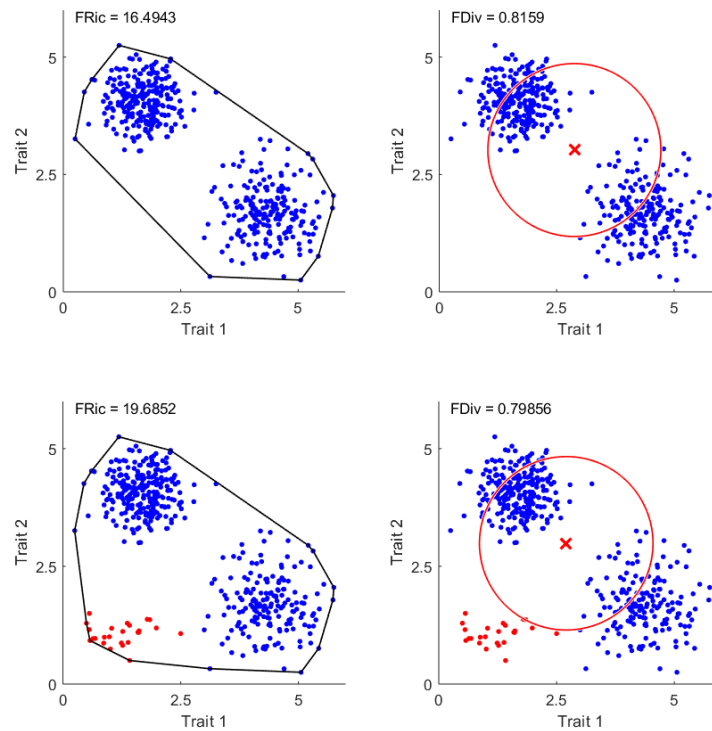


FIGURE 4.2: Effect of mixed pixels (red) on randomly generated data-points with clear differentiation/niche partitioning. Functional richness increases (left panels) and divergence decreases (right panels).

the correlations of the diversity maps in the subareas were sometimes much higher, as there were hardly any mixed pixels due to very rare forest edge and clearings within the subareas, compared to the whole ecosystem. Potential improvement of the forest mask especially at low resolutions, could greatly improve the presented results.

4.2.4 Adding Anthocyanin

The advantages of adding a fourth dimension to the functional trait space is not completely visible, and there is still no consensus on the best method for measuring the quality of functional spaces (Maire et al., 2015). Our four-dimensional analysis and the three-dimensional analysis achieved similar results on the A2 dataset. Consequently, three dimensions achieve a sufficient result, when four dimensions are not available. However, when comparing functional traits, Maire et al. (2015) found that functional trait spaces having at least four dimensions delivered the strongest results, compared to two-dimensional functional spaces. The information gain is therefore absolutely advantageous. The use of anthocyanin is further reasonable, as we were comparing calculations at two dates of the phenological year.

4.2.5 Seasonal development of mapped physiological diversity

The change of functional diversity through the seasons was compared by using datasets, which were collected at two points throughout the phenological year. The correlation of the seasons in-

creased with unit sizes, and more strongly for divergence than richness. Functional richness, as well as functional divergence increased in September, compared to July. This could be explained by the higher values of anthocyanin content. This observation, however, lays the foundation for further observation of changes in functional biodiversity during the course of the phenological year. Different stages of phenology being analyzed through the year could deliver valuable information on the phenology of ecosystems and the changes of functional diversity throughout the year and changes of the phenology of diversity in time lines. Doing so, using anthocyanin content seems even more reasonable, as anthocyanins are also common during the earliest stages of leaf development before the photosystems are fully functional (Gamon and Surfus, 1999; Ustin et al., 2009). Even though phenological development should be visible from chlorophyll, carotenoid and water content alone, adding anthocyanin adds valuable information. Furthermore, information could be gained by analyzing the development of traits and functional diversity throughout the day. In this context, unmanned aerial vehicles offer a lot of potential. They are affordable and suitable for repeated measurements, can be operated autonomously and represent an emerging field in airborne sensing that has the potential to extend and evolve Earth observing disciplines (Houborg, Fisher, and Skidmore, 2015).

4.2.6 Behavior of diversity metrics with neighborhood area

The relation of functional richness and square unit side length in the scale analysis could best be described with the power-law function ($r^2 > 0.99$), which agrees with observations by Schneider et al. (2017) regarding units smaller than 10 ha. The scale analysis of functional richness and the fitted functions are shown in Figure A.19. In order to observe the development at larger scales (units > 16 ha), a larger research area would be necessary, permitting larger unit areas to carry out the scale analysis. Thus, the logarithmic function could be tested for scale analysis in larger units. On the calculated functional diversity maps, a power-law and a logarithmic function were fitted to the mean functional richness for the resampled A20 datasets for different units with diameters up to 800 m, as shown in Figure A.20. At larger units, mean values of richness could be described better by the power-law function. This contrasts observations by Schneider et al. (2017) stating that from a unit size of 10 ha, development of the mean functional richness is described best by a logarithmic function. The observed flattening could be due to redundancy with regard to the functional traits at large scales. However, this redundancy was not observed at lower spatial resolution at the same units areas, but lower number of pixels per area. The missing, logarithmic behavior could be explained by the lower number of pixels and therefore the absence of redundancy at the same units area. The logarithmic behavior of the functional richness may be visible at larger areas, when calculated based on data with lower spatial resolution. The logarithmic behavior of the functional richness could be caused by redundancy in traits at a certain number of pixels per area.

The power-law function $y = a \cdot x^b$ is prominently used to model species-area relationships resulting in a linear function on the log-log scale. The slope of this function varies between ecosystems (exponent b of the power function) (Arrhenius, 1921; Gerstner et al., 2014; Schneider et al.,

2017). Results of Schneider et al. (2017) were similar to large-scale species models for temperate mixed forest, shown by Gerstner et al. (2014). Our results, within-unit functional richness in the scale analysis, showed higher values, as shown in Figure A.19 ($b = 0.4842$ in summer, $b = 0.4418$ in fall). This could probably be explained by only units smaller than 400 m taken into accounts, showing steeper increase at smaller units. Steep curves at smaller scales seem reasonable (Pereira, Borda-De-Água, and Martins, 2012). Larger units were not taken into account for 2 m pixels, due to calculation times. A larger research area could enable larger units and therefore improve the result, delivering a more accurate fit in the scale analysis. On the A20 mean functional richness graph in Figure A.20, the slope of the power function showed even higher values ($b = 0.8032$ in summer, $b = 0.7742$ in fall). This can be explained by the pixels averaging values and small scale information loss, as well as the much higher point of saturation for richness at lower spatial resolution. However, the values at the new scale level should be compared for different ecosystems, as they may show characteristic values for different ecosystems similar to observations by Gerstner et al. (2014). We expect higher values of b for ecosystems with a high level of diversity, such as tropical forests, and low values for ecosystems with low diversity such as boreal forests and deserts.

4.2.7 Outlook

Functional diversity was calculated and compared to randomly generated traits with no measurable auto-correlation. There are probably different reactions to different levels of auto-correlation. Possibly, one could use a scale analysis to deduce the degree of auto-correlation and the spatial scale of the trait or the functional diversity metric, and create different spatial categories. By doing so, one could deduce from the scale analysis the degree of auto-correlation and the scale of variability. As seen in the random model (see Figure A.13), the number of units is important, especially when calculating mean functional divergence. A larger extent of the research area would improve the result, and furthermore give more information on the suitability of the method at larger scales. This is especially needed since we are dealing with a lower spatial resolution. Furthermore, at a unit size of 500 m or higher, a larger research area would be reasonable, as the north-south extent of the research area is hardly larger than 500 m at the smallest distance. Future studies should further focus on the suitability and results of this method in other ecosystems. Ecosystems with more homogeneous forest stands at larger scales could be accessed more easily using satellites. Doing so, new traits should be defined for different ecosystems, in order to deliver reasonable results.

The values and their comparability are strongly dependent on the number of pixels per unit. Approaches, such as the one by Lanaras et al. (2018) of super-resolving arbitrary Sentinel-2 images without the need of retraining could enable the availability of 10 m pixel resolution for Sentinel-2 datasets. Such an improvement in resolution of 10 m pixel size would increase the number of pixels per unit by a factor of four compared to the 20 m resolution used here. This would increase the quality of the calculated diversity metrics by far, as well as decrease the information loss when rescaling to satellite resolution. Functional richness would be much higher and more comparable, as well as functional divergence saturating at smaller unit areas. Furthermore, the appearance and

the influence of mixed-pixels decrease with smaller pixels.

Despite the challenges remaining, this approach is a step towards mapping functional diversity from space. Doing so, satellite remote-sensing offers possibilities of observing biodiversity on a global scale (Skidmore and Pettorelli, 2015; Jetz et al., 2016). Biodiversity in all biomes is sensitive to global changes in environment (Sala et al., 2000). Being able to observe biodiversity continuously in time and space builds the basis for studying impacts, interaction and feedback of global environmental change on ecosystems and biodiversity globally, and especially in remote areas.

5 Conclusion

In this Master thesis we analyzed suitable approaches to transfer functional diversity metrics from airborne to spaceborne platforms. We investigated the influence of different spatial scales, different sensors and different seasons on mapping functional diversity continuously through space. We showed possibilities and limitations of investigated methods and sensors, to highlight suitable pathways and challenges, which have to be tackled in future research.

We identified four traits to describe physiological diversity, namely chlorophyll, anthocyanin, carotenoid, and water content. For all four traits, we selected corresponding indices, that could be applied to Sentinel-2 and APEX data, namely $CI_{red-edge}$, RGR , $PSRI$, and $NDII$. Functional diversity metrics were found to vary on larger scales, compared to the traits alone. Resampling across spatial scales affects those diversity metrics. For example, richness is considerably smaller at lower spatial resolutions. Likewise, divergence decreases and saturates at much larger unit sizes. In short, both metrics were found to be dependent on the number of pixels per unit (ppu). When mapped, some patterns can still be observed and interpreted at lower spatial resolutions, especially using richness. To a basic extent, we observed phenological development of functional traits and diversity metrics in July and September and pointed out the possibilities of observing phenological development of traits and diversity for the interpretation of the ecosystem. Comparing the original dataset with a spatially resampled version and a temporally corresponding satellite observation allowed to us differentiate between scaling and sensor-related influences. Direct comparison of diversity maps derived from datasets with different spatial resolutions is not recommended, but rather a qualitative comparison. We observed overall similar spatial patterns between the 2 m and 20 m resampled APEX datasets. However, this comparison varies, depending on structure, location, stand, mixture and size of the area in question. Mixed pixels play a major role in altering the diversity metrics, which imposes a major limitation on this method. We observe that increasing effects with lower resolution cause an increase in richness and a decrease in divergence. This effect is particularly important regarding the high heterogeneity in our research area. We therefore recommend that future studies could not only focus on the the improvement of the presented approach using new approaches of masking vegetation and including different traits, but on changes of functional traits and functional diversity over time throughout the phenological year or even throughout the day, on scaling effects in multiple different ecosystems and larger homogeneous areas, or on the impact of environmental change on diversity metrics.

Despite the challenges, studying biodiversity on a global scale bears large opportunities to advance research on global change. Once applied, this approach of mapping functional biodiversity enables continuous observations on ecosystem functioning as well as studying impacts of global environmental change on biodiversity continuously in time and space.

Bibliography

- Acker, S. A. et al. (2002). "Trends in bole biomass accumulation, net primary production and tree mortality in *Pseudotsuga menziesii* forests of contrasting age." In: *Tree Physiology* 22.2-3, pp. 213–217. ISSN: 0829-318X. DOI: 10.1093/treephys/22.2-3.213. URL: <https://academic.oup.com/treephys/article-lookup/doi/10.1093/treephys/22.2-3.213>.
- Arrhenius, Olof (1921). "Species and Area." In: *The Journal of Ecology* 9.1, p. 95. ISSN: 00220477. DOI: 10.2307/2255763. URL: <https://www.jstor.org/stable/2255763?origin=crossref>.
- Asner, Gregory P. and Roberta E. Martin (2015). "Spectroscopic remote sensing of non-structural carbohydrates in forest canopies." In: *Remote Sensing* 7.4, pp. 3526–3547. ISSN: 20724292. DOI: 10.3390/rs70403526.
- Asner, Gregory P, Roberta E Martin, and Affendi Bin Suhaili (2012). "Sources of Canopy Chemical and Spectral Diversity in Lowland Bornean Forest." In: *Ecosystems* 15, pp. 504–517. DOI: 10.1007/s10021-012-9526-2.
- Balvanera, Patricia et al. (2006). "Quantifying the evidence for biodiversity effects on ecosystem functioning and services." In: *Ecology Letters* 9.10, pp. 1146–1156. ISSN: 1461023X. DOI: 10.1111/j.1461-0248.2006.00963.x. URL: <http://doi.wiley.com/10.1111/j.1461-0248.2006.00963.x>.
- Bartomeus, Ignasi et al. (2013). "Biodiversity ensures plant-pollinator phenological synchrony against climate change." In: *Ecology Letters* 16.11, pp. 1331–1338. ISSN: 14610248. DOI: 10.1111/ele.12170.
- Bello, Francesco de et al. (2009). "Partitioning of functional diversity reveals the scale and extent of trait convergence and divergence." In: *Journal of Vegetation Science* 20.3, pp. 475–486. ISSN: 11009233. DOI: 10.1111/j.1654-1103.2009.01042.x. URL: <http://doi.wiley.com/10.1111/j.1654-1103.2009.01042.x>.
- Bello, Francesco de et al. (2011). "Quantifying the relevance of intraspecific trait variability for functional diversity." In: *Methods in Ecology and Evolution* 2.2, pp. 163–174. ISSN: 2041210X. DOI: 10.1111/j.2041-210X.2010.00071.x. URL: <http://doi.wiley.com/10.1111/j.2041-210X.2010.00071.x>.
- Brooks, Thomas M et al. (2002). "Habitat Loss and Extinction in the Hotspots of Biodiversity." In: *Brazil's Amazon forest remained largely intact until the "modern" era of deforestation began with the inauguration of the Transamazon Highway in 1970. Amazonian deforestation rates have trended upward since 1991, with clearing proceeding at a variable but* 16.4, pp. 909–923.
- Brooks, Thomas M. et al. (2015). "Harnessing biodiversity and conservation knowledge products to track the Aichi Targets and Sustainable Development Goals." In: *Biodiversity* 16.2-3, pp. 157–174. ISSN: 1488-8386. DOI: 10.1080/14888386.2015.1075903. URL: <http://www.tandfonline.com/doi/full/10.1080/14888386.2015.1075903>.

- Brown, Charles E. (1998). "Coefficient of Variation." In: *Applied Multivariate Statistics in Geohydrology and Related Sciences*. Berlin, Heidelberg: Springer Berlin Heidelberg, pp. 155–157. DOI: 10.1007/978-3-642-80328-4_{_}13. URL: http://www.springerlink.com/index/10.1007/978-3-642-80328-4_13.
- Buchanan-Wollaston, Vicky (1997). "The molecular biology of leaf senescence." In: *Journal of Experimental Botany* 48.307, pp. 181–199.
- Cadotte, Marc W., Kelly Carscadden, and Nicholas Mirotnick (2011). "Beyond species: Functional diversity and the maintenance of ecological processes and services." In: *Journal of Applied Ecology* 48.5, pp. 1079–1087. ISSN: 00218901. DOI: 10.1111/j.1365-2664.2011.02048.x.
- Cardinale, Bradley J. et al. (2013). "Biodiversity simultaneously enhances the production and stability of community biomass, but the effects are independent." In: *Ecology* 94.8, pp. 1697–1707. ISSN: 0012-9658. DOI: 10.1890/12-1334.1. URL: <http://doi.wiley.com/10.1890/12-1334.1>.
- Chen, Xiang et al. (2018). "The mixed pixel effect in land surface phenology: A simulation study." In: *Remote Sensing of Environment* 211. June 2017, pp. 338–344. ISSN: 00344257. DOI: 10.1016/j.rse.2018.04.030.
- Clevers, Jan et al. (2017). "Using Sentinel-2 Data for Retrieving LAI and Leaf and Canopy Chlorophyll Content of a Potato Crop." In: *Remote Sensing* 9.5, p. 405. ISSN: 2072-4292. DOI: 10.3390/rs9050405. URL: <http://www.mdpi.com/2072-4292/9/5/405>.
- Clevers, J.G.P.W. and A.A. Gitelson (2013). "Remote estimation of crop and grass chlorophyll and nitrogen content using red-edge bands on Sentinel-2 and -3." In: *International Journal of Applied Earth Observation and Geoinformation* 23, pp. 344–351. DOI: 10.1016/J.JAG.2012.10.008. URL: <https://www.sciencedirect.com/science/article/pii/S0303243412002097#bib0075>.
- Cornelissen, J. H.C. et al. (2003). *A handbook of protocols for standardised and easy measurement of plant functional traits worldwide*. DOI: 10.1071/BT02124. URL: www.publish.csiro.au/journals/ajb.
- Cusson, Mathieu et al. (2015). "Relationships between biodiversity and the stability of marine ecosystems: Comparisons at a European scale using meta-analysis." In: *Journal of Sea Research* 98, pp. 5–14. DOI: 10.1016/j.seares.2014.08.004. URL: <http://linkinghub.elsevier.com/retrieve/pii/S1385110114001609>.
- Dalponte, Michele et al. (2018). "Predicting stem diameters and aboveground biomass of individual trees using remote sensing data." In: *Ecological Indicators* 85, pp. 367–376. ISSN: 1470-160X. DOI: 10.1016/J.ECOLIND.2017.10.066. URL: <https://www.sciencedirect.com/science/article/pii/S1470160X17307033>.
- Dash, J. and P.J. Curran (2007). "Evaluation of the MERIS terrestrial chlorophyll index (MTCI)." In: *Advances in Space Research* 39.1, pp. 100–104. DOI: 10.1016/J.ASR.2006.02.034. URL: <https://www.sciencedirect.com/science/article/pii/S0273117706000834>.
- Daughtry, C.S.T et al. (2000). "Estimating Corn Leaf Chlorophyll Concentration from Leaf and Canopy Reflectance." In: *Remote Sensing of Environment* 74.2, pp. 229–239. DOI: 10.1016/S0034-4257(00)00113-9. URL: <https://www.sciencedirect.com/science/article/pii/S0034425700001139#TBL1>.
- Day, M. E., M. S. Greenwood, and A. S. White (2001). "Age-related changes in foliar morphology and physiology in red spruce and their influence on declining photosynthetic rates and productivity with tree age." In: *Tree Physiology* 21.16, pp. 1195–1204. ISSN: 0829-318X. DOI: 10.1093/

- treephys/21.16.1195. URL: <https://academic.oup.com/treephys/article-lookup/doi/10.1093/treephys/21.16.1195>.
- Demarez, V et al. (1999). "Seasonal variation of leaf chlorophyll content of a temperate forest. Inversion of the prospect model." In: *International Journal of Remote Sensing* 20.5, pp. 879–894. ISSN: 13665901. DOI: 10.1080/014311699212975. URL: <http://www.tandfonline.com/action/journalInformation?journalCode=tres20>.
- Dhindsa, Rajinder S, Pamela Plumb-Dhindsa, and Trevor A Thorpe (1981). "Leaf Senescence: Correlated with Increased Levels of Membrane Permeability and Lipid Peroxidation, and Decreased Levels of Superoxide Dismutase and Catalase." In: *Journal of Experimental Botany* 32.126, pp. 93–101. URL: https://oup.silverchair-cdn.com/oup/backfile/Content_public/Journal/jxb/32/1/10.1093/jxb/32.1.93/2/32-1-93.pdf.
- Dotzler, Sandra et al. (2015). "The Potential of EnMAP and Sentinel-2 Data for Detecting Drought Stress Phenomena in Deciduous Forest Communities." In: *Remote Sensing* 7.10, pp. 14227–14258. DOI: 10.3390/rs71014227. URL: <http://www.mdpi.com/2072-4292/7/10/14227>.
- Drusch, M. et al. (2012). "Sentinel-2: ESA's Optical High-Resolution Mission for GMES Operational Services." In: *Remote Sensing of Environment* 120, pp. 25–36. ISSN: 0034-4257. DOI: 10.1016/J.RSE.2011.11.026. URL: <https://www.sciencedirect.com/science/article/pii/S0034425712000636#t0005>.
- Ensminger, Ingo et al. (2004). "Intermittent low temperatures constrain spring recovery of photosynthesis in boreal Scots pine forests." In: *Global Change Biology* 10.6, pp. 995–1008. ISSN: 13541013. DOI: 10.1111/j.1365-2486.2004.00781.x. URL: <http://doi.wiley.com/10.1111/j.1365-2486.2004.00781.x>.
- ESA (2017). *Sentinel-2 MSI*. URL: <https://earth.esa.int/web/sentinel/user-guides/sentinel-2-msi>.
- Eugster, W et al. (2007). "Methodical study of nitrous oxide eddy covariance measurements using quantum cascade laser spectrometry over a Swiss forest." In: *Biogeosciences* 4.5, pp. 927–939. ISSN: 17264189. DOI: 10.5194/bg-4-927-2007. URL: www.biogeosciences.net/4/927/2007/.
- FAO (2018). *The state of the world's forests*. Tech. rep. URL: www.fao.org/publications.
- Fearnside, Philip M (2005). "Deforestation in Brazilian Amazonia : History , Rates , and Consequences." In: *Conservation Biology* 19.3, pp. 680–688.
- Finegan, Bryan (1984). "Forest succession." In: *Nature* 312.5990, pp. 109–114. ISSN: 0028-0836. DOI: 10.1038/312109a0. URL: <http://www.nature.com/articles/312109a0>.
- Gamon, J. A. and J. S. Surfus (1999). "Assessing leaf pigment content and activity with a reflectometer." In: *New Phytologist* 143.1, pp. 105–117. ISSN: 0028646X. DOI: 10.1046/j.1469-8137.1999.00424.x. URL: <http://doi.wiley.com/10.1046/j.1469-8137.1999.00424.x>.
- Gamon, John A et al. (2016). "A remotely sensed pigment index reveals photosynthetic phenology in evergreen conifers." In: *Proceedings of the National Academy of Sciences of the United States of America* 113.46, pp. 13087–13092. ISSN: 1091-6490. DOI: 10.1073/pnas.1606162113. URL: <http://www.ncbi.nlm.nih.gov/pubmed/27803333><http://www.pubmedcentral.nih.gov/articlerender.fcgi?artid=PMC5135292>.
- Gerstner, Katharina et al. (2014). "Accounting for geographical variation in species-area relationships improves the prediction of plant species richness at the global scale." In: *Journal of Biogeog-*

- raphy* 41.2. Ed. by Peter Pearman, pp. 261–273. ISSN: 03050270. DOI: 10.1111/jbi.12213. URL: <http://doi.wiley.com/10.1111/jbi.12213>.
- GIS-ZH (2018). *Das Geografische Informationssystem des Kantons Zürich*. URL: www.gis.zh.ch.
- Gitelson, A. A., O. B. Chivkunova, and M. N. Merzlyak (2009). “Nondestructive estimation of anthocyanins and chlorophylls in anthocyanic leaves.” In: *American Journal of Botany* 96.10, pp. 1861–1868. DOI: 10.3732/ajb.0800395. URL: <http://doi.wiley.com/10.3732/ajb.0800395>.
- Gitelson, Anatoly A. (2004). “Wide Dynamic Range Vegetation Index for Remote Quantification of Biophysical Characteristics of Vegetation.” In: *Journal of Plant Physiology* 161.2, pp. 165–173. ISSN: 0176-1617. DOI: 10.1078/0176-1617-01176. URL: <https://www.sciencedirect.com/science/article/pii/S0176161704705726>.
- Goodwin, T W (1958). “Studies in carotenogenesis. 24. The changes in carotenoid and chlorophyll pigments in the leaves of deciduous trees during autumn necrosis.” In: *The Biochemical journal* 68.3, pp. 503–11. URL: <http://www.ncbi.nlm.nih.gov/pubmed/13522652>.
- Grimm, Bernhard (2001). “Chlorophyll : Structure and Function.” In: *Encyclopedia of life sciences*. John Wiley & Sons. DOI: <http://dx.doi.org/10.1038/npg.els.0001310>.
- Grotzinger, J. et al. (2008). *Understanding Earth*. 5th ed. W. H. Freeman and Company. ISBN: 978-3-8274-1812-8.
- Haboudane, Driss et al. (2002). “Integrated narrow-band vegetation indices for prediction of crop chlorophyll content for application to precision agriculture.” In: *Remote Sensing of Environment* 81.2-3, pp. 416–426. DOI: 10.1016/S0034-4257(02)00018-4. URL: <https://www.sciencedirect.com/science/article/pii/S0034425702000184>.
- Hanfrey, Colin, Mark Fife, and Vicky Buchanan-Wollaston (1996). “Leaf senescence in *Brassica napus*: expression of genes encoding pathogenesis-related proteins.” In: *Plant Molecular Biology* 30, pp. 597–609. URL: <https://link.springer.com/content/pdf/10.1007%2F00049334.pdf>.
- Harley, Christopher D G (2011). “Climate change, keystone predation, and biodiversity loss.” In: *Science* 334.6059, pp. 1124–1127. ISSN: 10959203. DOI: 10.1126/science.1210199. URL: <http://www.ncbi.nlm.nih.gov/pubmed/22116885>.
- Hautier, Yann et al. (2015). “Anthropogenic environmental changes affect ecosystem stability via biodiversity.” In: *Science* 348.6232. URL: <http://science.sciencemag.org/content/348/6232/336>.
- Havaux, Michel (2014). “Carotenoid oxidation products as stress signals in plants.” In: *The Plant Journal* 79.4, pp. 597–606. ISSN: 09607412. DOI: 10.1111/tpj.12386. URL: <http://doi.wiley.com/10.1111/tpj.12386>.
- Hector, Andy and Robert Bagchi (2007). “Biodiversity and ecosystem multifunctionality.” In: *Nature* 448.7150, pp. 188–190. ISSN: 0028-0836. DOI: 10.1038/nature05947. URL: <http://www.nature.com/articles/nature05947>.
- Henebry, Geoffrey M. and Kirsten M. De Beurs (2013). “Remote Sensing of Land Surface Phenology: A Prospectus.” In: *Phenology: An Integrative Environmental Science*. Vol. 9789400769. Chap. 21, pp. 1–610. ISBN: 9789400769250. DOI: 10.1007/978-94-007-6925-0.

- Herms, Daniel A. and William J. Mattson (1992). "The Dilemma of Plants: To Grow or Defend." In: *The Quarterly Review of Biology* 67.3, pp. 283–335. ISSN: 0033-5770. DOI: 10.1086/417659. URL: <https://www.journals.uchicago.edu/doi/10.1086/417659>.
- Hill, Michael J. (2013). "Vegetation index suites as indicators of vegetation state in grassland and savanna: An analysis with simulated SENTINEL 2 data for a North American transect." In: *Remote Sensing of Environment* 137, pp. 94–111. ISSN: 0034-4257. DOI: 10.1016/J.RSE.2013.06.004. URL: <https://www.sciencedirect.com/science/article/pii/S0034425713001971#t0005>.
- Homolová, Lucie (2014). "Imaging spectroscopy for ecological analysis in forest and grassland ecosystems." In: URL: <http://library.wur.nl/WebQuery/wurpubs/fulltext/287261>.
- Houborg, Rasmus, Joshua B. Fisher, and Andrew K. Skidmore (2015). "Advances in remote sensing of vegetation function and traits." In: *International Journal of Applied Earth Observation and Geoinformation* 43, pp. 1–6. ISSN: 1872826X. DOI: 10.1016/j.jag.2015.06.001.
- Hsieh, Pi Fuei, Lou C. Lee, and Nai Yu Chen (2001). "Effect of spatial resolution on classification errors of pure and mixed pixels in remote sensing." In: *IEEE Transactions on Geoscience and Remote Sensing* 39.12, pp. 2657–2663. ISSN: 01962892. DOI: 10.1109/36.975000.
- Hueni, A. et al. (2009). "Structure, Components, and Interfaces of the Airborne Prism Experiment (APEX) Processing and Archiving Facility." In: *IEEE Transactions on Geoscience and Remote Sensing* 47.1, pp. 29–43. ISSN: 0196-2892. DOI: 10.1109/TGRS.2008.2005828. URL: <http://ieeexplore.ieee.org/document/4694063/>.
- Hueni, Andreas et al. (2017). "Field and Airborne Spectroscopy Cross Validation -Some Considerations." In: *IEEE Journal of Selected Topics in Applied Earth Observations and Remote Sensing* 10.3, pp. 1117–1135. ISSN: 21511535. DOI: 10.1109/JSTARS.2016.2593984.
- Huete, A et al. (2002). "Overview of the radiometric and biophysical performance of the MODIS vegetation indices." In: *Remote Sensing of Environment* 83.1-2, pp. 195–213. ISSN: 00344257. DOI: 10.1016/S0034-4257(02)00096-2. URL: <http://www.sciencedirect.com/science/article/pii/S0034425702000962>.
- Huete, A.R., HuiQing Liu, and W.J.D. van Leeuwen (1997). "The use of vegetation indices in forested regions: issues of linearity and saturation." In: *IGARSS'97. 1997 IEEE International Geoscience and Remote Sensing Symposium Proceedings. Remote Sensing - A Scientific Vision for Sustainable Development*. Vol. 4. IEEE, pp. 1966–1968. ISBN: 0-7803-3836-7. DOI: 10.1109/IGARSS.1997.609169. URL: <http://ieeexplore.ieee.org/document/609169/>.
- IPCC (2013). *Summary for Policymakers*. In: *Climate Change 2013: The Physical Science Basis. Contribution of Working Group I to the Fifth Assessment Report of the Intergovernmental Panel on Climate Change*. Tech. rep., pp. 1–29. DOI: 10.1017/CB09781107415324. URL: <http://medcontent.metapress.com/index/A65RM03P4874243N.pdf>.
- Jactel, Hervé and Eckehard G. Brockerhoff (2007). "Tree diversity reduces herbivory by forest insects." In: *Ecology Letters* 10.9, pp. 835–848. ISSN: 1461-023X. DOI: 10.1111/j.1461-0248.2007.01073.x. URL: <http://doi.wiley.com/10.1111/j.1461-0248.2007.01073.x>.
- Jay, Sylvain et al. (2017). "Estimating leaf chlorophyll content in sugar beet canopies using millimeter-to centimeter-scale reflectance imagery." In: *Remote Sensing of Environment* 198, pp. 173–186. DOI: <https://doi.org/10.1016/j.rse.2017.06.008>.

- Jetz, Walter et al. (2016). "Monitoring plant functional diversity from space." In: *Nature Plants* 2.3, pp. 1–5. ISSN: 2055-0278. DOI: 10.1038/nplants.2016.24. URL: <http://www.nature.com/articles/nplants201624>.
- Jiang, Z et al. (2008). "Development of a two-band enhanced vegetation index without a blue band." In: *Remote Sensing of Environment* 112.10, pp. 3833–3845. ISSN: 00344257. DOI: 10.1016/j.rse.2008.06.006. URL: <http://linkinghub.elsevier.com/retrieve/pii/S0034425708001971>.
- Jones, Hamlyn and Xavier Sirault (2014). "Scaling of Thermal Images at Different Spatial Resolution: The Mixed Pixel Problem." In: *Agronomy* 4.3, pp. 380–396. ISSN: 2073-4395. DOI: 10.3390/agronomy4030380. URL: <http://www.mdpi.com/2073-4395/4/3/380/>.
- Jucker, Tommaso et al. (2014). "Stabilizing effects of diversity on aboveground wood production in forest ecosystems: Linking patterns and processes." In: *Ecology Letters* 17.12, pp. 1560–1569. ISSN: 14610248. DOI: 10.1111/ele.12382.
- Karadimou, Elpida K. et al. (2016). "Functional diversity exhibits a diverse relationship with area, even a decreasing one." In: *Scientific Reports* 6.1, p. 35420. ISSN: 2045-2322. DOI: 10.1038/srep35420. URL: <http://www.nature.com/articles/srep35420>.
- Kattge, J. et al. (2011). "TRY - a global database of plant traits." In: *Global Change Biology* 17.9, pp. 2905–2935. ISSN: 13541013. DOI: 10.1111/j.1365-2486.2011.02451.x. URL: <http://doi.wiley.com/10.1111/j.1365-2486.2011.02451.x>.
- Knaeps, E. et al. (2012). "In situ evidence of non-zero reflectance in the OLCI 1020 nm band for a turbid estuary." In: *Remote Sensing of Environment* 120, pp. 133–144. ISSN: 0034-4257. DOI: 10.1016/J.RSE.2011.07.025. URL: <https://www.sciencedirect.com/science/article/pii/S0034425712000727>.
- Kokaly, Raymond F and Andrew K Skidmore (2015). "International Journal of Applied Earth Observation and Geoinformation Plant phenolics and absorption features in vegetation reflectance spectra near 1.66 μm." In: *International Journal of Applied Earth Observations and Geoinformation* 43, pp. 55–83. ISSN: 0303-2434. DOI: 10.1016/j.jag.2015.01.010. URL: <http://dx.doi.org/10.1016/j.jag.2015.01.010>.
- Kooistra, Lammert and Jan G.P.W. Clevers (2016). "Estimating potato leaf chlorophyll content using ratio vegetation indices." In: *Remote Sensing Letters* 7.6, pp. 611–620. ISSN: 21507058. DOI: 10.1080/2150704X.2016.1171925. URL: <http://dx.doi.org/10.1080/2150704X.2016.1171925>.
- Korhonen, Lauri et al. (2017). "Comparison of Sentinel-2 and Landsat 8 in the estimation of boreal forest canopy cover and leaf area index." In: *Remote Sensing of Environment* 195, pp. 259–274. ISSN: 00344257. DOI: 10.1016/j.rse.2017.03.021. URL: <http://www.sciencedirect.com/science/article/pii/S0034425717301256>.
- Koukoulas, S. and G. A. Blackburn (2004). "Quantifying the spatial properties of forest canopy gaps using LiDAR imagery and GIS." In: *International Journal of Remote Sensing* 25.15, pp. 3049–3072. DOI: 10.1080/01431160310001657786. URL: <https://www.tandfonline.com/doi/full/10.1080/01431160310001657786>.
- Lanaras, Charis et al. (2018). "Super-resolution of Sentinel-2 images: Learning a globally applicable deep neural network." In: *ISPRS Journal of Photogrammetry and Remote Sensing* 146, pp. 305–319. ISSN: 09242716. DOI: 10.1016/j.isprsjprs.2018.09.018.

- Laureto, Livia Maira Orlandi, Marcus Vinicius Cianciaruso, and Diogo Soares Menezes Samia (2015). "Functional diversity: an overview of its history and applicability." In: *Natureza & Conservação* 13.2, pp. 112–116. ISSN: 1679-0073. DOI: 10.1016/J.NCON.2015.11.001. URL: <https://www.sciencedirect.com/science/article/pii/S1679007315000390>.
- Lewandowska, M. and P. G. Jarvis (1977). "Changes in chlorophyll and carotenoid content, specific leaf area and dry weight fraction in Sitka Spruce, in response to shading and season." In: *New Phytologist* 79, pp. 247–256. URL: <https://nph.onlinelibrary.wiley.com/doi/pdf/10.1111/j.1469-8137.1977.tb02202.x>.
- Leys, Christophe et al. (2013). "Detecting outliers: Do not use standard deviation around the mean, use absolute deviation around the median." In: *Journal of Experimental Social Psychology* 49.4, pp. 764–766. ISSN: 0022-1031. DOI: 10.1016/J.JESP.2013.03.013. URL: <https://www.sciencedirect.com/science/article/pii/S0022103113000668>.
- Lillesand, Thomas, Ralph W. Kiefer, and Jonathan Chipman (2015). *Remote Sensing and Image Interpretation*. 7th. John Wiley & Sons.
- Liu, Wen and Fumio Yamazaki (2012). "Object-based shadow extraction and correction of high-resolution optical satellite images." In: *IEEE Journal of Selected Topics in Applied Earth Observations and Remote Sensing* 5.4, pp. 1296–1302. ISSN: 19391404. DOI: 10.1109/JSTARS.2012.2189558.
- Liu, Xiaojuan et al. (2016). "Linking individual-level functional traits to tree growth in a subtropical forest." In: *Ecology* 97.9, pp. 2396–2405. ISSN: 00129658. DOI: 10.1002/ecy.1445.
- Loehle, Craig (1988). "Tree life history strategies: the role of defenses." In: *Canadian Journal of Forest Research* 18.2, pp. 209–222. ISSN: 0045-5067. DOI: 10.1139/x88-032. URL: <http://www.nrcresearchpress.com/doi/10.1139/x88-032>.
- Loreau, M et al. (2001). "Biodiversity and ecosystem functioning: current knowledge and future challenges." In: *Science (New York, N.Y.)* 294.5543, pp. 804–8. ISSN: 0036-8075. DOI: 10.1126/science.1064088. URL: <http://www.ncbi.nlm.nih.gov/pubmed/11679658>.
- Loreau, Michel et al. (2003). *Biodiversity as spatial insurance in heterogeneous landscapes*. Tech. rep. URL: www.pnas.org/cgi/doi/10.1073/pnas.2235465100.
- Lukito, Hasta Pratopo, Kenji Kouno, and Tadao Ando (1998). "Phosphorus requirements of microbial biomass in a regosol and an andosol." In: *Soil Biology and Biochemistry* 30.7, pp. 865–872. ISSN: 0038-0717. DOI: 10.1016/S0038-0717(98)00011-X. URL: <https://www.sciencedirect.com/science/article/pii/S003807179800011X>.
- Maire, Eva et al. (2015). "How many dimensions are needed to accurately assess functional diversity? A pragmatic approach for assessing the quality of functional spaces." In: *Global Ecology and Biogeography* 24.6, pp. 728–740. ISSN: 1466822X. DOI: 10.1111/geb.12299. URL: <http://doi.wiley.com/10.1111/geb.12299>.
- Martin, M. E. et al. (2008). "A generalizable method for remote sensing of canopy nitrogen across a wide range of forest ecosystems." In: *Remote Sensing of Environment* 112.9, pp. 3511–3519. ISSN: 00344257. DOI: 10.1016/j.rse.2008.04.008.
- Mason, Norman W.H. et al. (2005). "Functional richness, functional evenness and functional divergence: The primary components of functional diversity." In: *Oikos* 111.1, pp. 112–118. ISSN: 00301299. DOI: 10.1111/j.0030-1299.2005.13886.x. URL: <http://doi.wiley.com/10.1111/j.0030-1299.2005.13886.x>.

- Matias, Miguel G. et al. (2013). "Ecological strategies shape the insurance potential of biodiversity." In: *Frontiers in Microbiology* 3, p. 432. ISSN: 1664-302X. DOI: 10.3389/fmicb.2012.00432. URL: <http://journal.frontiersin.org/article/10.3389/fmicb.2012.00432/abstract>.
- Matsushita, Bunkei et al. (2007). "Sensitivity of the Enhanced Vegetation Index (EVI) and Normalized Difference Vegetation Index (NDVI) to Topographic Effects: A Case Study in High-density Cypress Forest." In: *Sensors* 7.11, pp. 2636–2651. DOI: 10.3390/s7112636. URL: <http://www.mdpi.com/1424-8220/7/11/2636>.
- Menzel, Annette (2002). "Phenology: Its Importance to the Global Change Community." en. In: *Climatic Change* 54.4, pp. 379–385. ISSN: 1573-1480. URL: <http://link.springer.com/article/10.1023/A%3A1016125215496>.
- Merzlyak, Mark N, Alexei E Solovchenko, and Anatoly A Gitelson (2003). "Reflectance spectral features and non-destructive estimation of chlorophyll, carotenoid and anthocyanin content in apple fruit." In: *Postharvest Biology and Technology* 27.2, pp. 197–211. ISSN: 09255214. DOI: 10.1016/S0925-5214(02)00066-2. URL: <http://linkinghub.elsevier.com/retrieve/pii/S0925521402000662>.
- MeteoSwiss (2016). *Swiss phenology network*. URL: <http://www.meteoswiss.admin.ch/home/measurement-and-forecasting-systems/land-based-stations/swiss-phenology-network.html>.
- Morin, Xavier et al. (2011). "Tree species richness promotes productivity in temperate forests through strong complementarity between species." In: *Ecology Letters* 14.12, pp. 1211–1219. ISSN: 1461023X. DOI: 10.1111/j.1461-0248.2011.01691.x. URL: <http://doi.wiley.com/10.1111/j.1461-0248.2011.01691.x>.
- Morin, Xavier et al. (2014). "Temporal stability in forest productivity increases with tree diversity due to asynchrony in species dynamics." In: *Ecology Letters* 17.12, pp. 1526–1535. ISSN: 14610248. DOI: 10.1111/ele.12357.
- Mutanga, O. and L. Kumar (2007). "Estimating and mapping grass phosphorus concentration in an African savanna using hyperspectral image data." In: *International Journal of Remote Sensing* 28.21, pp. 4897–4911. ISSN: 13665901. DOI: 10.1080/01431160701253253.
- Nagendra, Harini and Duccio Rocchini (2008). "High resolution satellite imagery for tropical biodiversity studies: The devil is in the detail." In: *Biodiversity and Conservation* 17.14, pp. 3431–3442. ISSN: 09603115. DOI: 10.1007/s10531-008-9479-0.
- Nagler, Pamela L et al. (2003). "Cellulose absorption index (CAI) to quantify mixed soil–plant litter scenes." In: *Remote Sensing of Environment* 87.2-3, pp. 310–325. DOI: 10.1016/J.RSE.2003.06.001. URL: <https://www.sciencedirect.com/science/article/pii/S0034425703001883>.
- Obeso, Jose Ramon (2002). "The costs of reproduction in plants." In: *New Phytologist* 155.3, pp. 321–348. ISSN: 0028-646X. DOI: 10.1046/j.1469-8137.2002.00477.x. URL: <http://doi.wiley.com/10.1046/j.1469-8137.2002.00477.x>.
- Pandit, M. K. et al. (2007). "Unreported yet massive deforestation driving loss of endemic biodiversity in Indian Himalaya." In: *Biodiversity and Conservation* 16.1, pp. 153–163. ISSN: 0960-3115. DOI: 10.1007/s10531-006-9038-5. URL: <http://link.springer.com/10.1007/s10531-006-9038-5>.

- Peng, Yi and Anatoly A. Gitelson (2011). "Application of chlorophyll-related vegetation indices for remote estimation of maize productivity." In: *Agricultural and Forest Meteorology* 151.9, pp. 1267–1276. ISSN: 0168-1923. DOI: 10.1016/J.AGRFORMET.2011.05.005. URL: <https://www.sciencedirect.com/science/article/pii/S0168192311001493>.
- Penuelas, J, F Baret, and I Filella (1995). *Semi-empirical indices to assess carotenoids/chlorophyll a ratio from leaf spectral reflectance*. URL: <http://scholar.google.com/scholar?hl=en&btnG=Search&q=intitle:Semi-empirical+indices+to+assess+carotenoids/chlorophyll+a+ratio+from+leaf+spectral+reflectance#0>.
- Pereira, H M et al. (2013). "Ecology. Essential biodiversity variables." en. In: *Science (New York, N.Y.)* 339.6117, pp. 277–278. ISSN: 1095-9203. URL: <http://science.sciencemag.org/content/339/6117/277.abstract>.
- Pereira, Henrique Miguel, Luís Borda-De-Água, and Inês Santos Martins (2012). "Geometry and scale in species-area relationships." In: *Nature* 482.7386, E3–E4. ISSN: 00280836. DOI: 10.1038/nature10857. URL: <http://www.nature.com/doi/10.1038/nature10857>.
- Pérez-Harguindeguy, N. et al. (2013). "New handbook for standardised measurement of plant functional traits worldwide." In: *Australian Journal of Botany* 61.3, p. 167. ISSN: 0067-1924. DOI: 10.1071/BT12225. URL: <http://www.publish.csiro.au/?paper=BT12225>.
- Pettorelli, Nathalie et al. (2016). "Framing the concept of satellite remote sensing essential biodiversity variables: challenges and future directions." In: *Remote Sensing in Ecology and Conservation* 2.3. Ed. by Doreen Boyd, pp. 122–131. ISSN: 20563485. DOI: 10.1002/rse2.15. URL: <http://doi.wiley.com/10.1002/rse2.15>.
- Polley, H Wayne et al. (2013). "Plant functional traits improve diversity-based predictions of temporal stability of grassland productivity." In: *Oikos* 122.9, pp. 1275–1282. DOI: 10.1111/j.1600-0706.2013.00338.x. URL: http://sustainingnature.org/wp-content/uploads/2014/02/Polley_etal2013.pdf.
- Richter, R. and D. Schläpfer (2017). "Atmospheric / Topographic Correction for Satellite Imagery (ATCOR - 2/3 User Guide)." In: *ATCOR-2/3 User Guide, Version 9.1.2* January, pp. 1–71. ISSN: 1098-6596. DOI: 10.1017/CB09781107415324.004.
- Rufenacht, Dominic, Clement Fredembach, and Sabine Susstrunk (2014). "Automatic and accurate shadow detection using near-infrared information." In: *IEEE Transactions on Pattern Analysis and Machine Intelligence* 36.8, pp. 1672–1678. ISSN: 01628828. DOI: 10.1109/TPAMI.2013.229.
- Sala, Osvaldo E et al. (2000). "Global Biodiversity Scenarios for the Year 2100." In: *Science's Compass* 287.March, pp. 1770–1775.
- Schaepman, Michael E. et al. (2015). "Advanced radiometry measurements and Earth science applications with the Airborne Prism Experiment (APEX)." In: *Remote Sensing of Environment* 158, pp. 207–219. ISSN: 0034-4257. DOI: 10.1016/J.RSE.2014.11.014. URL: <https://www.sciencedirect.com/science/article/pii/S0034425714004568>.
- Schläpfer, D. and R. Richter (2002). "Geo-atmospheric processing of airborne imaging spectrometry data. Part 1: Parametric orthorectification." In: *International Journal of Remote Sensing* 23.13, pp. 2609–2630. ISSN: 0143-1161. DOI: 10.1080/01431160110115825. URL: <https://www.tandfonline.com/doi/full/10.1080/01431160110115825>.

- Schneider, Fabian D. et al. (2017). "Mapping functional diversity from remotely sensed morphological and physiological forest traits." In: *Nature Communications* 8.1, p. 1441. ISSN: 2041-1723. DOI: 10.1038/s41467-017-01530-3. URL: <http://www.nature.com/articles/s41467-017-01530-3>.
- Scholtz, Rheinhardt et al. (2018). "Quantifying variance across spatial scales as part of fire regime classifications." In: *Ecosphere* 9.7, e02343. ISSN: 21508925. DOI: 10.1002/ecs2.2343. URL: <http://doi.wiley.com/10.1002/ecs2.2343>.
- Silva Pedro, Mariana, Werner Rammer, and Rupert Seidl (2015). "Tree species diversity mitigates disturbance impacts on the forest carbon cycle." In: *Oecologia* 177.3, pp. 619–630. ISSN: 0029-8549. DOI: 10.1007/s00442-014-3150-0. URL: <http://link.springer.com/10.1007/s00442-014-3150-0>.
- Sims, Daniel A and John A Gamon (2002). "Relationships between leaf pigment content and spectral reflectance across a wide range of species, leaf structures and developmental stages." In: *Remote Sensing of Environment* 81.2-3, pp. 337–354. DOI: 10.1016/S0034-4257(02)00010-X. URL: <https://www.sciencedirect.com/science/article/pii/S003442570200010X>.
- Skidmore, Andrew K. and Nathalie Pettorelli (2015). "Agree on biodiversity metrics to track from space: ecologists and space agencies must forge a global monitoring strategy." In: *Nature* 523.7561, pp. 403–406. ISSN: 00280836. URL: <http://go.galegroup.com/ps/anonymou?id=GALE%7CA423049271&sid=googleScholar&v=2.1&it=r&linkaccess=abs&issn=00280836&p=AONE&sw=w>.
- Sodhi, Navjot S. et al. (2004). "Southeast Asian biodiversity: an impending disaster." In: *Trends in Ecology & Evolution* 19.12, pp. 654–660. ISSN: 0169-5347. DOI: 10.1016/J.TREE.2004.09.006. URL: <https://www.sciencedirect.com/science/article/pii/S0169534704002666>.
- Song, Conghe (2013). "Optical remote sensing of forest leaf area index and biomass." In: *Progress in Physical Geography* 37.1, pp. 98–113. ISSN: 0309-1333. DOI: 10.1177/0309133312471367. URL: <http://journals.sagepub.com/doi/10.1177/0309133312471367>.
- Srinivasan, Shruthi et al. (2015). "Terrestrial Laser Scanning as an Effective Tool to Retrieve Tree Level Height, Crown Width, and Stem Diameter." In: *Remote Sensing* 7.2, pp. 1877–1896. ISSN: 2072-4292. DOI: 10.3390/rs70201877. URL: <http://www.mdpi.com/2072-4292/7/2/1877>.
- Tilman, David, Forest Isbell, and Jane M. Cowles (2014). "Biodiversity and Ecosystem Functioning." In: *Annual Review of Ecology, Evolution, and Systematics* 45.1, pp. 471–493. ISSN: 1543-592X. DOI: 10.1146/annurev-ecolsys-120213-091917. URL: <http://www.annualreviews.org/doi/10.1146/annurev-ecolsys-120213-091917>.
- Tilman, David et al. (1997). "The Influence of Functional Diversity and Composition on Ecosystem Processes." In: *Science* 277.August, pp. 1300–1302.
- Tittensor, Derek P et al. (2014). "A mid-term analysis of progress toward international biodiversity targets." In: *Science (New York, N.Y.)* 346.6206, pp. 241–4. ISSN: 1095-9203. DOI: 10.1126/science.1257484. URL: <http://www.ncbi.nlm.nih.gov/pubmed/25278504>.
- Tsianou, Mariana A. and Athanasios S. Kallimanis (2016). "Different species traits produce diverse spatial functional diversity patterns of amphibians." In: *Biodiversity and Conservation* 25.1, pp. 117–132. ISSN: 15729710. DOI: 10.1007/s10531-015-1038-x.

- Tucker, C. J. and P. J. Sellers (1986). "Satellite remote sensing of primary production." In: *International Journal of Remote Sensing* 7.11, pp. 1395–1416. DOI: 10.1080/01431168608948944. URL: <http://www.tandfonline.com/doi/abs/10.1080/01431168608948944>.
- Ustin, Susan L. and John A. Gamon (2010). "Remote sensing of plant functional types." In: *New Phytologist* 186.4, pp. 795–816. ISSN: 0028646X. DOI: 10.1111/j.1469-8137.2010.03284.x. URL: <http://doi.wiley.com/10.1111/j.1469-8137.2010.03284.x>.
- Ustin, Susan L et al. (2009). "Retrieval of Foliar Information about Plant Pigment Systems from High Resolution Spectroscopy." In: p. 165. DOI: 10.1016/j.r. URL: <http://digitalcommons.unl.edu/natrespapers/165>.
- Verein GLOBE Schweiz (2017a). *PhaenoNet*. URL: <https://phaenonet.ch/de/>.
- (2017b). *Photo Instruction Fagus sylvatica*. URL: <https://www.globe-swiss.ch/files/Downloads/967/Download/FotoanleitungBuche.pdf>.
- Villéger, Mason, and Mouillot (2008). "New multidimensional functional diversity indices for a multifaceted framework in functional ecology." In: *Ecology* 89.8, pp. 2290–2301. ISSN: 00129658. DOI: 10.1890/07-1206.1.
- Violle, Cyrille et al. (2007). "Let the concept of trait be functional!" In: *Oikos* 116, pp. 882–892. ISSN: 18825176. DOI: doi:10.1111/j.2007.0030-1299.15559.x.
- Violle, Cyrille et al. (2012). "The return of the variance: intraspecific variability in community ecology." In: *Trends in Ecology & Evolution* 27.4, pp. 244–252. ISSN: 0169-5347. DOI: 10.1016/J.TREE.2011.11.014. URL: <https://www.sciencedirect.com/science/article/pii/S0169534711003375>.
- Vuolo, Francesco et al. (2012). "Methodologies and Uncertainties in the Use of the Terrestrial Chlorophyll Index for the Sentinel-3 Mission." In: *Remote Sensing* 4.5, pp. 1112–1133. DOI: 10.3390/rs4051112. URL: <http://www.mdpi.com/2072-4292/4/5/1112>.
- Whittaker, R. H. (1972). "Evolution and Measurement of Species Diversity." In: *Taxon* 21.2/3, p. 213. ISSN: 00400262. DOI: 10.2307/1218190. URL: <https://www.jstor.org/stable/1218190?origin=crossrefhttp://www.jstor.org/stable/1218190?origin=crossref>.
- Wiens, J. A. (1989). "Spatial Scaling in Ecology." In: *Functional Ecology* 3.4, p. 385. ISSN: 02698463. DOI: 10.2307/2389612. URL: <https://www.jstor.org/stable/2389612?origin=crossrefhttp://www.jstor.org/stable/2389612?origin=crossref>.
- Wijk, Mark T. van and Mathew Williams (2005). "Optical Instruments for Measuring Leaf Area Index in Low Vegetation : Application in Arctic Ecosystems." In: *Ecological Applications* 15.4, pp. 1462–1470.
- Wu, Chaoyang et al. (2008). "Estimating chlorophyll content from hyperspectral vegetation indices: Modeling and validation." In: *Agricultural and Forest Meteorology* 148.8-9, pp. 1230–1241. DOI: 10.1016/J.AGRFORMET.2008.03.005. URL: <https://www.sciencedirect.com/science/article/pii/S0168192308000920#tb12>.
- Zhang, Yongqin, Jing M Chen, and Sean C Thomas (2007). "Retrieving seasonal variation in chlorophyll content of overstory and understory sugar maple leaves from leaf-level hyperspectral data." In: *Canadian Journal of Remote Sensing* 33.5, pp. 406–415. ISSN: 17127971. DOI: 10.5589/m07-037.

A Appendix - Additional Figures and Tables

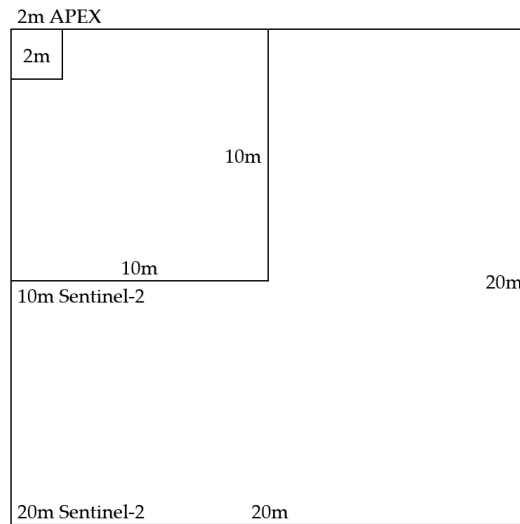


FIGURE A.1: Comparison of APEX (2 m) and Sentinel-2 (10 m and 20 m) pixels. The spatial resolution of the APEX datasets being 2 m through all bands, while the spatial resolution of Sentinel-2 being 10 m for bands of the visible (band 2 – 4) and the NIR (band 8) part of the spectrum and 20 m for red-edge bands (bands 5 – 7), NIR narrow (band 8a), as well as SWIR bands (band 11 and 12).

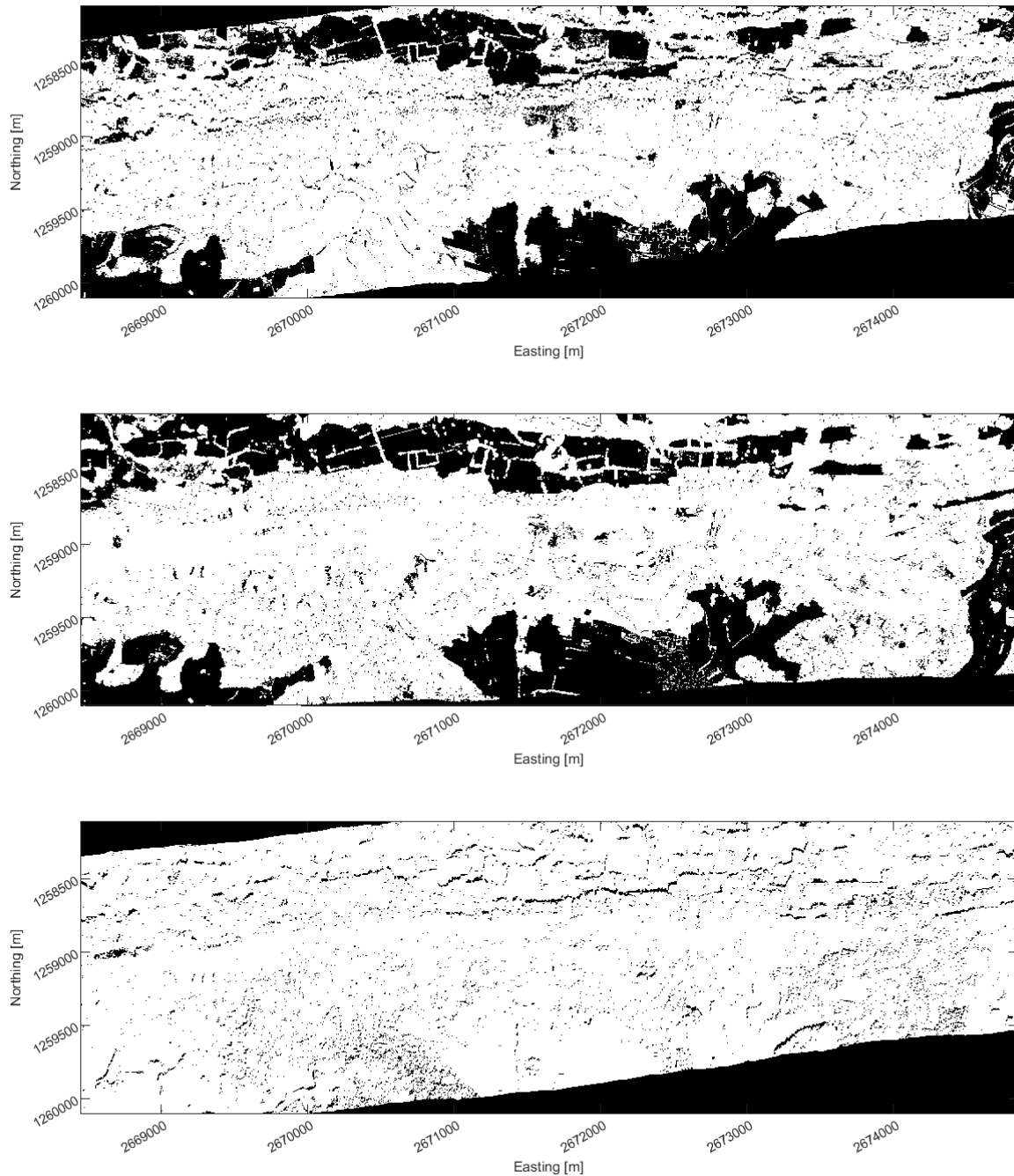


FIGURE A.2: Three vegetation masks created for the APEX 2 m scene for summer and fall combined in case of *NDVI* and shadow. The masks were combined afterwards. A pixel which was assigned the value 1 on all of the requirements was selected for the forest mask.

top: *NDVI* Mask. Pixels values of ≥ 0.7 were assigned 1, pixels with a value < 0.7 were assigned 0.

middle: Vegetation height mask based on the CHM. Pixels values of 4 m and higher were assigned 1, pixels smaller than 4 m were assigned 0.

bottom: Shadow mask. The lowest 2.5% of the summed channels 7 – 10 were assigned 0.

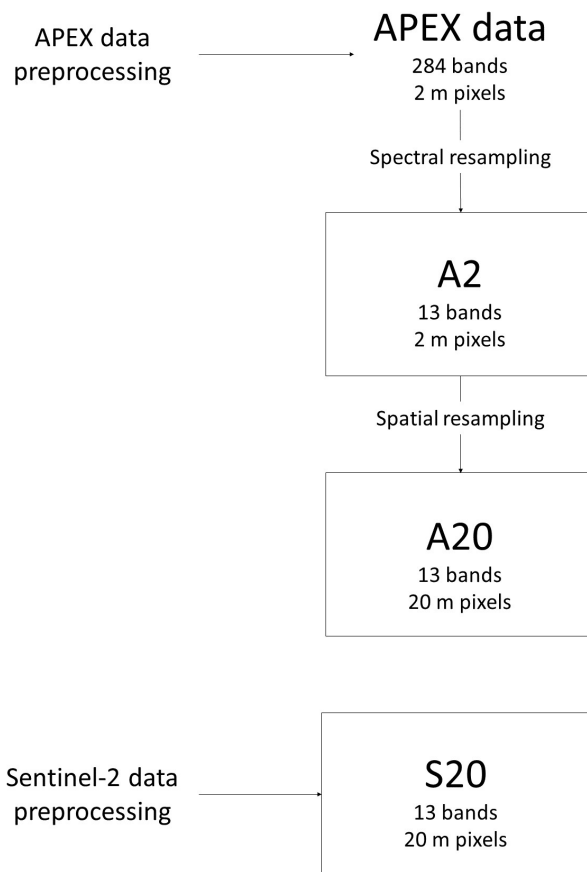


FIGURE A.3: Graphic representation of the three types of dataset, the spectrally resampled APEX dataset (A2), the spectrally and spatially resampled APEX dataset (A20) and the Sentinel-2 dataset (S20). Each type of dataset was analyzed in both summer and fall.

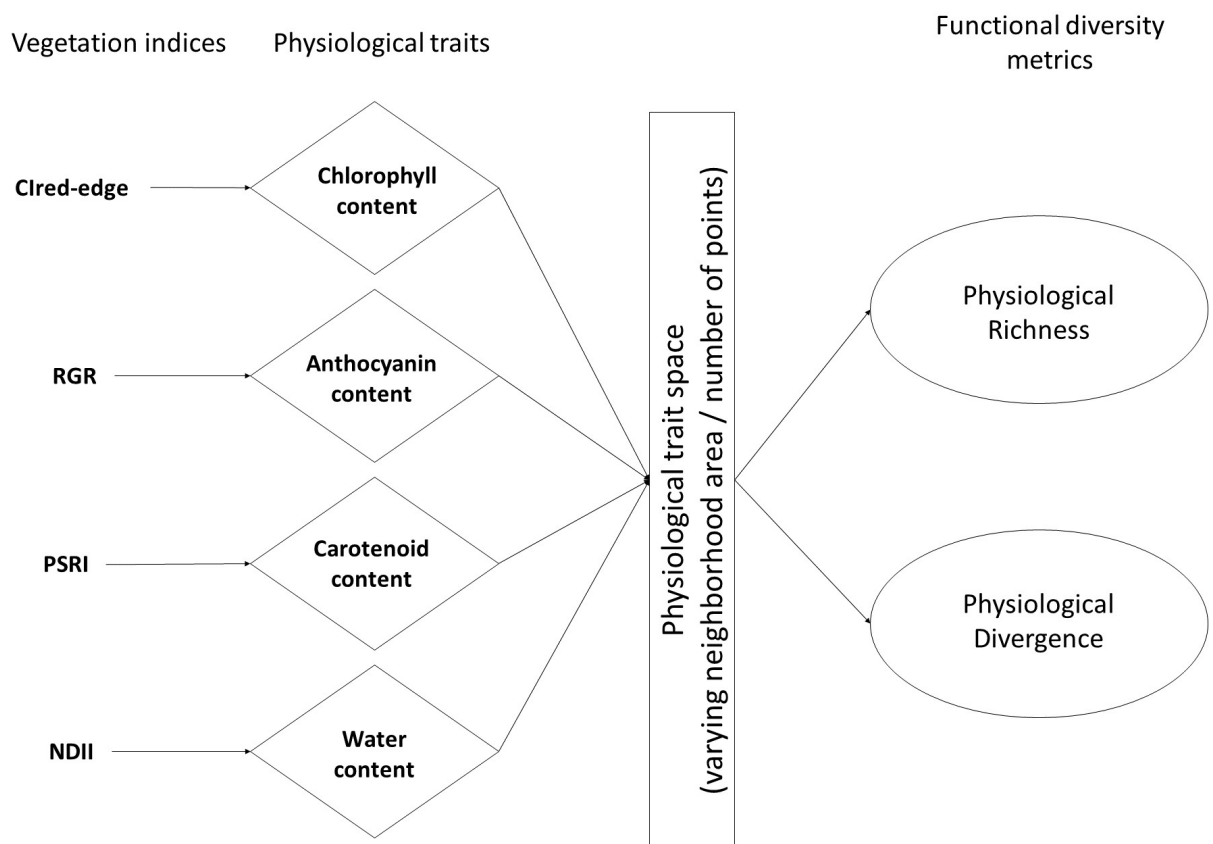


FIGURE A.4: Graphic representation of the basic work-flow from remotely-sensed vegetation indices (VI) data to physiological diversity metrics. Which was implemented on all of the datasets (A2, A20, S20) for each summer and fall. Based on the original by Schneider et al. 2017.

0	0	0	0.1	0.39	0.49	0.39	0.1	0	0	0
0	0	0.48	0.98	1	1	1	0.98	0.48	0	0
0	0.48	1	1	1	1	1	1	1	0.48	0
0.1	0.98	1	1	1	1	1	1	1	0.98	0.1
0.39	1	1	1	1	1	1	1	1	1	0.39
0.49	1	1	1	1	1	1	1	1	1	0.49
0.39	1	1	1	1	1	1	1	1	1	0.39
0.1	0.98	1	1	1	1	1	1	1	0.98	0.1
0	0.48	1	1	1	1	1	1	1	0.48	0
0	0	0.48	0.98	1	1	1	0.98	0.48	0	0
0	0	0	0.1	0.39	0.49	0.39	0.1	0	0	0

FIGURE A.5: Example of circular pixel neighborhood and its weighing. A unit with a diameter of 10 pixel corresponds to the square unitsize of $8.86 \cdot 8.86$ pixels and an area of 78.54 pixel.

TABLE A.1: Correlation of tested indices with each other, calculated based on A20 datasets averaged over seasons summer and fall. The corresponding traits are chlorophyll (green), anthocyanin (red), carotenoid (orange) and water content (blue).

Index	Cired-edge	Cgreen	MTCI	NDRE1	NDRE2	REP	MCARI/ OSAVI	TCARI/ OSAVI	ARI1	ARI2	RGR	CRI1	PSRI	NDII	MSI
CI red-edge	1	0,92	0,84	0,90	1,00	0,62	0,55	0,81	0,44	0,55	-0,60	0,26	-0,20	0,65	0,69
CI green	0,92	1	0,80	0,87	0,91	0,48	0,60	0,83	0,46	0,50	-0,42	0,18	-0,47	0,47	0,54
MTCI	0,84	0,80	1	0,88	0,84	0,32	0,70	0,54	0,08	0,33	-0,59	-0,14	-0,16	0,53	0,67
NDRE1	0,90	0,87	0,88	1	0,91	0,23	0,76	0,70	0,24	0,54	-0,78	0,13	-0,03	0,55	0,67
NDRE2	1,00	0,91	0,84	0,91	1	0,61	0,54	0,81	0,45	0,55	-0,61	0,27	-0,18	0,66	0,69
REP	0,62	0,48	0,32	0,23	0,61	1	-0,19	0,55	0,58	0,22	0,08	0,35	-0,39	0,49	0,36
MCARI/OSAVI	0,55	0,60	0,70	0,76	0,54	-0,19	1	0,22	-0,33	0,44	-0,72	-0,24	0,10	0,20	0,40
TCARI/OSAVI	0,81	0,83	0,54	0,70	0,81	0,55	0,22	1	0,79	0,41	-0,34	0,45	-0,37	0,57	0,52
CRI1	0,44	0,46	0,08	0,24	0,45	0,58	-0,33	0,79	1	0,20	0,09	0,65	-0,42	0,43	0,27
ARI1	0,55	0,50	0,33	0,54	0,55	0,22	0,44	0,41	0,20	1	-0,53	0,70	0,08	0,35	0,33
ARI2	-0,60	-0,42	-0,59	-0,78	-0,61	0,08	-0,72	-0,34	0,09	-0,53	1	-0,14	-0,58	-0,51	-0,61
RGR	0,26	0,18	-0,14	0,13	0,27	0,35	-0,24	0,45	0,65	0,70	-0,14	1	0,04	0,35	0,17
PSRI	-0,20	-0,47	-0,16	-0,03	-0,18	-0,39	0,10	-0,37	-0,42	0,08	-0,58	0,04	1	0,14	0,15
NDII	0,65	0,47	0,53	0,55	0,66	0,49	0,20	0,57	0,43	0,35	-0,51	0,35	0,14	1	0,94
MSI	0,69	0,54	0,67	0,67	0,69	0,36	0,40	0,52	0,27	0,33	-0,61	0,17	0,15	0,94	1

TABLE A.2: Correlation of tested indices with each other, calculated based on S20 datasets averaged over seasons summer and fall. The corresponding traits are chlorophyll (green), anthocyanin (red), carotenoid (orange) and water content (blue).

Index	Cired-edge	Cgreen	MTCI	NDRE1	NDRE2	REP	MCARI/ OSAVI	TCARI/ OSAVI	ARI1	ARI2	RGR	CRI1	PSRI	NDII	MSI
<i>Cired-edge</i>	1	0,75	0,85	0,96	0,99	0,72	-0,17	0,59	0,22	0,49	-0,42	0,29	-0,21	0,53	0,38
<i>Cgreen</i>	0,75	1	0,43	0,72	0,75	0,45	0,21	0,67	0,64	0,51	-0,22	0,41	-0,59	0,11	-0,06
<i>MTCI</i>	0,85	0,43	1	0,85	0,83	0,60	-0,48	0,43	-0,04	0,23	-0,15	0,06	-0,20	0,52	0,43
<i>NDRE1</i>	0,96	0,72	0,85	1	0,97	0,53	-0,11	0,59	0,21	0,52	-0,49	0,30	-0,18	0,54	0,39
<i>NDRE2</i>	0,99	0,75	0,83	0,97	1	0,71	-0,17	0,62	0,24	0,50	-0,45	0,31	-0,20	0,53	0,38
<i>REP</i>	0,72	0,45	0,60	0,53	0,71	1	-0,44	0,45	0,13	0,15	-0,05	0,12	-0,18	0,36	0,25
<i>MCARI/OSAVI</i>	-0,17	0,21	-0,48	-0,11	-0,17	-0,44	1	-0,29	-0,02	0,36	-0,43	0,02	0,11	-0,17	-0,21
<i>TCARI/OSAVI</i>	0,59	0,67	0,43	0,59	0,62	0,45	-0,29	1	0,78	0,31	-0,13	0,64	-0,42	0,15	0,04
<i>CRI1</i>	0,22	0,64	-0,04	0,21	0,24	0,13	-0,02	0,78	1	0,14	0,12	0,62	-0,60	-0,29	-0,42
<i>ARI1</i>	0,49	0,51	0,23	0,52	0,50	0,15	0,36	0,31	0,14	1	-0,59	0,66	0,04	0,37	0,32
<i>ARI2</i>	-0,42	-0,22	-0,15	-0,49	-0,45	-0,05	-0,43	-0,13	0,12	-0,59	1	-0,32	-0,60	-0,50	-0,43
<i>RGR</i>	0,29	0,41	0,06	0,30	0,31	0,12	0,02	0,64	0,62	0,66	-0,32	1	-0,08	0,02	-0,07
<i>PSRI</i>	-0,21	-0,59	-0,20	-0,18	-0,20	-0,18	0,11	-0,42	-0,60	0,04	-0,60	-0,08	1	0,35	0,42
<i>NDII</i>	0,53	0,11	0,52	0,54	0,53	0,36	-0,17	0,15	-0,29	0,37	-0,50	0,02	0,35	1	0,95
<i>MSI</i>	0,38	-0,06	0,43	0,39	0,38	0,25	-0,21	0,04	-0,42	0,32	-0,43	-0,07	0,42	0,95	1

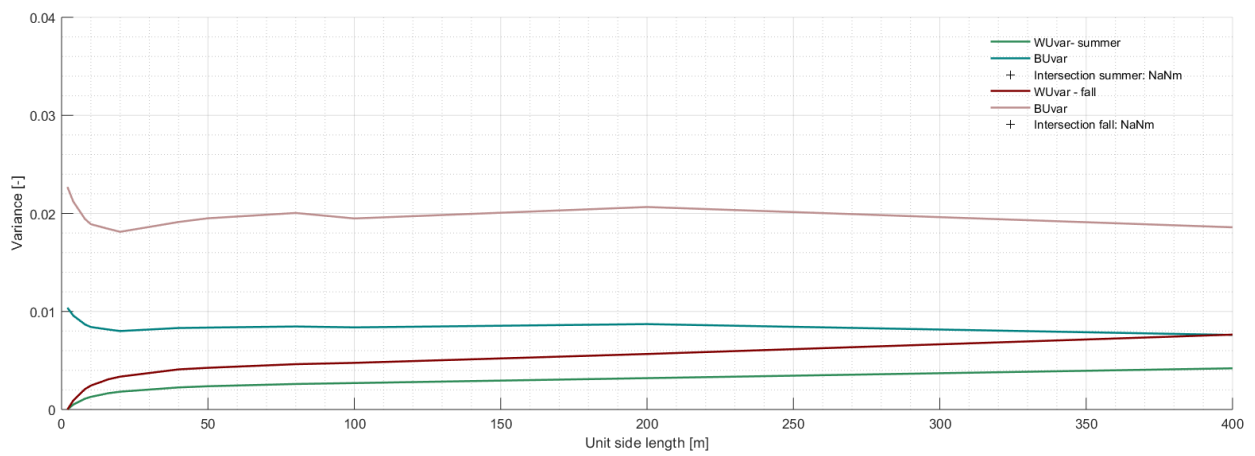


FIGURE A.6: Performance of *CRI1* in the one-dimensional scale analysis. Carotenoid describing *CRI1* seemed to not work properly on the APEX data.

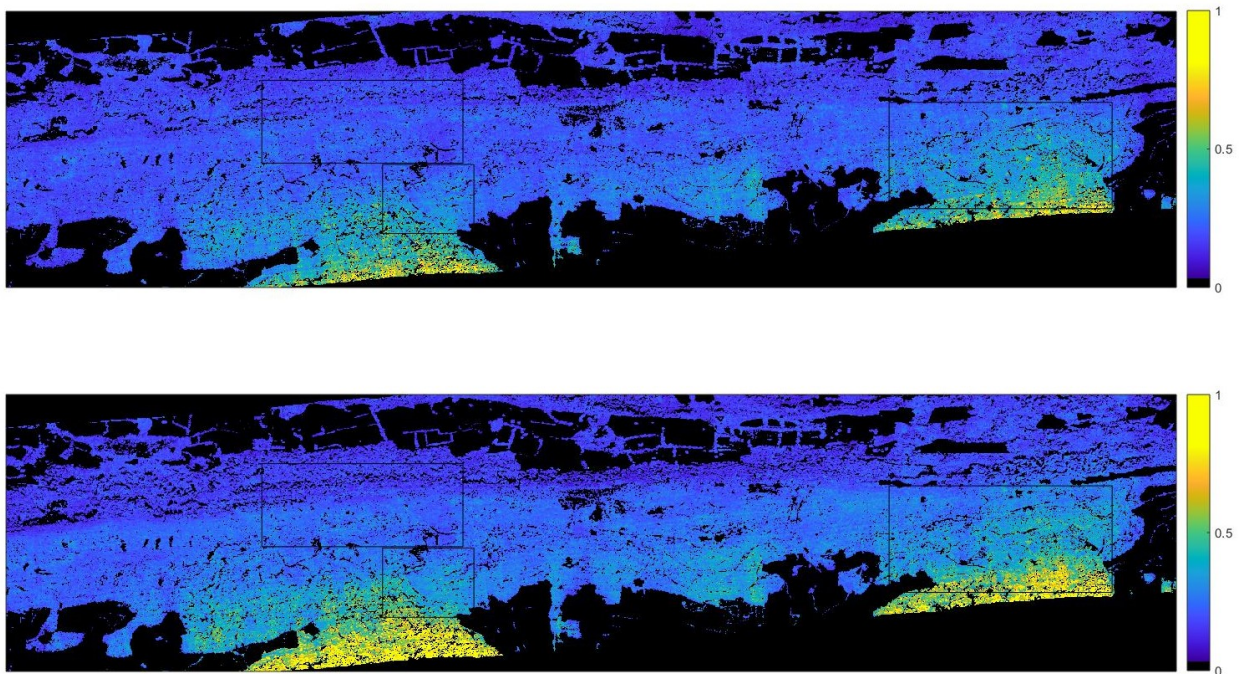


FIGURE A.7: Carotenoid describing *CRI1* calculated on the A2 dataset. *CRI1* seemed to not work properly on the APEX data.

TABLE A.3: Calculated variables of tested indices, calculated based on A20 and S20 datasets for each sensor at both summer and fall. The corresponding traits are chlorophyll (green), anthocyanin (red), carotenoid (orange) and water content (blue).

Index	Sensor difference of means [-]	Sensor difference of <i>cv</i> [-]	Mean of <i>cvs</i> [-]	Outliers [%]
<i>CIred – edge</i>	0.0976	7.84	17.06	0.0282
<i>CIgreen</i>	0.0433	2.48	8.35	0.0241
<i>MTCI</i>	0.1512	11.46	26.32	0.0208
<i>NDRE1</i>	0.0720	3.90	10.74	0.0419
<i>NDRE2</i>	0.0253	2.60	3.81	0.0466
<i>REP</i>	0.0432	5.76	7.97	0.0049
<i>MCARI/OSAVI</i>	0.0067	4.84	1.82	0.0195
<i>TCARI/OSAVI</i>	0.0595	1.47	8.94	0.0619
<i>ARI1</i>	0.0243	0.53	6.41	0.0388
<i>ARI2</i>	0.0664	1.61	14.79	0.0147
<i>RGR</i>	0.0079	2.56	1.98	0.0329
<i>CR11</i>	0.1168	19.67	38.70	0.0581
<i>PSRI1</i>	0.0187	2.26	4.35	0.0273
<i>NDII</i>	0.0870	0.73	15.78	0.0373
<i>MSI</i>	0.0220	1.90	3.54	0.0349

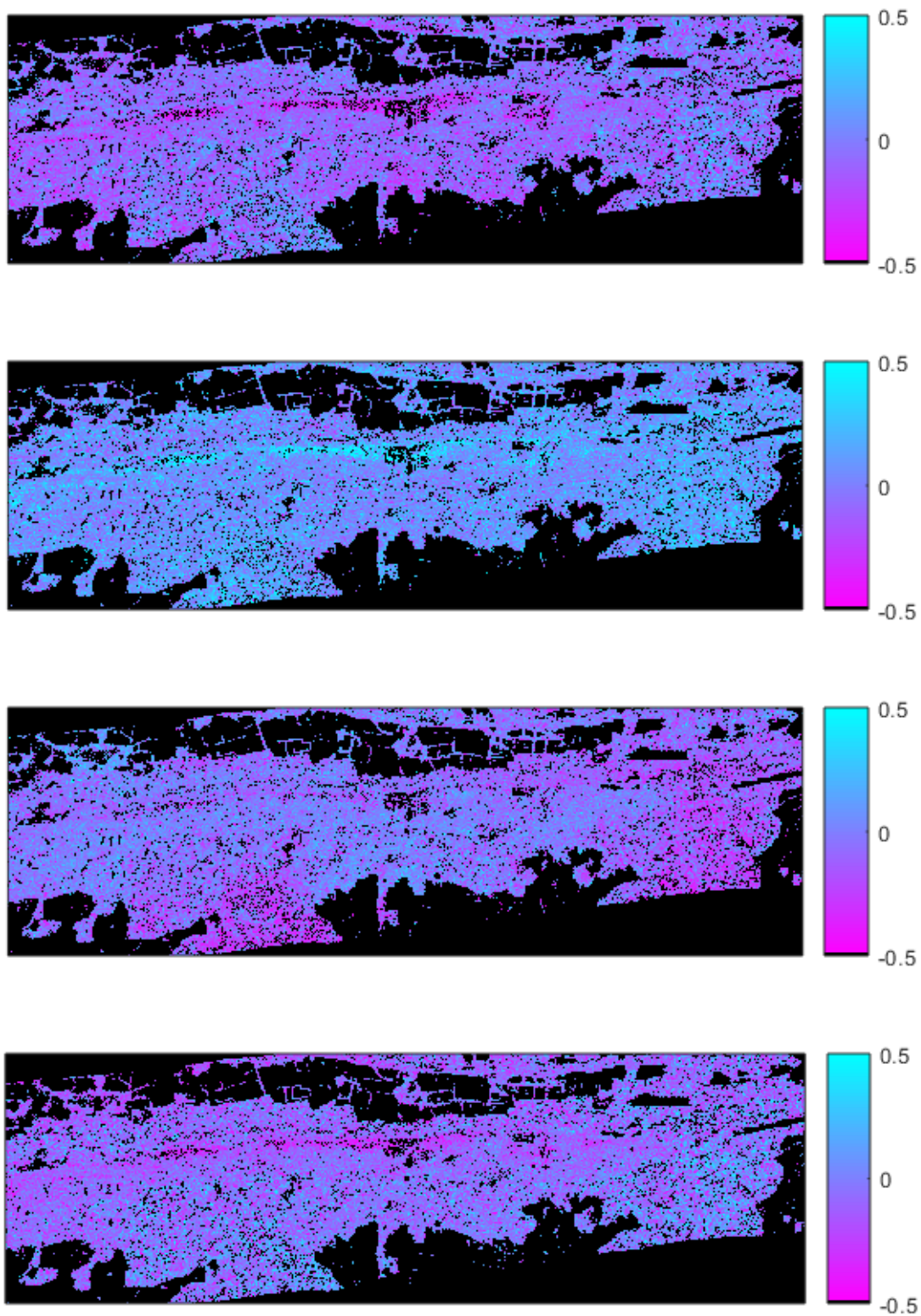


FIGURE A.8: Difference of all functional traits (fall-summer) calculated based on the A2 datasets. Blue being the increase and pink being the decrease of the trait value for chlorophyll content, anthocyanin content, carotenoid content and water content (from top to bottom).

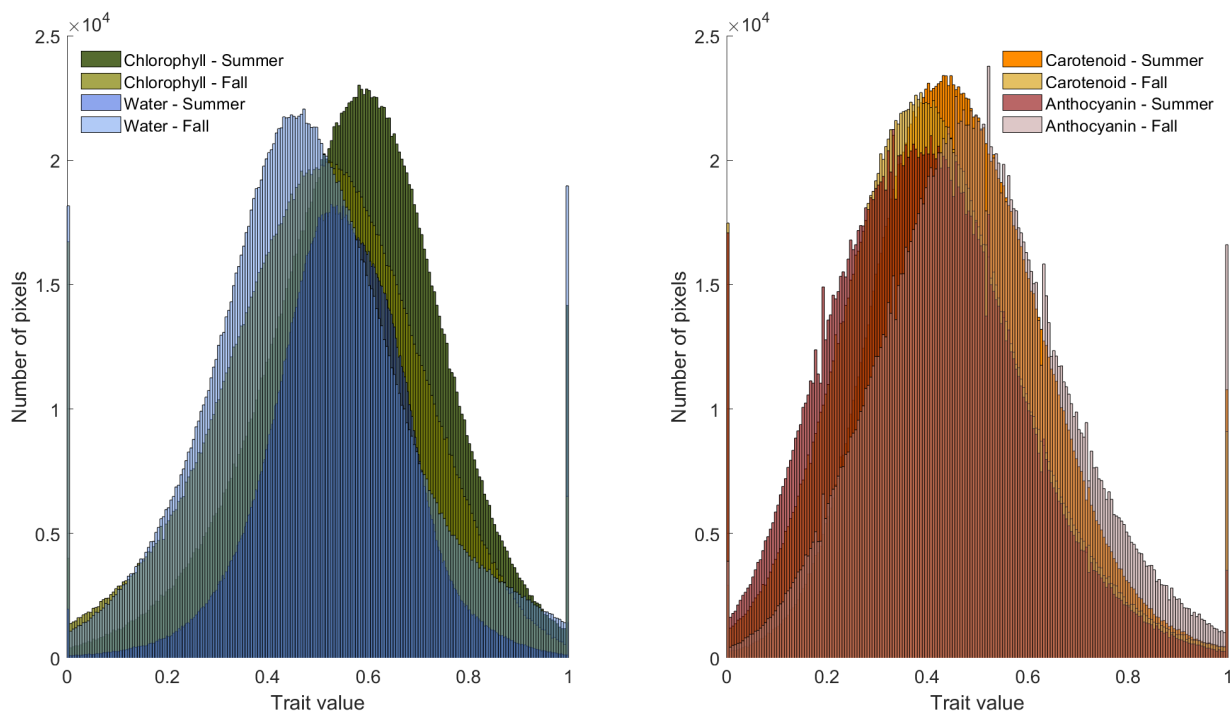


FIGURE A.9: Histograms showing the mapped functional traits chlorophyll (green), anthocyanin (red), carotenoid (orange) and water content (blue) on the research site for both summer (dark color) and fall (light color).

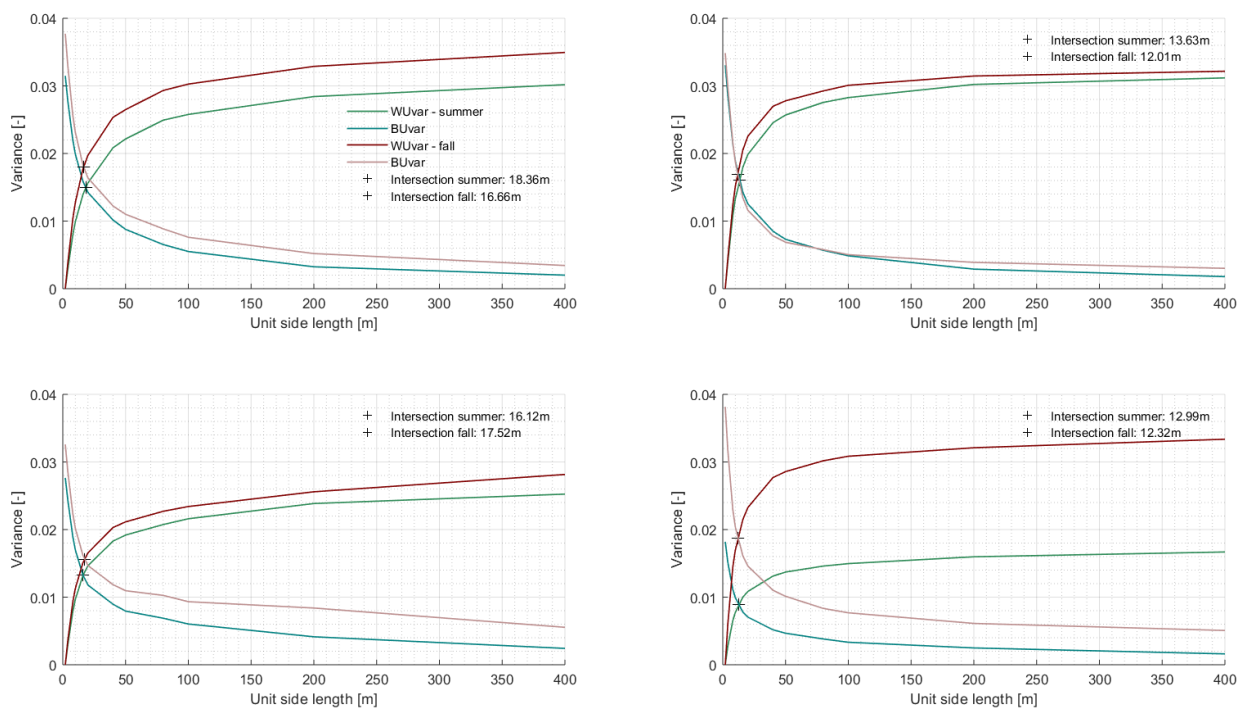


FIGURE A.10: One-dimensional scale analysis for each of the functional traits, based on the A2 datasets. The functional traits are chlorophyll (top left), anthocyanin (top right), carotenoid (bottom left) and water content (bottom right).

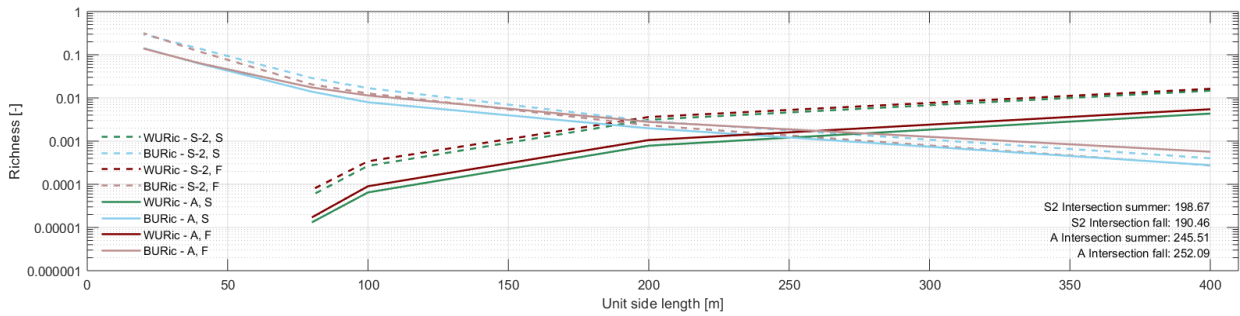


FIGURE A.11: Scale analysis of A20 (solid) and S20 (dashed) datasets, calculating functional richness.

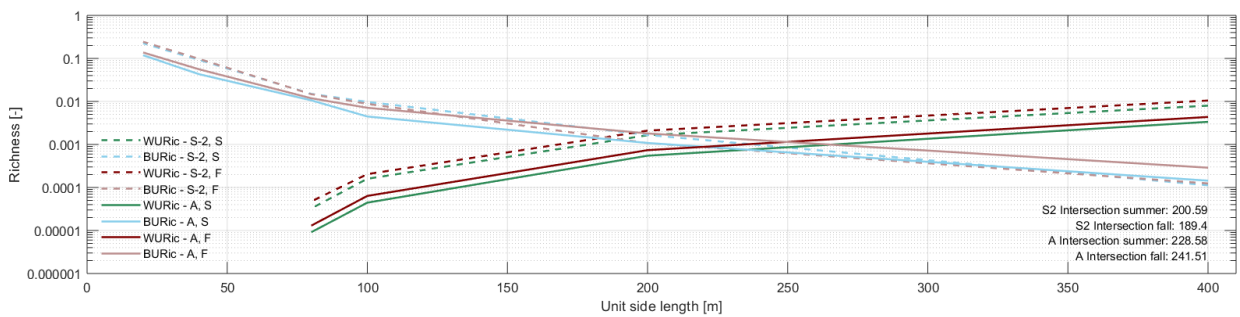


FIGURE A.12: Scale analysis of A20 (solid) and S20 (dashed) datasets, calculating functional richness. Chlorophyll content is here described by Cl_{green} instead of $Cl_{red - edge}$.

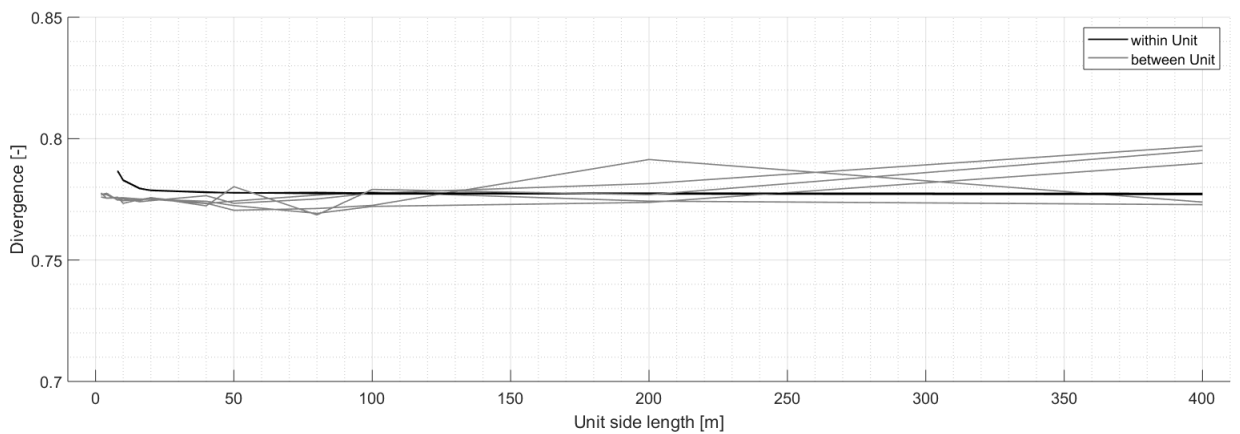


FIGURE A.13: Scale analysis of randomly generated, normally distributed trait data calculated functional divergence five times. Between-unit divergence (grey) shows strong differences in each calculation which can probably be explained by the insufficient number of units at larger unit sizes not delivering stable results.

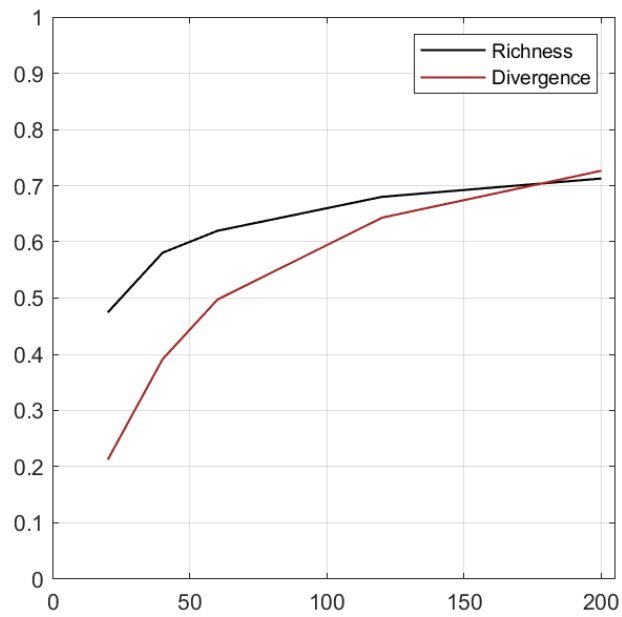


FIGURE A.14: Correlation of seasons for both functional richness (black) and divergence (red) maps, calculated from A2 data.

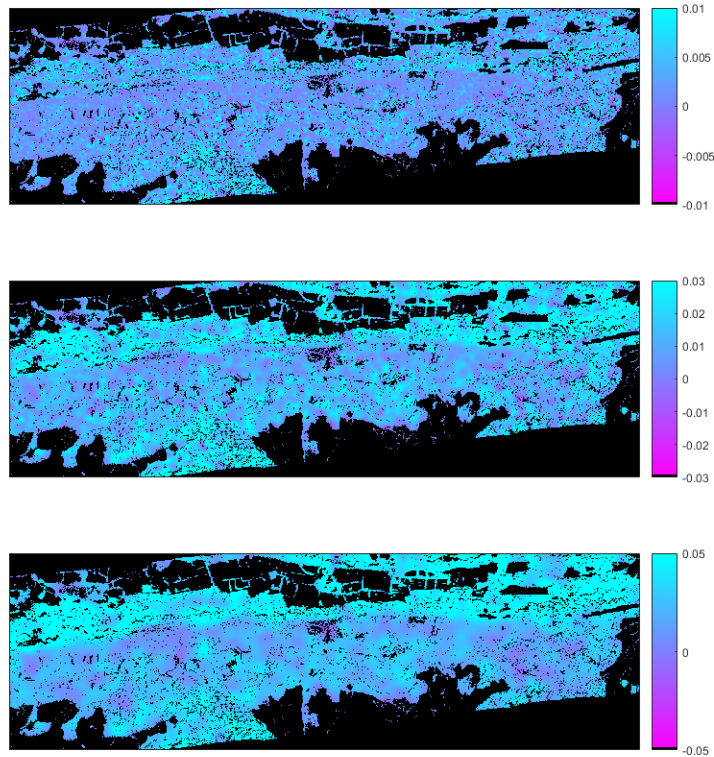


FIGURE A.15: Spatial detail of seasonal difference of functional richness, calculated at 20 m (top) 60 m (middle) and 120 m diameter (bottom).

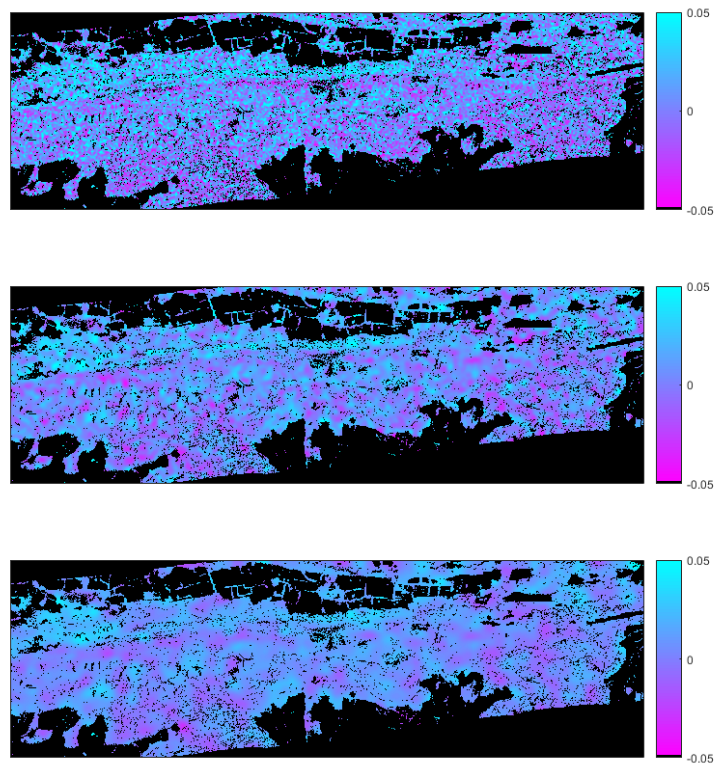


FIGURE A.16: Spatial detail of seasonal difference of functional divergence, calculated at 20 m (top) 60 m (middle) and 120 m diameter (bottom).

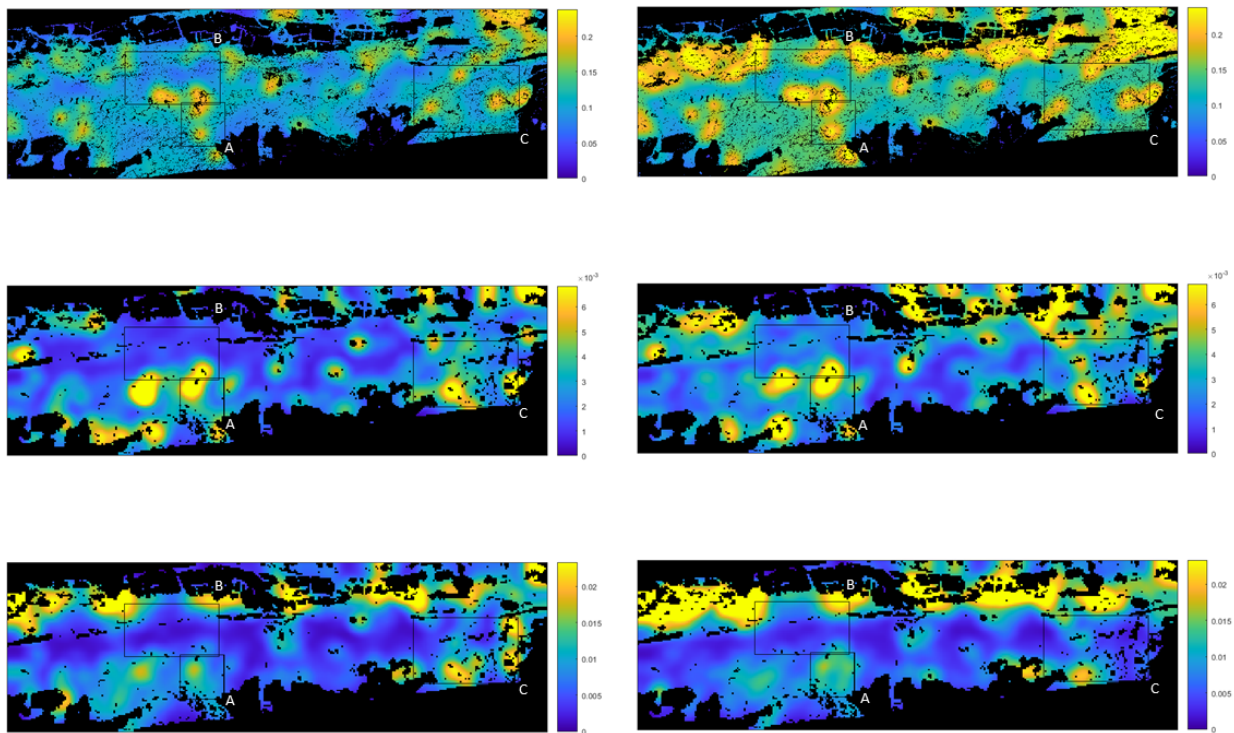


FIGURE A.17: Functional richness calculated based on the A2 dataset (top), the A20 dataset (middle) and S20 dataset (bottom) in summer (left) and fall (right) based on 200 m unit size.

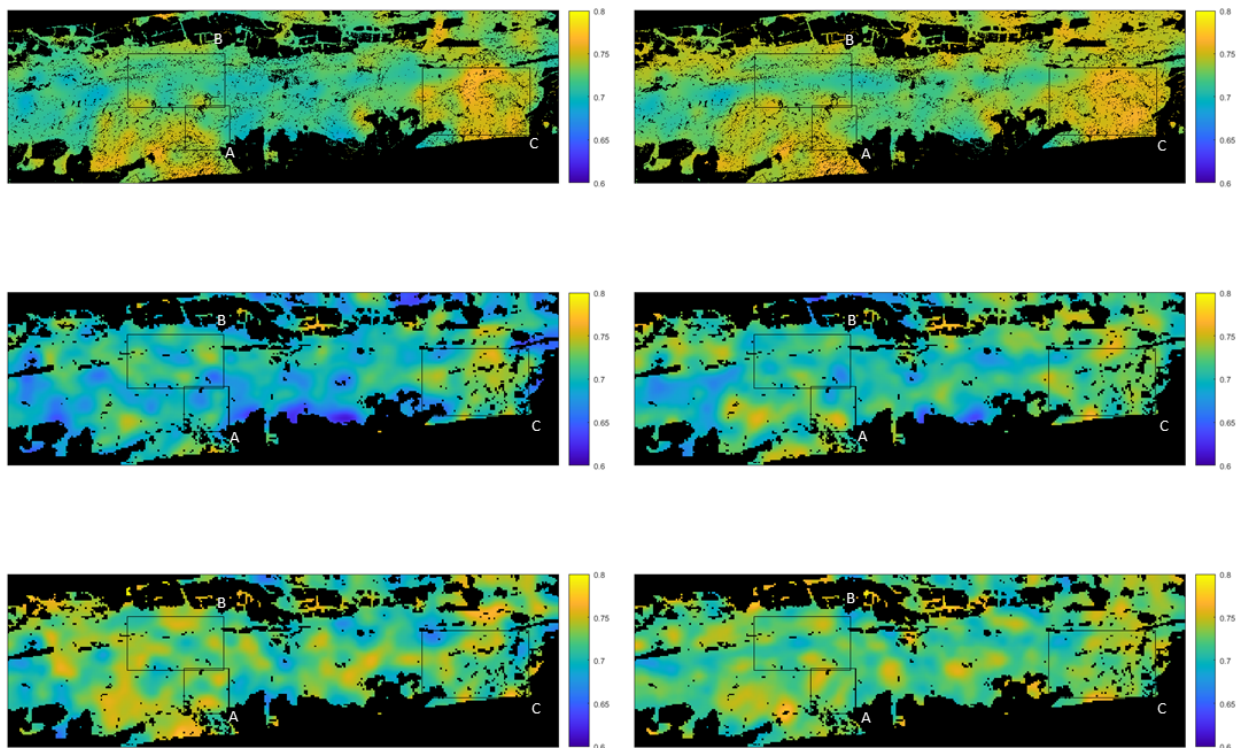


FIGURE A.18: Functional divergence calculated based on the A2 dataset (top), the A20 dataset (middle) and S20 dataset (bottom) in summer (left) and fall (right) based on 200 m unit size.

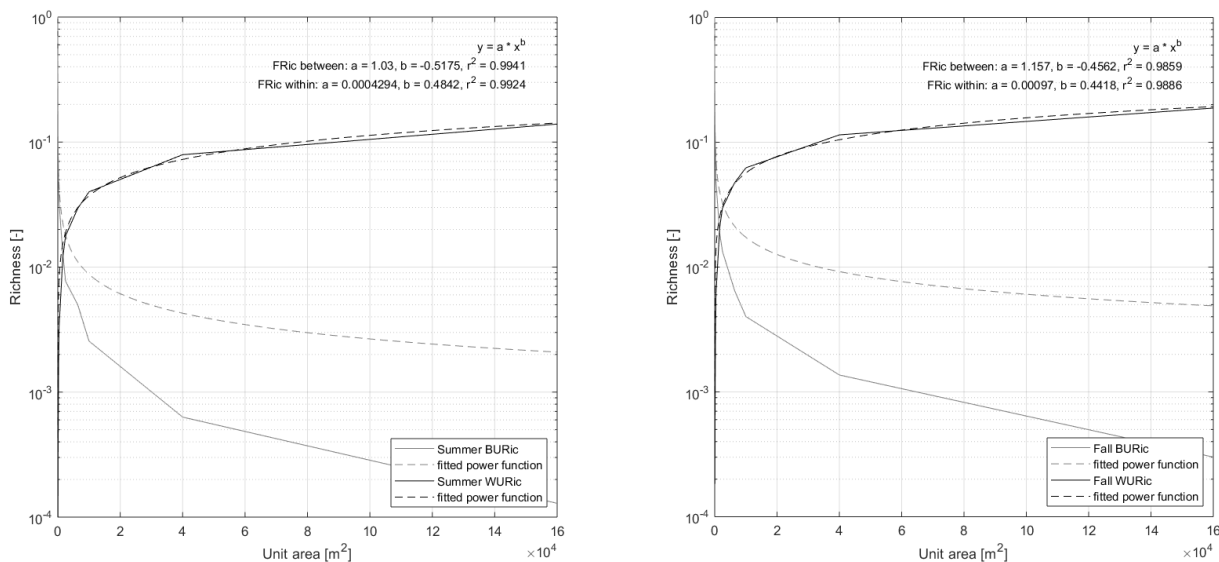


FIGURE A.19: Development of within- and between-unit functional richness with increasing unit size in summer (left) and fall (right) in the four-dimensional scale analysis based on the A2 datasets. Attempts of fitting power law functions and logarithmic functions (Schneider et al., 2017), are shown in dashed and dotted lines.

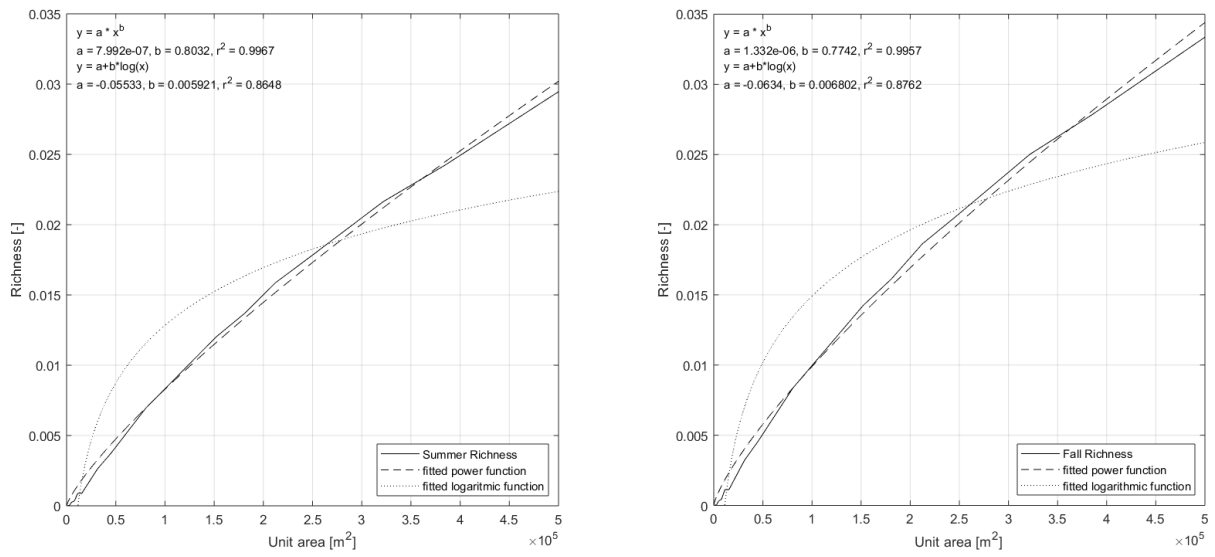


FIGURE A.20: Development of mean functional richness calculated based on the A20 datasets, with increasing unit area in summer (left) and fall (right). Attempts of fitting power law functions and logarithmic functions (Schneider et al., 2017), are shown in dashed and dotted lines.

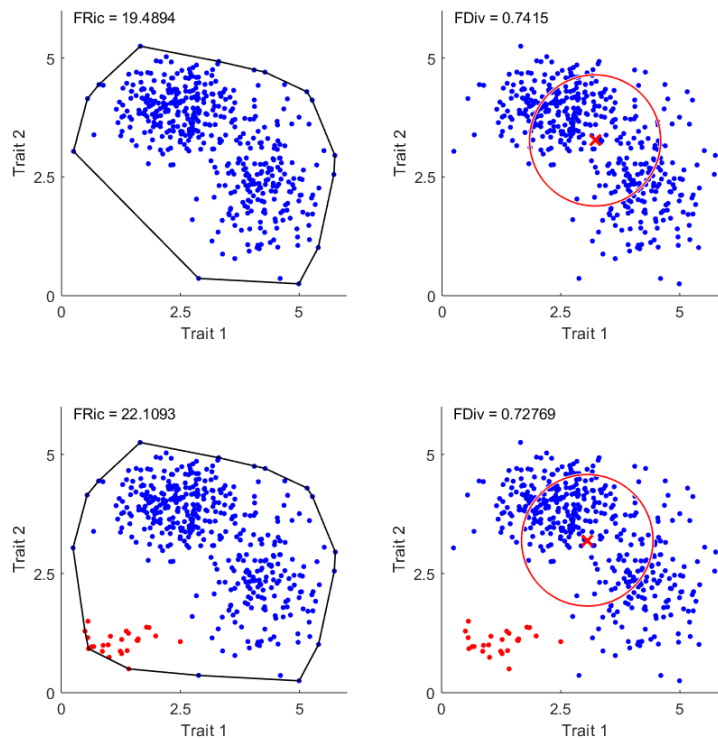


FIGURE A.21: Effect of mixed pixels (red) on randomly generated, normally distributed data-points without clear differentiation/niche partitioning. Functional richness increases (left panels) and divergence decreases (right panels).

B Appendix - List of Abbreviations

B.1 Terms and Abbreviations

α -diversity	diversity within a community
β -diversity	diversity between communities
γ -diversity	sum of α - and β -diversity
ρ	surface reflectance [0-1]
A2	spectrally resampled APEX data, with 13 spectral bands and a pixel size of 2 m
A20	spectrally and spatially resampled APEX data, with 13 spectral bands and a pixel size of 20 m
S20	Sentinel-2 spaceborne derived dataset, with 13 spectral bands and a pixel size of 20 m
a. s. l.	above sea level
BRDF	Bidirectional Reflectance Distribution Function
CHM	Canopy Height Model
DOY	day of year
EBV	essential biodiversity variable
LAI	Leaf Area Index [$\frac{m^2}{m^2}$]
MERIS	Medium Resolution Imaging Spectrometer on the Envisat satellite
MSI	Multi-Spectral Instrument on Sentinel-2
NIR	Near Infrared part of the spectrum
OLCI	Ocean and Land Color Instrument on Sentinel-3
SWIR	Short wave infrared part of the spectrum
RE	red-edge part of the spectrum
VI	Vegetation Index
VIS	visible part of the spectrum (R = red, G = green, B = blue)

B.2 Abbreviations

<i>BU</i>	between-unit
<i>WU</i>	within-unit
<i>i</i>	intersection of within- and between-unit variance
<i>t</i>	80% of the variance within-/between-unit
<i>maxvar</i>	between-unit variance at original pixel size
<i>BUvar(20)</i>	between-unit variance remaining at 20 m (absolute or relative)
<i>cv</i>	coefficient of variation
<i>dim</i>	number of dimensions
<i>d</i>	circular unit diameter
<i>ppu</i>	pixels per unit
<i>BUvar</i>	between-unit variance
<i>WUvar</i>	within-unit variance
<i>BURic</i>	between-unit richness
<i>WURic</i>	within-unit richness
<i>BUDiv</i>	between-unit divergence
<i>WUDiv</i>	within-unit divergence
<i>n</i>	number of units
U_{ppu}	pixel values
<i>l</i>	square unit side length
<i>FRic</i>	Functional Richness
<i>FDiv</i>	Functional Divergence
<i>Chl</i>	Chlorophyll content
<i>Ant</i>	Anthocyanin content
<i>Car</i>	Carotenoid content
<i>Wat</i>	Water content
<i>S</i>	Summer (July)
<i>F</i>	Fall (September)

B.3 Vegetation indices

<i>ARI</i>	Anthocyanin Reflectance Index
<i>CI_{green}</i>	Green chlorophyll index
<i>CI_{red-edge}</i>	Red-edge chlorophyll index
<i>EVI</i>	Enhanced vegetation index
<i>NDVI</i>	Normalized Difference Vegetation Index
<i>SR</i>	Simple Ratio
<i>MTCI</i>	MERIS terrestrial chlorophyll index
<i>NDRE</i>	Normalized difference red-edge
<i>OTCI</i>	OLCI Terrestrial Chlorophyll Index
<i>REP</i>	Red-edge position
<i>MCARI</i>	Modified chlorophyll absorption ratio index
<i>TCARI</i>	Transformed chlorophyll absorption ratio index
<i>SAVI</i>	Optimized soil-adjusted vegetation index
<i>RGR</i>	Red Green Ratio
<i>CRI1</i>	Carotenoid Reflectance Index 1
<i>SIPI</i>	Structure-insensitive pigment index
<i>PSRI</i>	Plant Senescence Reflectance Index
<i>NDII</i>	Normalized Difference Infrared Index
<i>NDWI</i>	Normalized Difference Water Index
<i>MSI</i>	Moisture Stress Index

B.4 Organizations

ESA	European Space Agency https://www.esa.int/ESA
FAO	Food and Agriculture Organization of the United Nations http://www.fao.org/home/en/
MeteoSwiss	Swiss federal office of Meteorology and Climatology https://www.meteoswiss.admin.ch/home.html?tab&overview
swisstopo	Swiss federal office of topography https://www.swisstopo.admin.ch/en/home.html
UN	United Nations http://www.un.org/en/index.html

B.5 Missions

Envisat Mission	https://earth.esa.int/web/guest/missions/esa-operational-eo-missions/envisat
Sentinel-2 Mission	https://sentinel.esa.int/web/sentinel/missions/sentinel-2
Sentinel-3 Mission	https://sentinel.esa.int/web/sentinel/missions/sentinel-3

B.6 Software

- ATCOR3 Atmospheric and Topographic Correction 3
<https://www.rese-apps.com/software/atcor-3-satellites/index.html>
- ATCOR4 Atmospheric and Topographic Correction 4
<http://www.rese.ch/products/atcor/atcor4/>
- ENVI Environment for Visualizing Images
<https://www.harrisgeospatial.com/Software-Technology/ENVI>
- MATLAB <https://ch.mathworks.com/products/matlab.html>

Acknowledgements

First of all, many thanks go to Michael, Devis and Rogier for inspiring my enthusiasm for science and motivating me to apply for the specialized Master's program. A really big thank you goes to Hendrik for multiple reasons, which can be shortened to being always around, offering an open ear and a helping hand whenever needed. Next, I would like to thank Fabian for his exorbitant amount of patience, his time and every appointment. These turned out to be trickier than it sounds, once he moved to the other side of the world. Furthermore, I would like to thank my fellow students, especially Ewa, Joan, Manuel and Marius for their help, support, patience and company. Lastly, I would like to thank everyone proofreading parts of this thesis, listening to my never changing topic number one, this Master thesis, supporting and believing in me. This includes all the people mentioned above, my friends and my family. During the last two years I learned so much thanks to everyone of you.

Personal Declaration

I hereby declare that the submitted thesis is the result of my own, independent work. All external sources are explicitly acknowledged in the thesis.

Date

December 29, 2018

Signature

Isabelle Helfenstein